MACTEC

APPENDIX B

CPT TESTING REPORT FROM APPLIED RESEARCH SERVICES

CONE PENETRATION TESTING
SUBSURFACE INVESTIGATION FOR SOUTHERN NUCLEAR OPERATING COMPANY, INC.

ADVANCED LIGHT WATER REACTOR EARLY SITE PERMIT

ALVIN W. VOGTLE NUCLEAR PLANT
WAYNESBORO, GEORGIA

Prepared for:

MACTEC Engineering and Consulting, Inc.
396 Plasters Avenue
Atlanta, Georgia

Prepared by:

Applied Research Associates, Inc.
New England Division
415 Waterman Road
South Royalton, Vermont 05068

ARA Report No. 17087

February 10, 2006

TABLE OF CONTENTS

SECTION **Page**

CONE PENETROMETER TESTING SUBSURFACE INVESTIGATION FOR ALVIN W. VOGTLE NUCLEAR PLANT WAYNESBORO, GEORGIA 1
- INTRODUCTION 1
- TEST LOCATIONS 1
- REPORT OUTLINE 1

TESTING EQUIPMENT AND PROCEDURES 5
- INTRODUCTION 5
- PIEZO-ELECTRIC CONE PENETROMETER EQUIPMENT AND TEST 5
  - Saturation of the Piezo-Cone 7
  - Field Calibrations 8
  - Penetration Data Format 9
  - Pore Pressure Correction of Tip Stress 9
  - Numerical Editing of the Penetration Data 13
- SEISMIC CONE PENETROMETER EQUIPMENT AND TEST 13
- PORE PRESSURE DISSIPATION RESULTS 16

DATA ANALYSIS TECHNIQUES 20
- OVERVIEW 20
- LOCATION OF THE SITE WATER TABLE 20
- SOIL BEHAVIOR TYPE 20
- STANDARD PENETRATION TEST 24
- FRICTION ANGLE (ϕ') 25
- UNDRAINED SHEAR STRENGTH (S_U) 26
- PRESENTATION OF ϕ AND S_U VALUES 26
- ESTIMATES OF OVERCONSOLIDATION RATIO (OCR) 27
- COEFFICIENT OF LATERAL CONSOLIDATION (C_H) 27
- COEFFICIENT OF LATERAL PERMEABILITY (K_H) 28

LIST OF REFERENCES 31

APPENDICES
- APPENDIX A: CONE PENETOMETER DATA
- APPENDIX B: SEISMIC TIME HISTORIES AND VELOCITIES
- APPENDIX C: PORE PRESSURE DISSIPATION DATA

LIST OF TABLES

Table **Page**

Summary of CPT testing at the Alvin W. Vogtle Nuclear Plants Subsurface Investigation ..3

LIST OF ILLUSTRATIONS

Figure **Page**

Figure 1. CPT Locations Table 4
Figure 2. Schematic of ARA's Peizo-Electric Cone Penetrometer 6
Figure 3. Typical CPT Profile from the A. W. Vogtle Site 11
Figure 4. High Energy Shear Wave Hammer 14
Figure 5. Typical Shear Wave Traces 15
Figure 6. Classic Dissipation Profile from the A. W. Vogtle Plant Site 18
Figure 7. Dissipation Test Showing a Dilating Condition 19
Figure 8. 1986 Soil Behavior Charts 21
Figure 9. 1990 Soil Behavior Charts 22
Figure 10. Dissipation Curves for a 60° Cone According to Linear Isotropic Uncoupled Solution (after Baligh and Levadoux, 1980) 29
Figure 11. Estimation of the Constrained Modulus, M, for Clays (after Robertson and Campanella, 1988) 30

SECTION 1

CONE PENETROMETER TESTING SUBSURFACE INVESTIGATION FOR ALVIN W. VOGTLE NUCLEAR PLANT WAYNESBORO, GEORGIA

SOUTHERN NUCLEAR OPERATING COMPANY, INC. ADVANCED LIGHT WATER REACTOR EARLY SITE PERMIT INVESTIGATION

INTRODUCTION

Applied Research Associates, Inc. (ARA) under contract to MACTEC Engineering and Consulting, Inc., conducted Electric Cone Penetration Tests with seismic measurements (S-CPT) in support of the subsurface investigation for Southern Nuclear Operating Company, Inc.'s Alvin W. Vogtle Nuclear Plant's Advanced Light Water Reactors Early Site Permit, in Waynesboro, Georgia. This report documents ARA's site investigation efforts, test techniques, and analysis of the data for fieldwork conducted September 1 through September 8, 2005. Presented in this report are the field-testing methods, data analysis techniques, and hardcopies of the test results.

TEST LOCATIONS

Twelve cone penetrometer test soundings were conducted at the site**.** Two additional soundings (C-1001A and C-1009A) from were offset and conducted due to shallow refusal at (C-1001 and C-1009). All the soundings were advanced from ground surface. Tip stress, sleeve stress, and penetration pore pressure were measured in all the CPTs. Seismic shear wave measurements were obtained at five-foot intervals at three locations. Compression wave measurements were not obtained as part of this investigation.

Table 1 lists the penetrations and relevant information about each location. All locations were grouted upon retraction of the rod string using a standard tremie grout method. The surveyed coordinates and elevations for all CPTs are listed on Figure 1. MACTEC Engineering and Consulting, Inc. provided the site map and survey data.

REPORT OUTLINE

This report is organized into 4 Sections and 3 Appendices. Section 2 discusses the CPT

equipment, field procedures, and daily calibrations. Section 3 describes the methods used to interpret the CPT results. Section 4 lists references. Appendix A presents the piezo-cone data. Seismic test wave histories and velocities are located in Appendix B. Appendix C contains pore pressure dissipation plots and a summary of these data, along with estimated values of constrained modulus, coefficient of lateral consolidation, and coefficient of lateral permeability.

Table 1. Summary of CPT testing at the Alvin W. Vogtle Nuclear Plants Subsurface Investigation

Project : MACTEC Engineering & Consulting, Inc.
Southern Nuclear Operating Company, inc.
Advanced Light Water Reactor Early Site Permit

Probe Diameter: 1.75 (in)

Test ID	Surface Elevation (ft)	Predrilled Depth	Depth of CPT (ft)	Seismic CPT	Water Table Depth (ft)	Water Table Elev (ft)	Test Depth (ft)	Test Elev (ft)	Static Pressure (psi)	Maximum Pressure (psi)	50 % Pressure (psi)	Tip Stress (tsf)	Tip Stress (psi)	Alpha	Constrained Modulus (psi)	Time 50% (min)	Lateral Consolidation (in2/s)	Lateral Consolidation (cm2/sec)	Lateral Permeability (cm/s)
C-1001	248.57	0.0	13.0	No	NA	NA	NA	NA											
C-1001A	248.57	0.0	116.7	No	NA	NA	NA	NA											
C-1002	222.13	0.0	78.5	No	NA	NA	NA	NA											
C-1003	219.80	0.0	80.0	Yes	44.6	175.20	68.31	151.5	10.3	10.45	10.4	487.3	6768.1	1.0	6768.1	0.09	7.80E-01	5.03E+00	1.06E-05
C-1003	219.80	0.0	80.0	Yes	51.8	168.00	79.07	140.7	11.8	13.68	12.7	198.1	2751.4	1.0	2751.4	1.0	6.95E-02	4.48E-01	2.32E-06
C-1004	220.82	0.0	77.0	No	NA	NA	66.25	154.6	NA	317.44	158.72	43.3	601.4	1.0	601.39	10.61	6.61E-03	4.27E-02	1.01E-06
C-1005	223.81	0.0	82.0	Yes	34.01	189.80	56.08	167.7	9.6	86.59	48.1	12.0	166.7	1.0	166.67	4.44	1.58E-02	1.02E-01	8.70E-06
C-1005	223.81	0.0	82.0	Yes	47.84	175.97	73.14	150.7	11.0	75.19	43.1	12.5	173.6	1.0	173.6	8.37	8.38E-03	5.41E-02	4.43E-06
C-1005	223.81	0.0	82.0	Yes	NA	NA	81.97	141.8											
C-1006	222.80	0.0	74.0	No	NA	NA	NA	NA											
C-1007	222.81	0.0	81.7	No	NA	NA	NA	NA											
C-1008	221.30	0.0	76.0	No	NA	NA	NA	NA											
C-1009	218.93	0.0	6.0	Yes	NA	NA	NA	NA											
C-1009A	218.93	0.0	99.0	Yes	49.97	168.96	60.12	158.8	4.4	4.45	4.4	128.6	1786.1		1786.1				
C-1009A	218.93	0.0	99.0	Yes	49.53	169.40	77.04	141.9	11.9	11.96	11.9	292.7	4065.3		4065.28				
C-1009A	218.93	0.0	99.0	Yes	NA	NA	90.07	128.9	39.0	283.76	141.88	68.2	1.89	1.0	947.22	16.28	4.31E-03	2.78E-02	4.17E-07
C-1009A	218.93	0.0	99.0	Yes	44.9	15.97	99.07	119.9	23.5	710.47	367.0	140.3	1948.6	1.0	1948.61	2.31	3.04E-02	1.96E-01	1.43E-06
C-1010	219.06	0.0	96.0	No	NA	NA	NA	NA	0.0										

Note 1: Dissipation analysis conducted on profiles exhibiting classic dissipation profile only.
Note 2: Dissipation tests C-1005.82, C-1009A-60, and C-1009A-77 exhibit a dilating condition not appropriate for permeability estimate.

MACTEC Engineering and Consulting, Inc.
and
Bechtel Corporation, Inc.

September 1 - 8, 2005

Alvin W. Vogtle Nuclear Plant
Cone Penetrometer Testing (CPT) Geotechnical Investigation

Southern Nuclear Operating Company, Inc.
Waynesboro, Georgia

Test Identification	Type of Test	ARA Filename	Northing	Easting	Elevation	Final Depth
C-1001	PCPT	202S0503	8028.12	6355.96	248.57	13.00
C-1001A	PCPT	202S0504	NA	NA	NA	116.70
C-1002	PCPT	206S0501	7667.64	6574.64	222.13	78.50
C-1003	SCPT	207L0506	7669.31	7477.87	219.80	80.00
C-1004	PCPT	201S0501	7646.13	8361.84	220.82	77.00
C-1005	SCPT	208S0501	7995.26	8174.60	223.81	82.00
C-1006	PCPT	201S0504	8001.46	7261.58	222.80	74.00
C-1007	PCPT	202S0502	8270.62	8055.05	222.81	81.70
C-1008	PCPT	202S0501	8268.48	6930.89	221.30	76.00
C-1009	SCPT	207S0501	5979.62	6798.49	218.93	6.00
C-1009A	SCPT	207S0505	NA	NA	NA	99.00
C-1010	PCPT	208S0502	6008.34	7754.15	219.06	96.00

Note: PCPT: Peizo-Cone Penetrometer Test; SCPT: Seismic Cone Penetrometer Test;
CPT locations C-1001A and C-1009A were offset by approximately 5-10 feet due to refusal. MACTEC to provide elevations and cooridinates for these soundings.

Figure 1. CPT Locations Table

SECTION 2

TESTING EQUIPMENT AND PROCEDURES

INTRODUCTION

The electric cone penetrometer test (CPT) was originally developed for use in soft soil. Over the years, cone and push system designs have evolved to the point where they can now be used in strong cemented soils and even soft rock. ARA's penetrometer consists of an instrumented probe that is forced into the ground using a hydraulic load frame mounted on a heavy truck with the weight of the truck providing the necessary reaction mass. The probe has a conical tip and a friction sleeve that independently measure vertical resistance beneath the tip as well as frictional resistance on the side of the probe as a function of depth. A schematic view of ARA's penetrometer probe is shown in Figure 2. A pressure transducer in the cone is used to measure the pore water pressure as the probe is pushed into the ground (P-CPT). This probe also includes three geophones aligned along the X, Y, and Z-axis for measuring shear and compressional waves velocities.

PIEZO-ELECTRIC CONE PENETROMETER EQUIPMENT AND TEST

The cone penetrometer tests were conducted using the ARA penetrometer truck (Mack 1). The penetrometer equipment is mounted inside a van body attached to a ten-wheel truck chassis. Ballast in the form of weights is added to the truck to achieve an overall push capacity of 60,000 lbs. Penetration force is supplied by a pair of large hydraulic cylinders bolted to the truck frame. If the push cylinders measure 15,000 to 20,000 pounds per square inch (psi), ARA's crew chief may declare a sounding refusal. Multiple attempts to penetrate the identified stratigraphy will be conducted prior to abandoning the sounding within the subject area.

A 15-cm^2 penetrometer probe (which has 1.75-inch diameter, 60° conical tip, and a 1.75-inch diameter by 6.5-inch long friction sleeve) was used on this project. This probe size is in conformance with ASTM D 5778 (Ref. 1). The shoulder between the base of the tip and the porous filter, shown in Figure 2, is 0.08 inch long. The penetrometer is advanced vertically into the soil at a constant rate of 48 inches/minute (2 cm/second), although this rate must sometimes be reduced as hard layers are encountered. The electric cone penetrometer test is conducted in accordance with ASTM D 5778 (Ref. 1).

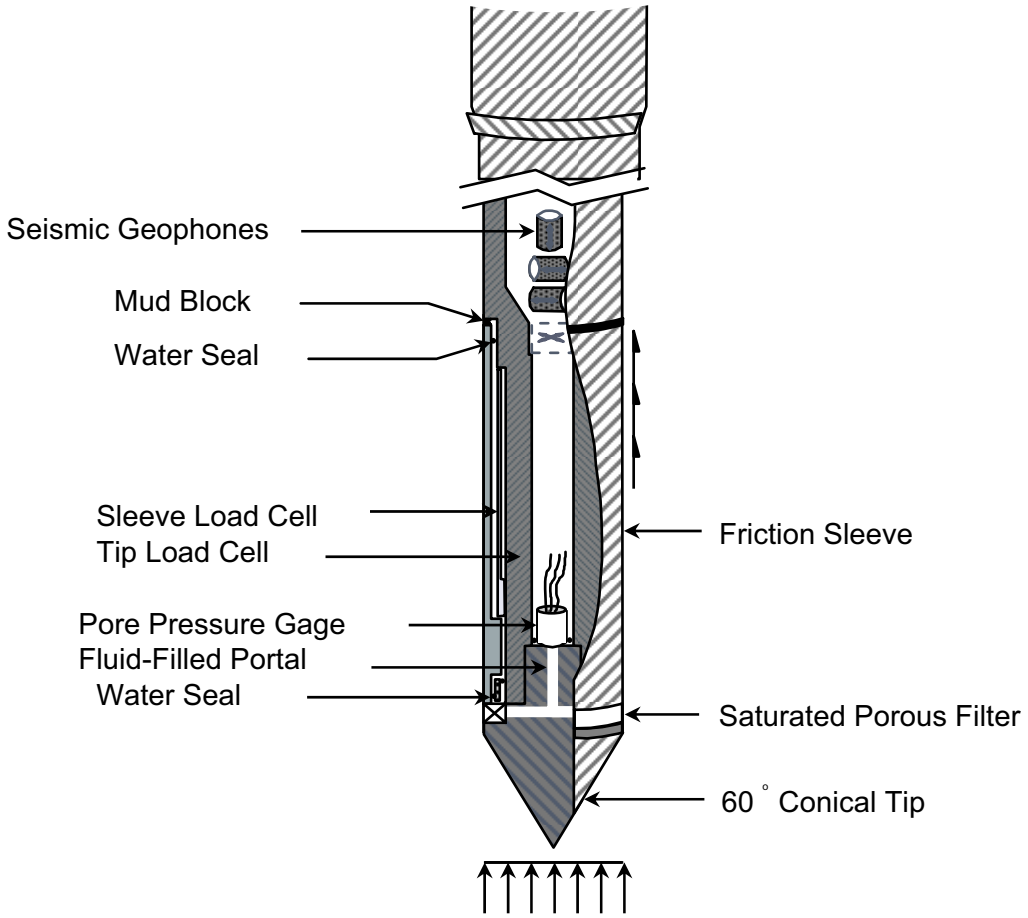

Figure 2. Schematic of ARA's Peizo-Electric Cone Penetrometer

Inside the probe, two load cells independently measure the vertical resistance against the conical tip and the side friction along the sleeve. Each load cell is a cylinder of uniform cross section instrumented with four strain gages in a full-bridge circuit. The forces are sensed by the load cells and the data are transmitted from the probe assembly via a cable running through the push rods. The analog data are digitized, recorded, and plotted by computer in the penetrometer truck. A set of data is normally recorded each second, for a minimum resolution of about one data point every 0.8 inch of cone advance. The depth of penetration is measured using a string

potentiometer mounted on the push frame.

Electronic data acquisition equipment for the cone penetrometer consists of a computer with a graphics monitor and eight signal conditioners. Analog signals are transmitted from the probe to the signal conditioners where the CPT data are amplified and filtered at 1 Hz. Once amplified, the analog signals are transmitted to a high-speed analog-to-digital converter board, where the signals are digitized, usually at the rate of one sample per second for the penetration data. The digital data are then read into memory and written to the internal hard disk for future processing. Upon completion of the test, the penetration data are plotted. The digital data are brought to ARA's New England Division in South Royalton, Vermont, for analysis and preparation of report plots.

Saturation of the Piezo-Cone

Penetration pore pressure is measured with a pressure transducer located behind the tip in the lower end of the probe. Water pressures in the soil are sensed through a 250 micro-inch porous polyethylene filter that is 0.25-inch high and 0.202-inch thick. The pressure transducer is connected to the porous filter through a fluid-filled pressure port as shown in Figure 2.

In order for the pressure transducer to respond rapidly and correctly to changing pore pressures during the penetration, the filter and pressure port must be saturated with silicone oil upon assembly of the probe. A vacuum pump is used to de-air the silicone oil before use and also to saturate the porous filters with oil. The probe is assembled with the pressure transducer facing upwards and the cavity above the pressure transducer is filled with de-aired oil. A previously saturated filter is then placed on a tip and oil is poured over the threads. When the cone tip is screwed into place, excess oil is ejected through the pressure port and filter, thereby forcing out any trapped air. The high viscosity of the silicone oil, coupled with the small pore space in the filter, prevents the loss of saturation as the cone is pushed through dry soils. Saturation of the cone is verified with a calibration check at the completion of the penetration. Extensive field experience has proven the reliability of this technique.

Field Calibrations

Many factors can effectively change the calibration factors used to convert the raw instrument readouts, measured in volts, to units of force or pressure. As a quality control measure, as well as a check for instrument damage, the load cells and the pressure transducer are routinely calibrated in the field. Calibrations are performed at the start of each day when the probe is ready to insert into the ground so that any factor affecting any component of the instrumentation system will be included and detected during the calibration.

The tip and sleeve load cells are calibrated with the conical tip and friction sleeve in place on the probe. For each calibration, the probe is placed in the push frame and loaded onto a precision reference load cell. The reference load cell is periodically calibrated in ARA's laboratory against instruments traceable to NIST standards. To calibrate the pore pressure transducer, the saturated probe is inserted into a pressure chamber with air pressure supplied by the compressor on the truck. The reference transducer in the pressure chamber is also periodically calibrated against an NIST-traceable instrument in ARA's laboratory. Additionally, the linear displacement transducer used to measure the depth of penetration is periodically checked against a tape measure. All records of device and load cell calibrations are maintained at ARA's New England Division.

Each instrument is calibrated using a specially developed computer code that displays the output from the reference device and the probe instrument in graphical form. During the calibration procedure, the operator checks for linearity and repeatability in the instrument output. At the completion of each calibration, this code computes the calibration factors using a linear regression algorithm. At a minimum, each probe instrument is calibrated at the beginning of each day of field-testing. Furthermore, the pressure transducer is recalibrated each time the porous filter is changed and the cone re-saturated. Calibrations are also performed to verify the operation of any instrument if any damage is suspected.

Penetration Data Format

Figure 3 presents a typical CPT profile from the A.W. Vogtle Nuclear Plant site investigation. This plot presents friction sleeve stress, tip stress, friction ratio, and penetration pore pressure. Additionally, presented on the second page of the plot profile is probe inclination, soil behavior type and stratigraphy based on corrected friction ratio. As shown in Figure 2, the piezo-cone probe senses the pore pressure immediately behind the tip. Currently, there is no accepted standard for the location of the pore pressure sensing element. ARA chose to locate this sensing element behind the tip to protect the filter from the direct thrust of the penetrometer and so that the measured pore pressure can be used to correct the tip resistance data as recommended in Reference 2. The magnitude of the penetration pore pressure is a function of the soil compressibility and, most importantly, permeability. In freely draining soil layers, the measured pore pressures will be very close to the hydrostatic pressure computed from the elevation of the water table. When low permeability soil layers are encountered, excess pore pressures generated by the penetration process cannot dissipate rapidly and this results in measured pore pressures that are significantly higher than the hydrostatic pressures. Whenever the penetrometer is stopped to add another section of push pipe or when a pore pressure dissipation test is run, the excess pore pressure may begin to dissipate. When the penetration is resumed, the pore pressure quickly rises to the level measured before the penetrometer was stopped. This process causes some of the spikes that appear in the penetration pore pressure data.

Pore Pressure Correction of Tip Stress

Cone penetrometers, by necessity, must have a joint between the tip and sleeve. Pore pressure acting behind the tip decreases the total tip resistance that would be measured if the penetrometer was without joints. The influence of pore pressure in these joints is compensated for by using the net area concept (Ref. 2).

The corrected tip resistance is given by:

$$q_t = q_c + u\,[1 - A_n / A_T] \qquad \textbf{(2.1)}$$

where:

q_t = corrected tip resistance (psi)
q_c = measured tip resistance (psi)
u = penetration pore pressure measured behind the tip (psi)

A_n = net area behind the tip not subjected to the pore pressure (1.897 in^2)
A_T = projected area of the tip (2.351 in^2).

Hence, for the ARA cone design, the tip resistance is corrected as:

$$q_t = q_c + u(0.1931) \qquad \textbf{(2.2)}$$

Laboratory calibrations have verified Equation 2.2 for ARA's piezo-cone design.

A joint also exists behind the top of the friction sleeve (see Figure 2). However, since the sleeve is designed to have the same cross sectional area on both ends, the pore pressures acting on the sleeve cancel out. Laboratory tests have verified that the sleeve is not subjected to unequal end area effects. Thus, no correction for pore pressure is needed for the friction sleeve data.

The net effect of applying the pore pressure correction is to increase the tip resistance. Generally, this correction is only significant when the measured tip resistance is very low.

The following figure graphically displays versus elevation a typical CPT sounding from the Alvin W. Vogtle Nuclear Plant limited investigation. Sleeve friction, (Sleeve Stress) is presented inversely of corrected tip resistance (Tip Stress COR) column. The friction ratio is defined as the ratio between sleeve friction and cone resistance (Ratio COR). The measured insitu pore pressures are displayed adjacently. The continuation of the Figure 3 depicts the CPT probes north-south inclination (X inclination) and east-west (Y inclination) as it is advanced. The following columns are Soil Behavior Type (SBT) based on Normalized Friction Ratio Classification Chart (Class. Fr, (Robertson 1990)) and the correlating stratigraphy are depicted.

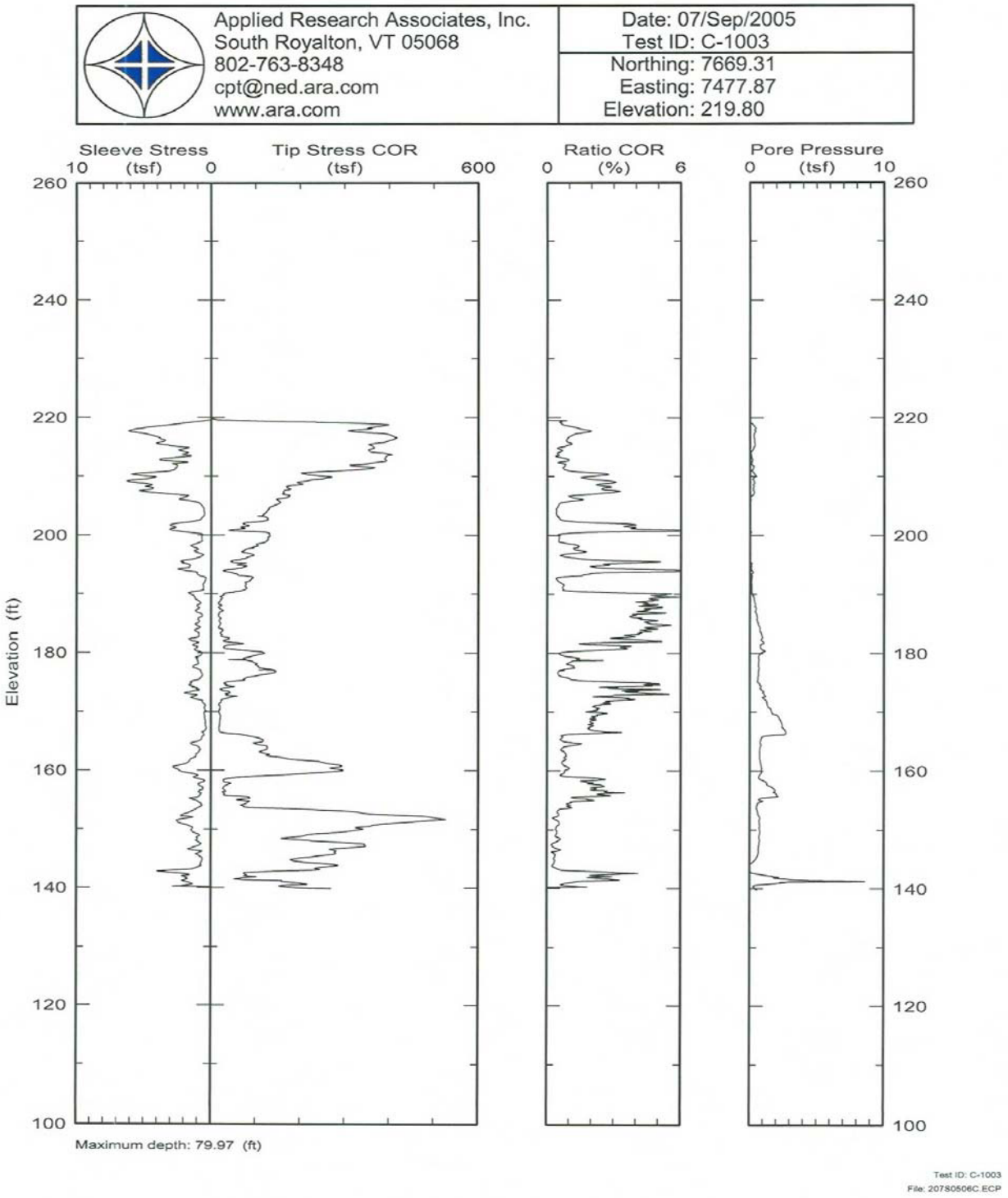

Figure 3. Typical CPT Profile from the A. W. Vogtle Site

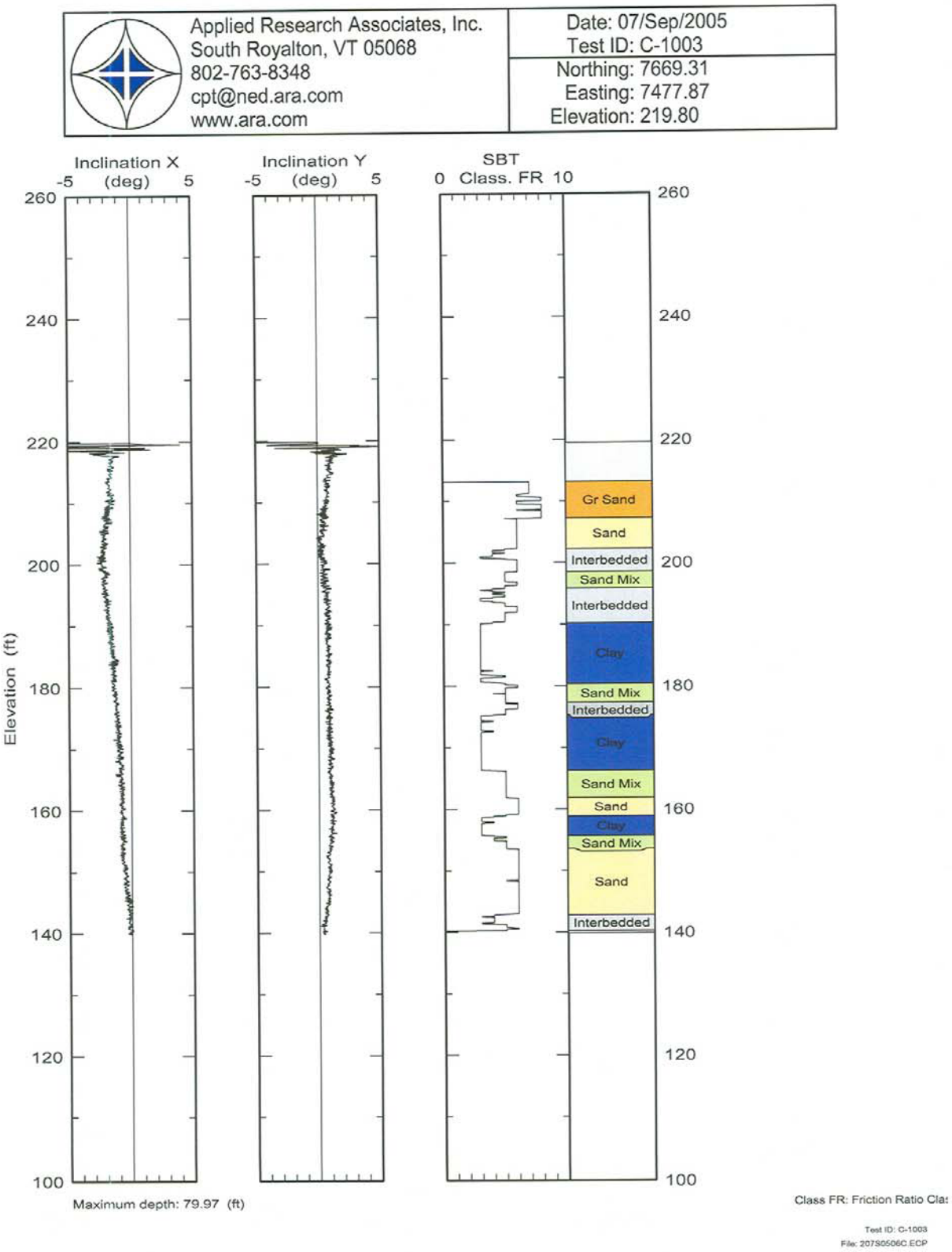

Figure 3. Typical CPT Profile from the A. W. Vogtle Site (concluded)

Numerical Editing of the Penetration Data

Any time that the cone penetrometer is stopped or pulled back during a test, misleading data can result. For instance, when the probe is stopped to add the next push rod section or when a pore pressure dissipation test is run, the excess pore pressures will dissipate towards the hydrostatic pore pressure. When the penetration is resumed, the pore pressure rises very quickly to the pressures experienced prior to the pause in the test. In addition, to penetrate stronger layers, the probe is sometimes pulled back and cycled up and down at intervals in deep holes to reduce soil friction on the push tubes. This results in erroneous tip stress data when the cone is advanced in the previously penetrated hole.

To eliminate this misleading data from the penetration profile, the data are numerically edited before plotting or use in further analysis. Each time the penetrometer stops or backs up, as apparent from the depth data, the penetration data are not plotted. Plotting of successive data is resumed only after the tip is fully re-engaged in the soil by one tip length of new penetration. In addition, each time the probe stops, the previous 0.5 inch of penetration data is filtered out. This filter is required to remove data that were recorded while the operator was in the process of stopping the probe. This algorithm also eliminates any data acquired at the ground surface before the tip has been completely inserted into the ground. The sleeve data are similarly treated and this results in the first data point not occurring at the ground surface. These procedures ensure that all of the penetration data that are plotted and used for analysis were acquired with the probe advancing fully into undisturbed soil. All raw measurements are subjected to this procedure. An undefined value is represented by (-99) in data columns.

SEISMIC CONE PENETROMETER EQUIPMENT AND TEST

The seismic cone penetrometer test was developed in the early 1980s and is gaining rapid acceptance in the geotechnical community. As with the conventional electric cone penetrometer test, initial development work was concentrated in weak materials. ARA's seismic cone equipment and field procedures were developed specifically for both weak soils and strong, dry, cemented soils. The seismic cone penetrometer test utilizes three geophones (Geospace Model GS-14-L9 velocity gages) mounted inside the penetrometer probe to detect the arrival at depth of seismic waves generated on the surface. Two horizontal transducers monitor shear wave (S-

wave) arrivals from which the shear wave velocity can be determined. A third geophone, mounted vertically, is used to measure the compression wave (P-wave) arrivals and to subsequently derive the compression wave velocity.

In the Seismic Cone Penetrometer Test (S-CPT), the cone is stopped at prescribed depth intervals, and S- and P-waves are generated on the ground surface near the push tubes. Both average downhole velocities and velocities between the depth intervals can be computed from the arrival time or time of peak data. High-energy shear waves are generated by an automated shear wave source in the front pad of the CPT rig (Figure 4). This system consists of a double-acting hydraulic cylinder used to

Figure 4. High Energy Shear Wave Hammer

horizontally move a large hammer. The hammer impacts either end of the front lifting pad of the penetrometer truck and induces a horizontal shear wave. By striking the pad on either end, polarized shear waves can be generated. This pad is 1 ft wide and about 8 ft long and oriented parallel to the axles of the truck. The point of impact of the shear hammers is located 36 inches

horizontally from the penetrometer push rod. Typical seismic traces for this investigation are shown in Figure 5, where time of first peak shear wave motions are indicated.

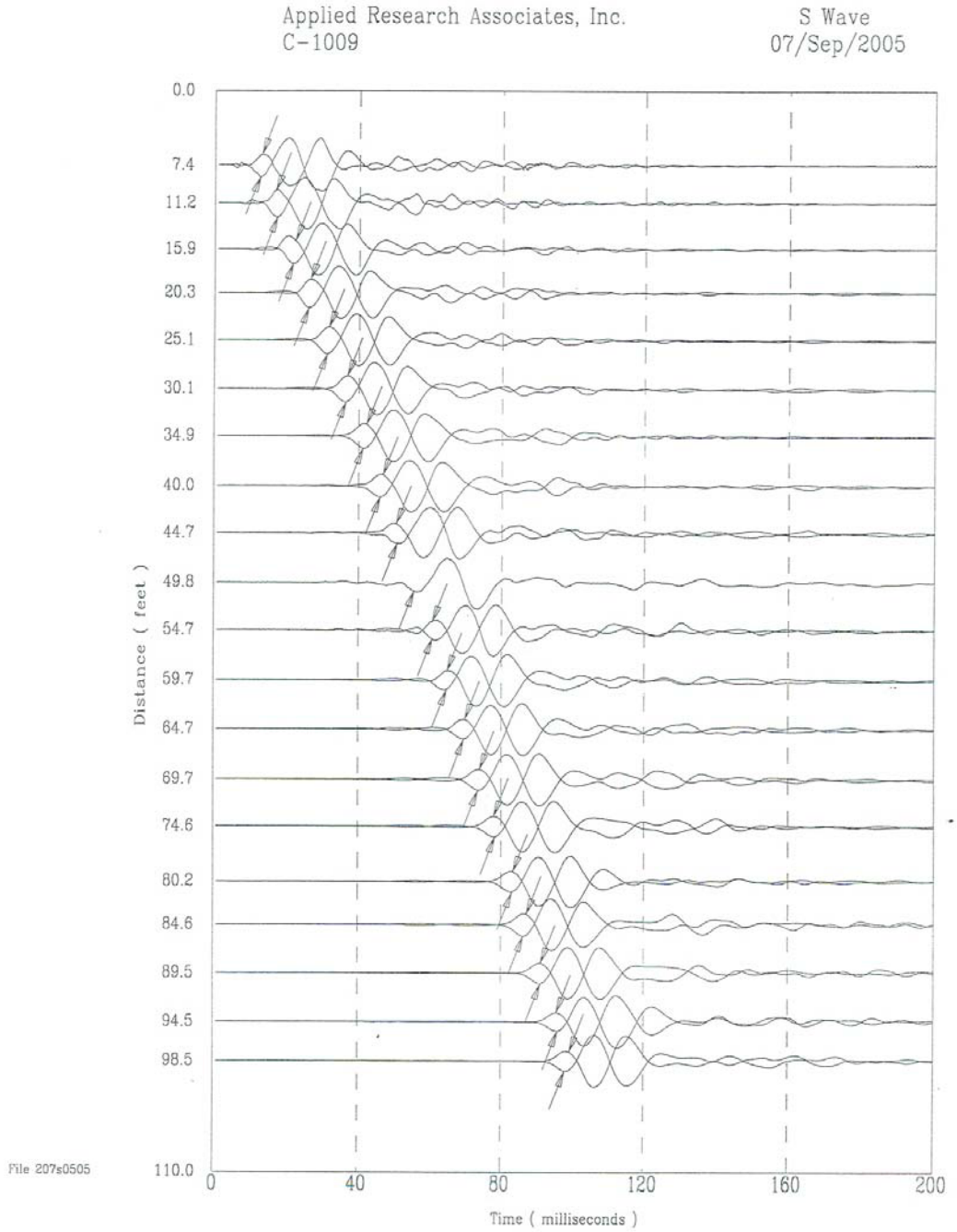

Figure 5. Typical Shear Wave Traces

The first major shear wave is used to select the shear time of peak as denoted by the arrows. The use of polarized shear waves clarifies this time of peak. Compression wave traces and/or analysis were not part of this investigation.

As discussed in Section 2, the seismic cone penetrometer utilizes two shear wave geophones and one compression wave geophone. When a seismic shear wave is generated at the surface it is recorded by both horizontal geophones. The geophone positioned in the most optimal orientation to record the cleanest seismic wave is selected by the operator and written to the seismic data file. Often times, no one trace stands out as being optimal, an occurrence that may be caused by geologic conditions or testing conditions (i.e., geophone orientation). When this occurs, the operator selects the seismic time history he feels is most optimal.

Prior to reporting, all seismic time histories are plotted, as they appear in Appendix B, and reviewed. When anomalous seismic waves are identified, and it is obvious the trace is not consistent with other traces from the same sounding, it is removed from the plot so as not to affect data analysis. Consequently, some seismic wave time history plots will have gaps where seismic waves were removed.

PORE PRESSURE DISSIPATION RESULTS

At selected depths, penetration of the penetrometer is stopped and the dissipation of excess pore pressure is observed. Pore pressures, as sensed by the pressure transducer, are recorded at regular time intervals (typically 1 second, but the sample rate can be adjusted for local site conditions) and plotted on the graphics monitor. Dissipation tests are usually run until at least 50 percent of the excess pore pressure has dissipated. This length of time, $t_{50,}$ can be used to estimate the lateral coefficient of consolidation and permeability in the given soil layer. Depending on site conditions, t_{50} can range from a few minutes to several hours. These tests are sometimes run to complete dissipation to measure the hydrostatic pore pressure.

During the dissipation test, the penetrometer is stationary with no downward force applied by the penetrometer truck.

A classic dissipation profile in a clay soil is shown in Figure 6. Total pore pressure is

presented on a semi-log plot versus time, and the value of P_n at the top of Figure 6 is the average of the last ten pore pressure measurements. The classic dissipation curve will show a dissipation rate that decreases with time. If the dissipation test is allowed to run long enough, P_n will be equal to the static pore pressure. This value can also be determined from the water table elevation at some sites. Knowing the static pore pressure, u_o, as well as the peak pressure observed during the test, u_p, the pore pressure at 50 percent of dissipation, u_{50}, can be determined. Time to 50% dissipation, t_{50}, can then be read directly from the dissipation profile.

Some of the penetration profiles from the work at the A. W Vogtle Nuclear Plant site exhibit the classic shape as depicted in Figure 6. At some locations, however, the dissipations start with a vacuum condition due to dilatation occurring during the penetration. From this condition the pore pressures increase as presented in Figure 7. This curve shape does not permit the traditional dissipation analysis algorithms used to determine hydraulic conductivity or depth of groundwater surface. Therefore, hydraulic conductivities for these dissipation tests are not included in the analysis table presented in Appendix C.

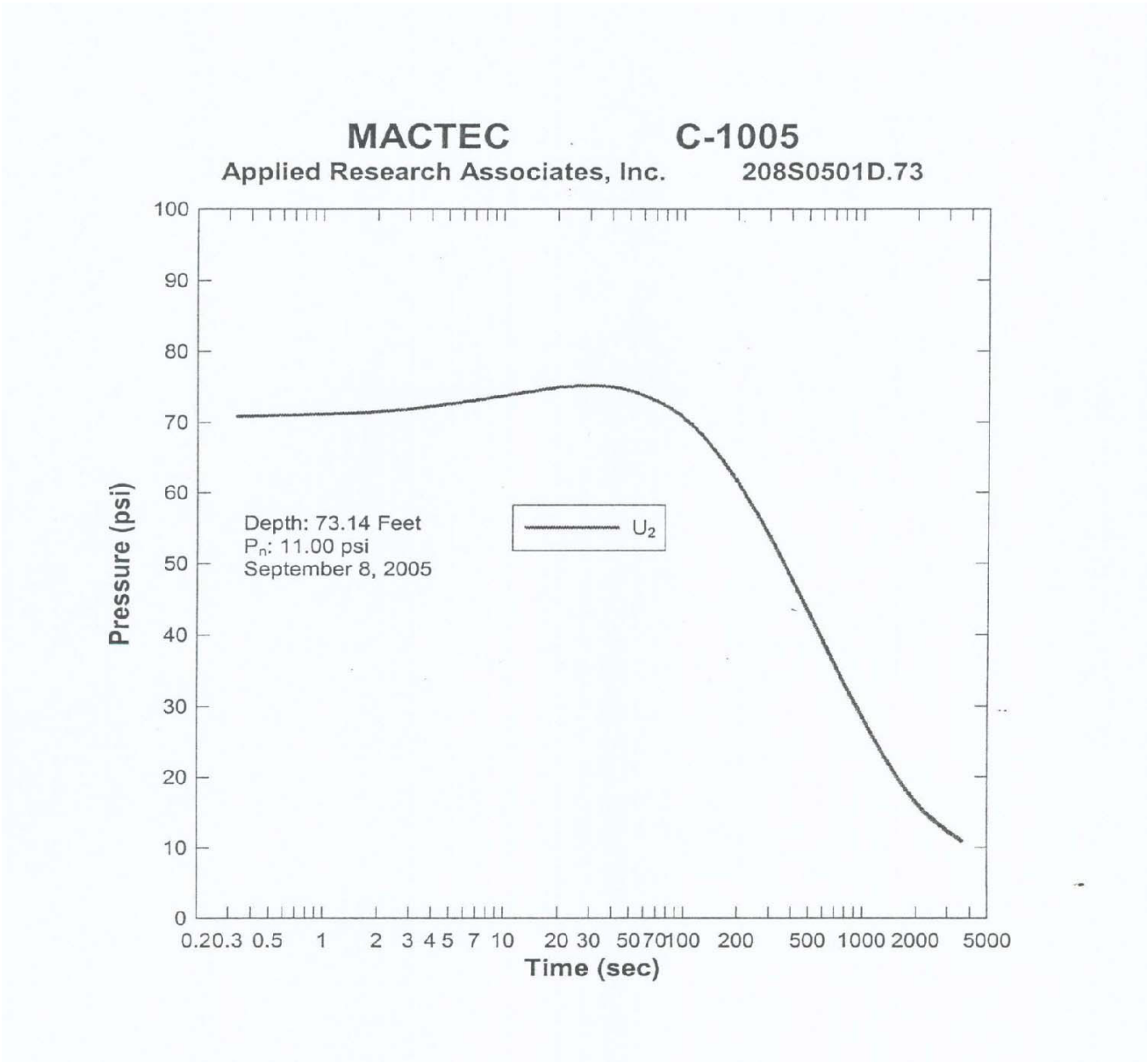

Figure 6. Classic Dissipation Profile from the A. W. Vogtle Plant Site

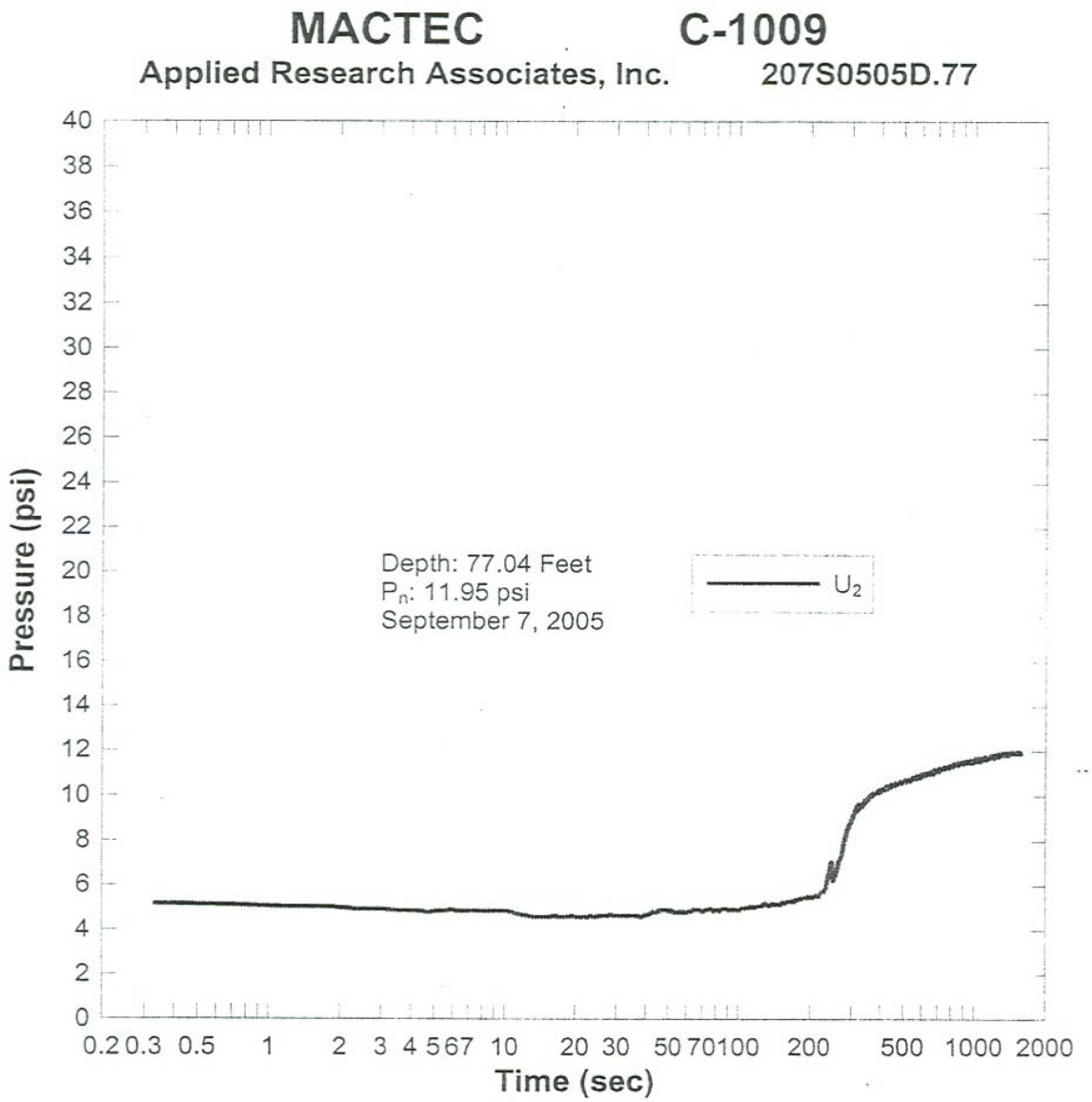

Figure 7. Dissipation Test Showing a Dilating Condition

SECTION 3

DATA ANALYSIS TECHNIQUES

OVERVIEW

Presented in this section is a description of analysis techniques used to determine engineering parameters. The methods used to determine the soil type information from the CPT are also discussed.

LOCATION OF THE SITE WATER TABLE

Generally, the static water table at a given site can be identified from the penetration pore pressures, since it will be equal to the hydrostatic pore pressure in freely draining soil layers. When no such layers are present, pore pressure dissipation tests can be performed to determine hydrostatic pressures. This information is used in the soil classification routines for the calculation of effective stress of the soil materials. Bechtel Corporation personnel supplied ARA with values for saturated unit weights for soil density ((pcf) per cubic foot)). The design dry density for the upper sands is 94 pcf, and the moisture content is 25%. This results in a saturated unit weight of 117.5 pcf. The values of the marl are 88 pcf and 35%, resulting in a saturated unit weight of 118.8 pcf.

SOIL BEHAVIOR TYPE

The tip resistance, friction ratio, and pore pressure values from CPT profiles can be used to determine a soil stratigraphy profile. To estimate soil behavior type, empirical charts were developed by Robertson and Campanella (Ref. 2) showing the relationship between tip resistance (q_t) versus friction ratio (f_s) and tip resistance (q_t) versus pore pressure ratio (B_q) Figure 8. The charts were later refined by Robertson (Ref. 5) to utilize normalized tip resistance (Q_t) versus normalized friction ratio (F_r) and normalized tip stress (Q_t) versus pore pressure ratio (B_q) Figure 9.

CPT Soil Behavior Type Legend
(Robertson et al. 1986)

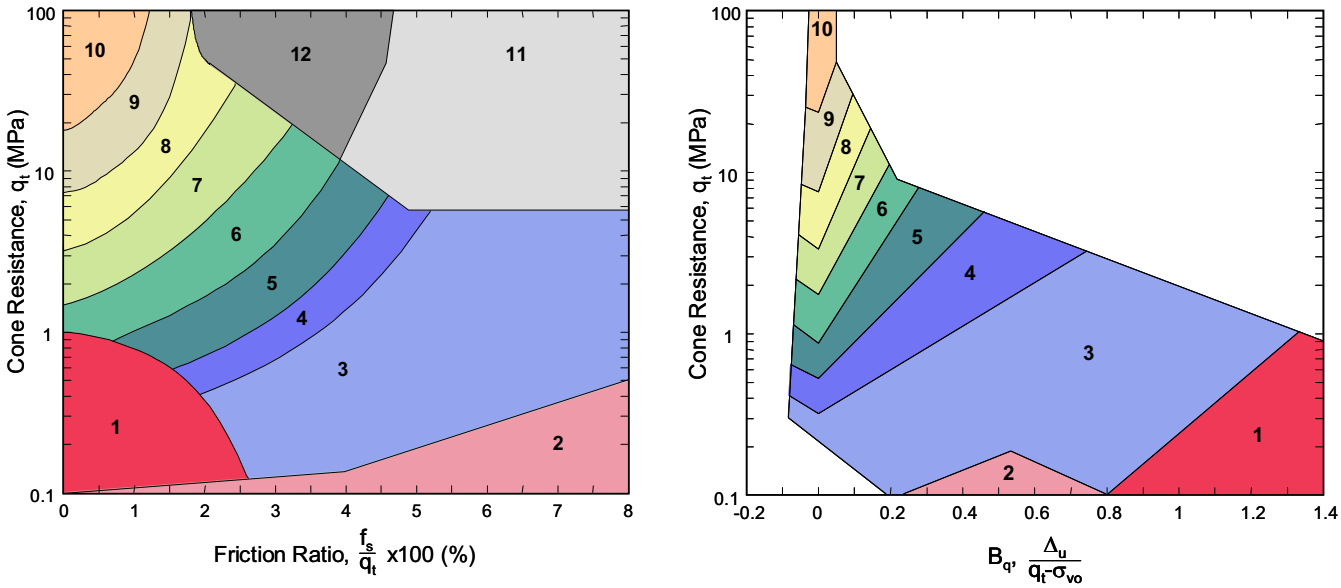

Zone	Soil Behavior Type
1	Sensitive, Fine Grained
2	Organic Material
3	Clay
4	Silty Clay to Clay
5	Clayey Silt to Silty Clay
6	Sandy Silt to Clayey Silt
7	Silty Sand to Sandy Silt
8	Sand to Silty Sand
9	Sand
10	Gravelly Sand to Sand
11	Very Stiff Fine Grained*
12	Sand to Clayey Sand*

*Overconsolidated or Cemented

Figure 8. 1986 Soil Behavior Charts

CPT Soil Behavior Type Legend
(Robertson et al. 1990)

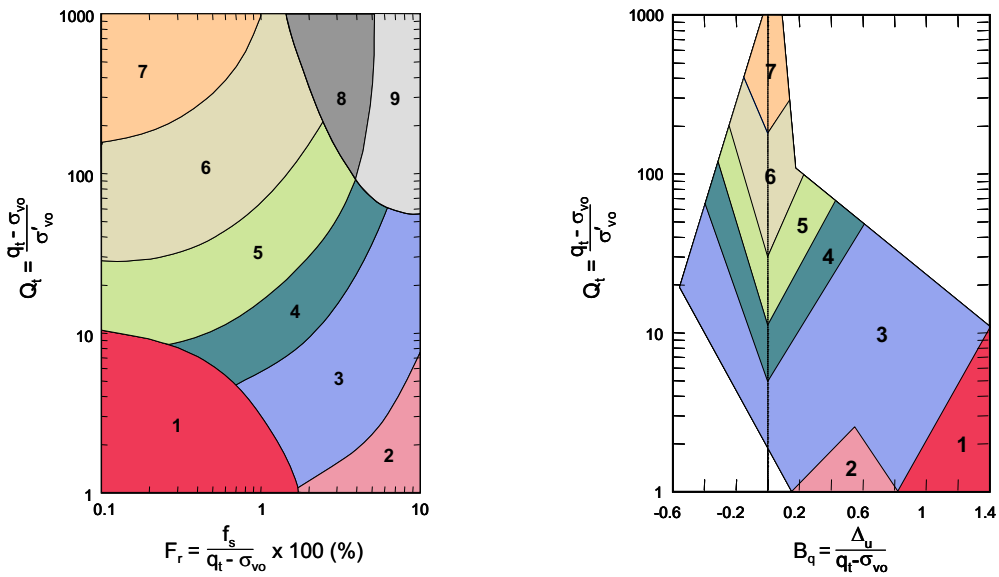

Zone	Soil Behavior Type
1	Sensitive, Fine Grained
2	Organic Soils-Peats
3	Clays; Clay to Silty Clay
4	Silt Mixtures; Clayey Silt to Silty Clay
5	Sand Mixtures; Silty Sand to Sandy Silt
6	Sands; Clean Sands to Silty Sands
7	Gravelly Sand to Sand
8	Very Stiff Sand to Clayey Sand*
9	Very Stiff Fine Grained*

*Overconsolidated or Cemented

Figure 9. 1990 Soil Behavior Charts

The normalized tip resistance is defined as:

$$Q_t = \frac{q_t - \sigma_{vo}}{\sigma'_{vo}} \quad \textbf{(3.1)}$$

The normalized friction ratio is defined as:

$$F_r = \frac{f_s}{q_t - \sigma_{vo}} x\, 100 \quad \textbf{(3.2)}$$

where: f_s = sleeve friction

q_t = corrected tip resistance

σ_{vo} = total overburden stress

σ'_{vo} = effective overburden stress

The intersection point of the Q_t and F_r values normally falls in a classification zone**.** Each zone corresponds to a Soil Behavior Type (SBT), which is identified by the descriptions shown in Figures 8 and 9. The graphical representation of zone numbers and the corresponding soil behavior types are plotted numerically and are identified in Figures 8 and 9. At some depths, the CPT data will fall outside of the range of the chart. When this occurs, the SBT is undefined and a break is seen in the SBT profile. This occasionally occurs at the top of a penetration where the effective vertical stress is very small, which results in normalized cone resistances greater than 1000.

The classification profiles are very detailed due to the high rate of data acquisition every 2 cm (0.8 in) for CPT profiles. Frequently significant variability in soil types over small changes in elevation can be observed in the profiles. To provide a simplified soil stratigraphy for comparison to standard boring logs, a layering and generalized classification system was implemented. Layer thicknesses are determined based on the variability of the SBT profile. The layering sequence is begun at the ground surface and layer thicknesses are determined by changes in the soil behavior type. The friction ratio is used to identify potential changes in soil layering. The SBT modal value for each potential layer is compared to the previous layer. Whenever the modal value changes, a new layer is started. The SBT for the layer is the mode of

the SBT values of the complete layer.

Although not presented on the CPT profiles included in Appendix A, the electronic text and/or numerical files contain classification values based on the pore pressure ratio. This method uses the normalized corrected tip stress in bars and the pore pressure ratio B_q. (Ref. 2).

$$B_q = \frac{u_{meas} - u_o}{q_t - \sigma_{vo}} \tag{3.3}$$

where: u_{meas} = measured penetration pore pressure

u_o = static pore pressure, determined from the water table elevation

q_t = corrected tip resistance

σ_{vo} = total overburden stress

The intersection point of the Q_t and B_q values normally fall in a SBT zone. The SBT zone number corresponds to a soil behavior type as shown in Figure 9. when this occurs, the SBT is undefined and a break is seen in the SBT profile. Close analysis of this chart indicates that as the zone numbers vary, so does the soil grain size. What is missing in these charts are mixed soils, such as sandy clays or clayey sands. This type of mixed soil represents special cases, which may be misclassified as silts.

STANDARD PENETRATION TEST

Data correlations between the cone penetrometer tip stress measurements, q_c, and standard penetration test blow count, (N), have been made by a number of researchers. Robertson and Campanella (Ref. 2) summarized many of these studies and presented a relationship between q_c, N, and soil type. The blow count corresponding to 60 percent of the energy transferred to the sampler can be estimated from a ratio based on the soil behavior type number applicable for the soil behavior type. Robertson and Campanella used the 1986 soil behavior chart (Figure 8) when determining these ratios. These SBT values are included in the electronic files. The ratios used to compute the N value were as follows:

Zone	Soil Behavior Type *(Robertson et al. 1986)*	$(q_c/p_a)/N$ Ratio
1	Sensitive fine grained	2
2	Organic material	1
3	Clay	1
4	Silty clay to clay	1.5
5	Clayey silt to silty clay	2
6	Sandy silt to clayey silt	2.5
7	Silty sand to sandy silt	3
8	Sand to silty sand	4
9	Sand	5
10	Gravelly sand to sand	6
11	Veru stiff fine grained	1
12	Sand to clayey sand	2

The correlation between q_c and N_{60} should be considered an estimate only, because rapid fluctuations in tip stress can result in large variations in the calculated blow count. Also, the techniques used in performing the SPT test in any geographical area need to be considered. If the energy level normally transferred to the sampler is not nearly 60 percent of the theoretical maximum, the local correlation will be either higher or lower than the data presented in this report.

FRICTION ANGLE (ϕ')

The effective stress friction angle in granular soils can be estimated from the tip resistance data using an empirical correlation derived between laboratory triaxial tests on sands and penetration tests performed through sands in large calibration chambers. The triaxial tests were performed at confining stresses equal to the horizontal effective stress in the calibration chamber.

The tip stress data were then correlated with peak effective friction angle as (Ref. 2):

$$\tan \phi' = 0.38 \left[\log_{10} \frac{q_c}{\sigma'_{vo}} \right] + 0.1 \qquad \textbf{(3.4)}$$

where: ϕ' = effective internal friction angle (deg)
q_c = total measured tip stress
σ'_{vo} = effective overburden stress

UNDRAINED SHEAR STRENGTH (S_u)

Estimates of the undrained shear strength in fine grained saturated soils can be made using the empirical relationship (Ref.2):

$$S_u = \frac{q_c - \sigma_{vo}}{N_k} \qquad \textbf{(3.5)}$$

where: S_u = undrained shear strength
q_c = total measured tip stress
σ_{vo} = total overburden stress
N_k = cone factor, assumed to be 15 for A. W. Vogtle Nuclear Plant site data

The cone factor, N_k falls between 11 and 19 with an average of 15. In the absence of field vane shear data, as is the case for the A. W. Vogtle Nuclear Plant investigation, Robertson and Campanella (Ref. 2) recommend assuming N_k to be 15. If N_k is 19 for a given material, using N_k of 15 overestimates the undrained shear strength by 27%; and if N_k is 11, the strength is underestimated by 27%.

PRESENTATION OF ϕ AND S_u VALUES

Conventional engineering considers only friction angles (ϕ') to be appropriate in granular soil deposits such as sands. Similarly, undrained shear strength (S_u) values are used in saturated, low permeability layers such as clays. The distinction between which parameter is appropriate at

a given depth is based on the soil behavior type. When the average SBT number is greater than 4, the granular material is assumed to dominate and the friction angle is plotted. Conversely, if the SBT number is less than or equal to 5, the fine-grained material is assumed to dominate and the undrained shear strength is plotted. These SBT numbers are found in the electronic files supplied with this report. Both values are plotted for SBT values of 4 and 5. When the data do not fall within the range of the classification system, neither ϕ' or S_u values are presented.

ESTIMATES OF OVERCONSOLIDATION RATIO (OCR)

A soil is termed normally consolidated if the current stress is the maximum to which the material has ever been subjected. The overconsolidation ratio (OCR) is defined as:

$$\text{OCR} = \frac{(\sigma'_{vo})_{\text{max.past}}}{(\sigma'_{vo})_{\text{present}}} \qquad \textbf{(3.6)}$$

where: $(\sigma'_{vo})_{\text{max.past}}$ = maximum past vertical effective overburden pressure

$(\sigma'_{vo})_{\text{present}}$ = present effective vertical overburden pressure

For a normally consolidated soil, $(\sigma'_{vo})_{\text{max.past}} = (\sigma'_{vo})_{\text{present}}$ and OCR = 1, while an overconsolidated soil has an OCR > 1.

OCR calculations for the A. W. Vogtle Nuclear Plant investigation were reported for all soil behavior types and are based on a publication by Mayne (Ref. 3) where OCR is directly correlated to excess pore pressure measured on the cone tip and only apply to cohesive soils. As determined from a linear regression of published data, this equation is:

$$\text{OCR} = 0.33\left[\frac{u_{\text{meas}} - u_o}{\sigma'_{vo}}\right]^{1.42} \qquad \textbf{(3.7)}$$

COEFFICIENT OF LATERAL CONSOLIDATION *(C_H)*

Horizontal coefficients of consolidation can be calculated from the pore pressure

dissipation tests using a theoretical model developed by Baligh and Levadoux (Ref. 4) and measured dissipation rates. Calculations are performed at 50% of the excess pore pressure dissipation, U_{50}. Using the theoretical curves in Figure 10, C_H is calculated as:

$$C_H = \frac{T_{50} R^2}{t_{50}} \qquad \textbf{(3.8)}$$

where: T_{50} = theoretical time factor at 50% dissipation

R = radius of cone in centimeters, 2.22 cm for the 1.75-inch diameter cone used at the A. W. Vogtle Nuclear Plant site

t_{50} = measured time at 50% dissipation in seconds

Pore pressure measurements are made just behind the tip; hence, curve 3 in Figure 10 is used to determine T_{50} equals 5.5. Estimates of C_H for the applicable dissipation test locations are contained in the summary table in Appendix C.

COEFFICIENT OF LATERAL PERMEABILITY *(K_H)*

The coefficient of lateral permeability is calculated based on the coefficient of lateral consolidation estimated from the pore pressure dissipation test described above and an estimate of the in situ constrained modulus, *M*, obtained from measured tip resistance values and soil classification according to:

$$K_H = \frac{C_H \gamma_w}{M} \qquad \textbf{(3.9)}$$

where: C_H = coefficient of lateral consolidation

γ_w = unit weight of water

M = constrained modulus

The constrained modulus, *M*, can be estimated using the empirical relationship:

$$M = \alpha\, q_c = \frac{1}{m_v} \qquad \textbf{(3.10)}$$

This method is discussed by Robertson and Campanella (Ref. 2).

where: α = empirical factor

q_c = measured tip resistance, not corrected for pore pressure effects

m_V = volumetric compressibility.

The factor α is obtained from (Ref. 2) is based on the uncorrected tip resistance and soil type. Estimates of M and K_H are contained in the summary table in Appendix C. Values for q_c are obtained from the depth interval closest to the depth of dissipation test.

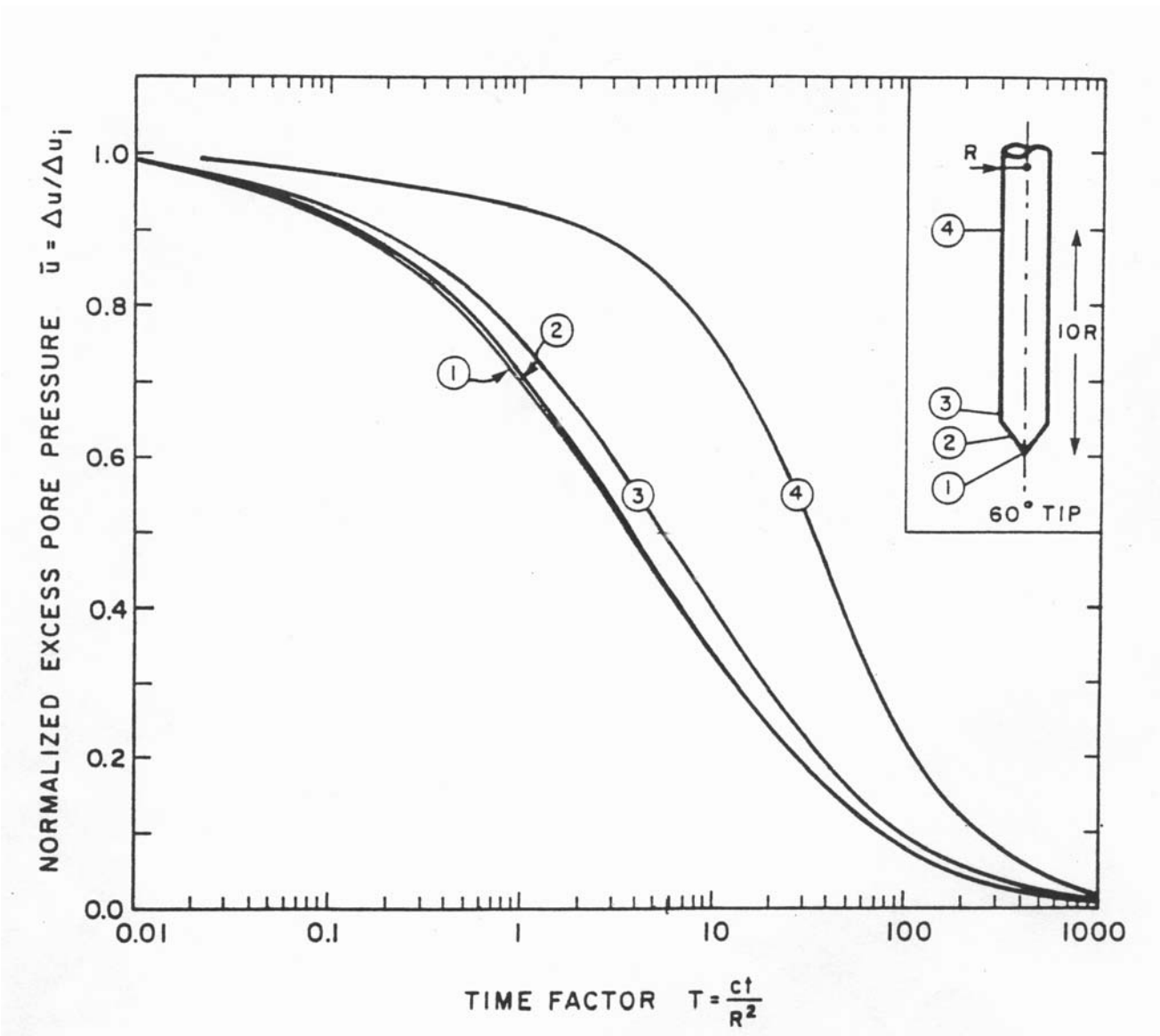

Figure 10. Dissipation Curves for a 60° Cone According to Linear Isotropic Uncoupled Solution (after Baligh and Levadoux, 1980)

$$M = \frac{1}{m_v} = \alpha . q_c$$

$q_c < 7$ bar	$3 < \alpha < 8$	
$7 < q_c < 20$ bar	$2 < \alpha < 5$	Clay of low plasticity (CL)
$q_c > 20$ bar	$1 < \alpha < 2.5$	
$q_c > 20$ bar	$3 < \alpha < 6$	Silts of low plasticity (ML)
$q_c < 20$ bar	$1 < \alpha < 3$	
$q_c < 20$ bar	$2 < \alpha < 6$	Highly plastic silts & clays (MH, CH)
$q_c < 12$ bar	$2 < \alpha < 8$	Organic silts (OL)
$q_c < 7$ bar:		
$50 < w < 100$	$1.5 < \alpha < 4$	Peat and organic clay (P_t, OH)
$100 < w < 200$	$1 < \alpha < 1.5$	
$w > 200$	$0.4 < \alpha < 1$	

Figure 11. Estimation of the Constrained Modulus, M, for Clays (after Robertson and Campanella, 1988)

SECTION 4

LIST OF REFERENCES

1. American Society for Testing and Materials, "Standard Test Method for Performing Electric Friction Cone and Piezo-Cone Penetration Testing of Soil," ASTM Designation: D5778, 1995.

2. Robertson, P. K. and R. G. Campanella, *Guidelines for Using the CPT, CPTU and Marchetti DMT for Geotechnical Design*, Vol. II, University of British Columbia, Vancouver, BC, Canada, March 1988.

3. Mayne, P.W., "CPT Indexing of In Situ OCR in Clays," included in *Use of In Situ Test in Geotechnical Engineering*, S. P. Clemence, ed., Geotechnical Special Publications No. 6, proceedings of In Situ '86 Conference, sponsored by Geotechnical Engineering Division of the American Society of Civil Engineers, Blacksburg, VA, June 1986.

4. Baligh, M. M. and J. N. Levadoux, Pore Pressure Dissipation After Cone Penetration, Massachusetts Institute of Technology, Cambridge, MA, April 1980.

5. Robertson, P.K, "Soil classification using the cone penetration test," Canadian Geotechnical Journal, 27(1).

APPENDIX A

PIEZO-CONE PROFILES

Applied Research Associates, Inc.
South Royalton, VT 05068
802-763-8348
cpt@ned.ara.com
www.ara.com

Date: 02/Sep/2005
Test ID: C-1001
Northing: 8028.12
Easting: 6255.96
Elevation: 248.57

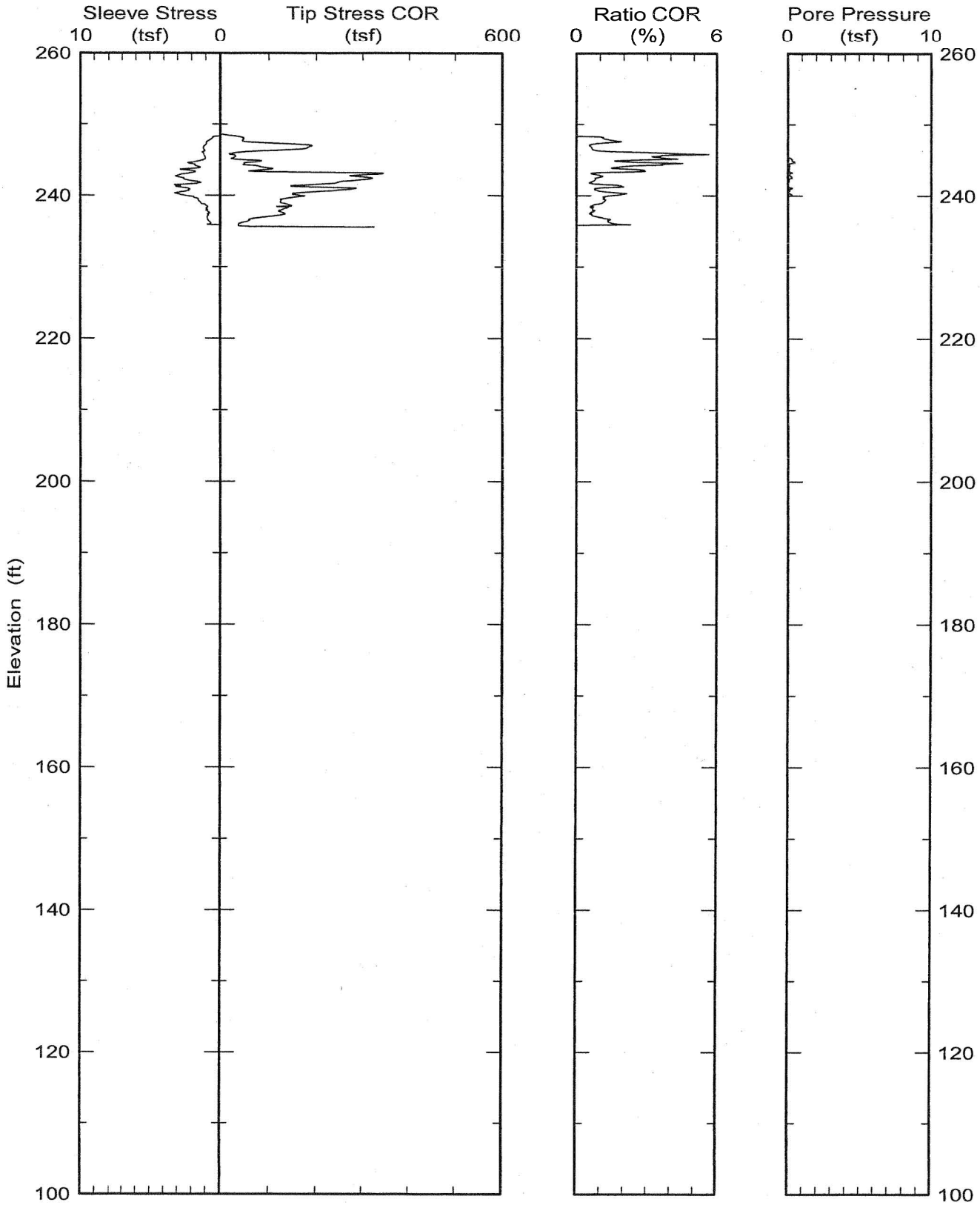

Maximum depth: 13.02 (ft)

Applied Research Associates, Inc.
South Royalton, VT 05068
802-763-8348
cpt@ned.ara.com
www.ara.com

Date: 02/Sep/2005
Test ID: C-1001
Northing: 8028.12
Easting: 6255.96
Elevation: 248.57

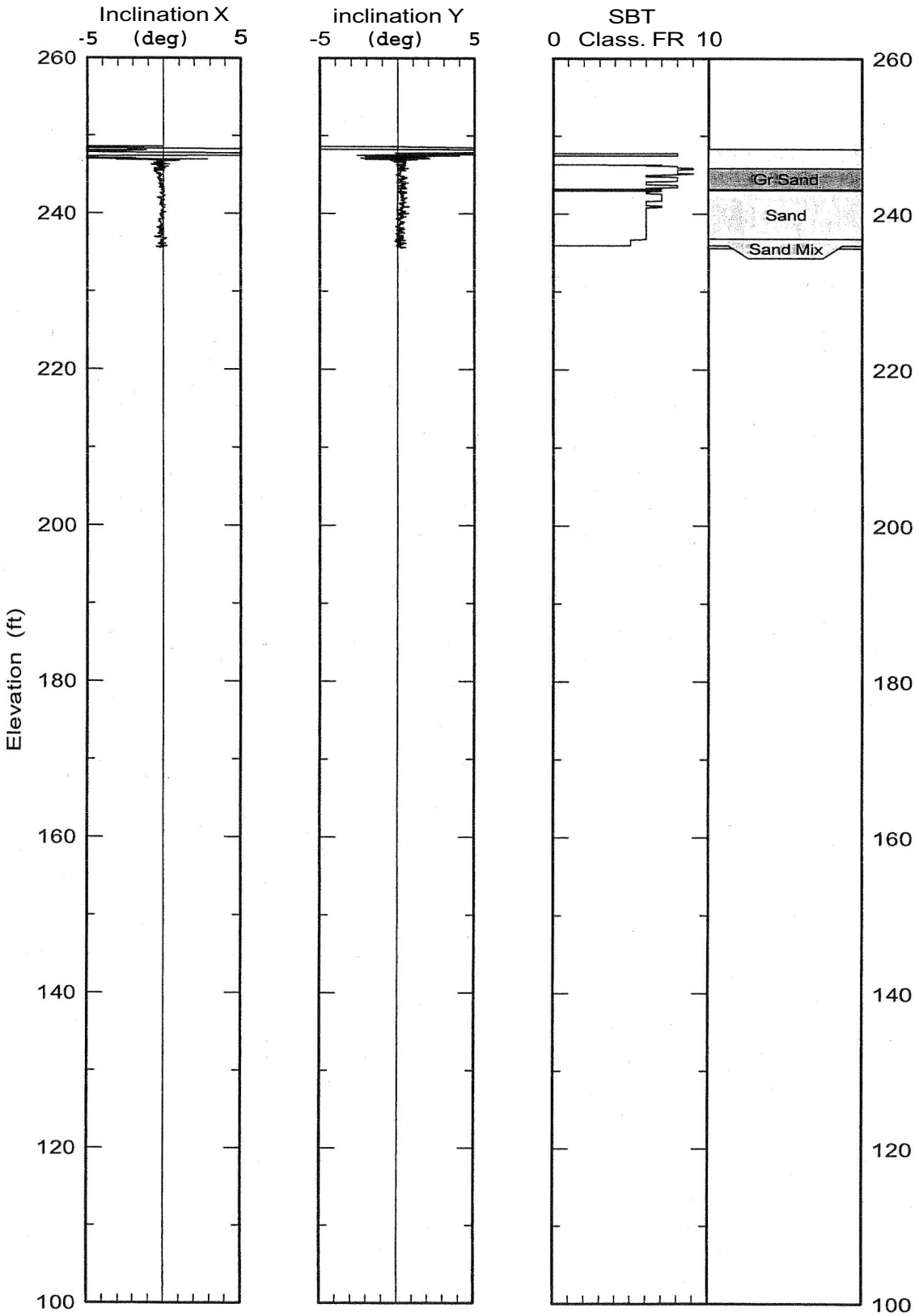

Maximum depth: 13.02 (ft)

Class FR: Friction Ratio Clas

Applied Research Associates, Inc.
South Royalton, VT 05068
802-763-8348
cpt@ned.ara.com
www.ara.com

Date: 02/Sep/2005
Test ID: C-1001A
Northing: 8028.12
Easting: 6255.96
Elevation: 248.57

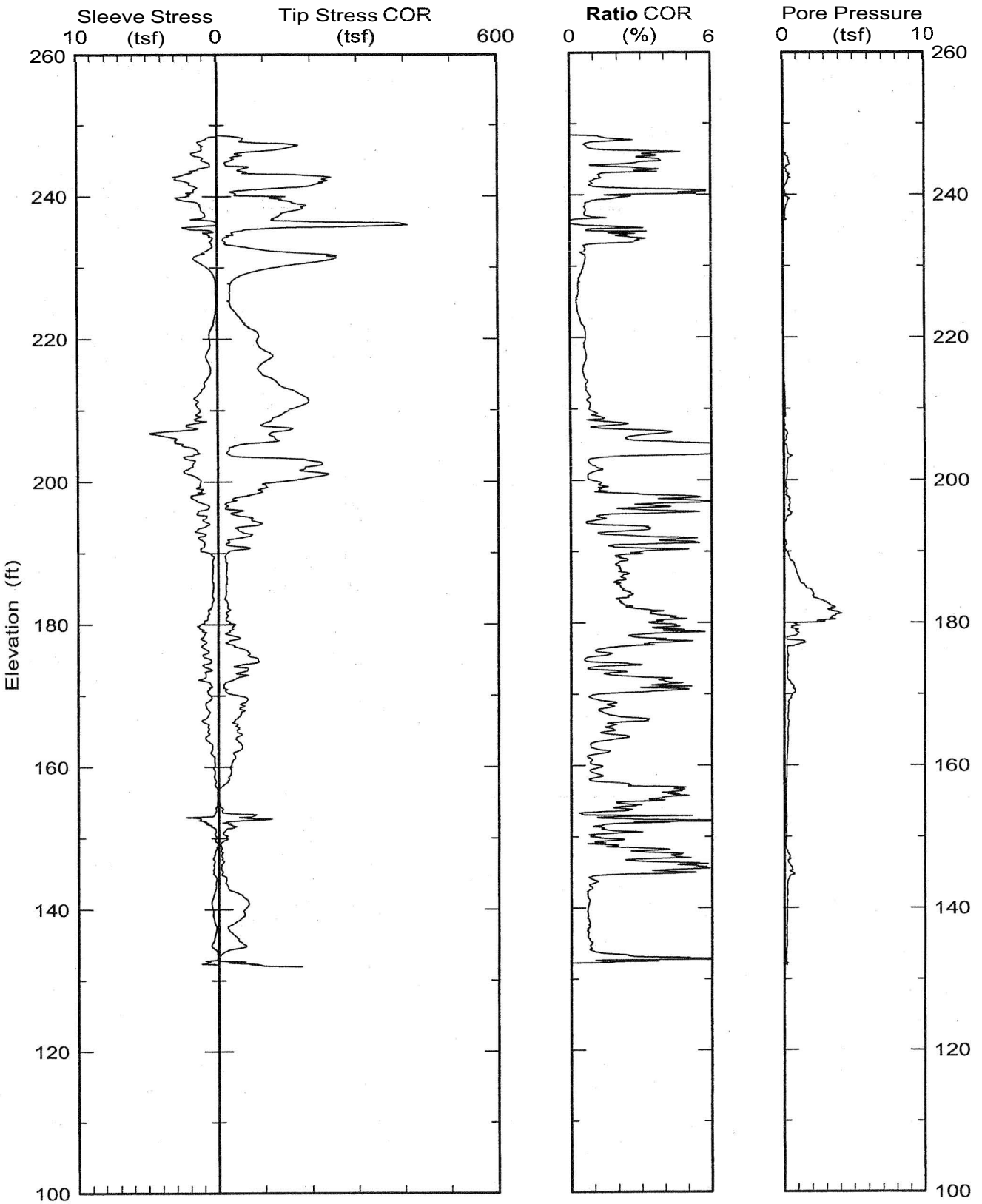

Maximum depth: 116.65 (ft)

Applied Research Associates, Inc.
South Royalton, VT 05068
802-763-8348
cpt@ned.ara.com
www.ara.com

Date: 02/Sep/2005
Test ID: C-1001A
Northing: 8028.12
Easting: 6255.96
Elevation: 248.57

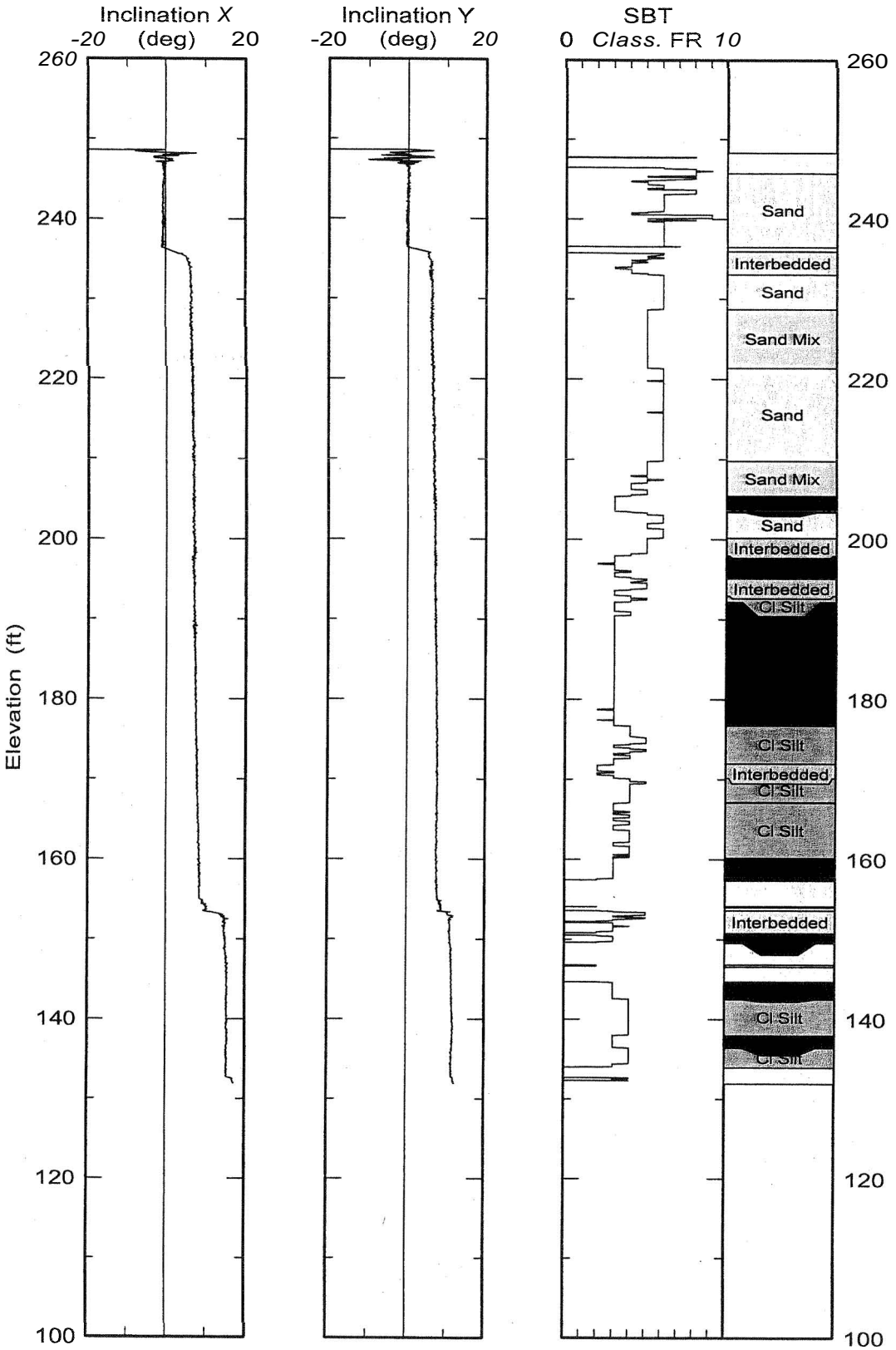

Maximum depth: 116.65 (ft)

Class FR: Friction Ratio Clas

Test ID: C-1001A

Applied Research Associates, Inc. South Royalton, VT 05068 802-763-8348 cpt@ned.ara.com www.ara.com	Date: 06/Sep/2005 Test ID: C-1002 Northing: 7667.64 Easting: 6574.64 Elevation: 222.13

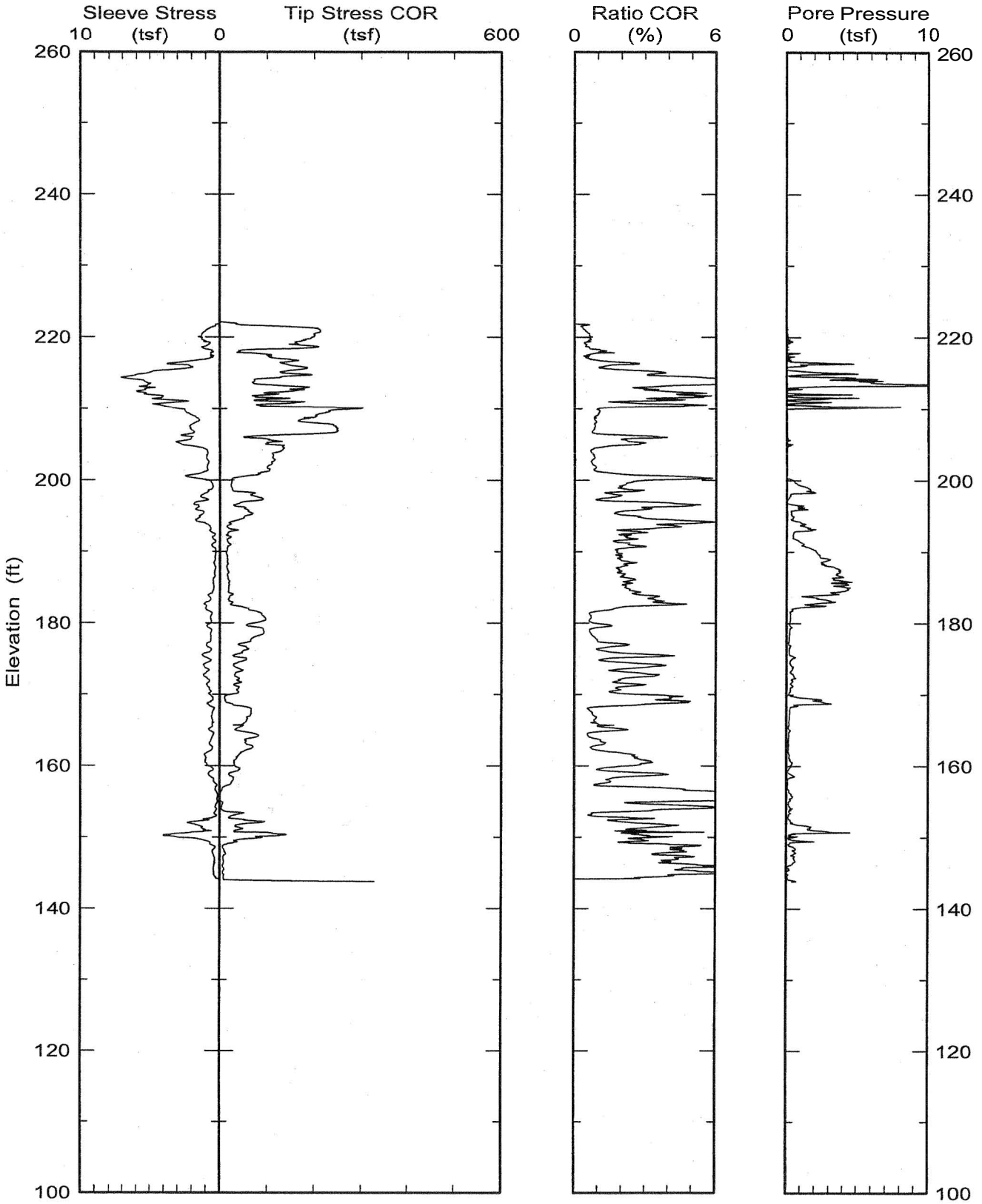

Maximum depth: *78.33* (ft)

Applied Research Associates, Inc.
South Royalton, VT 05068
802-763-8348
cpt@ned.ara.com
www.ara.com

Date: 06/Sep/2005
Test ID: C-1002

Northing: 7667.64
Easting: 6574.64
Elevation: 222.13

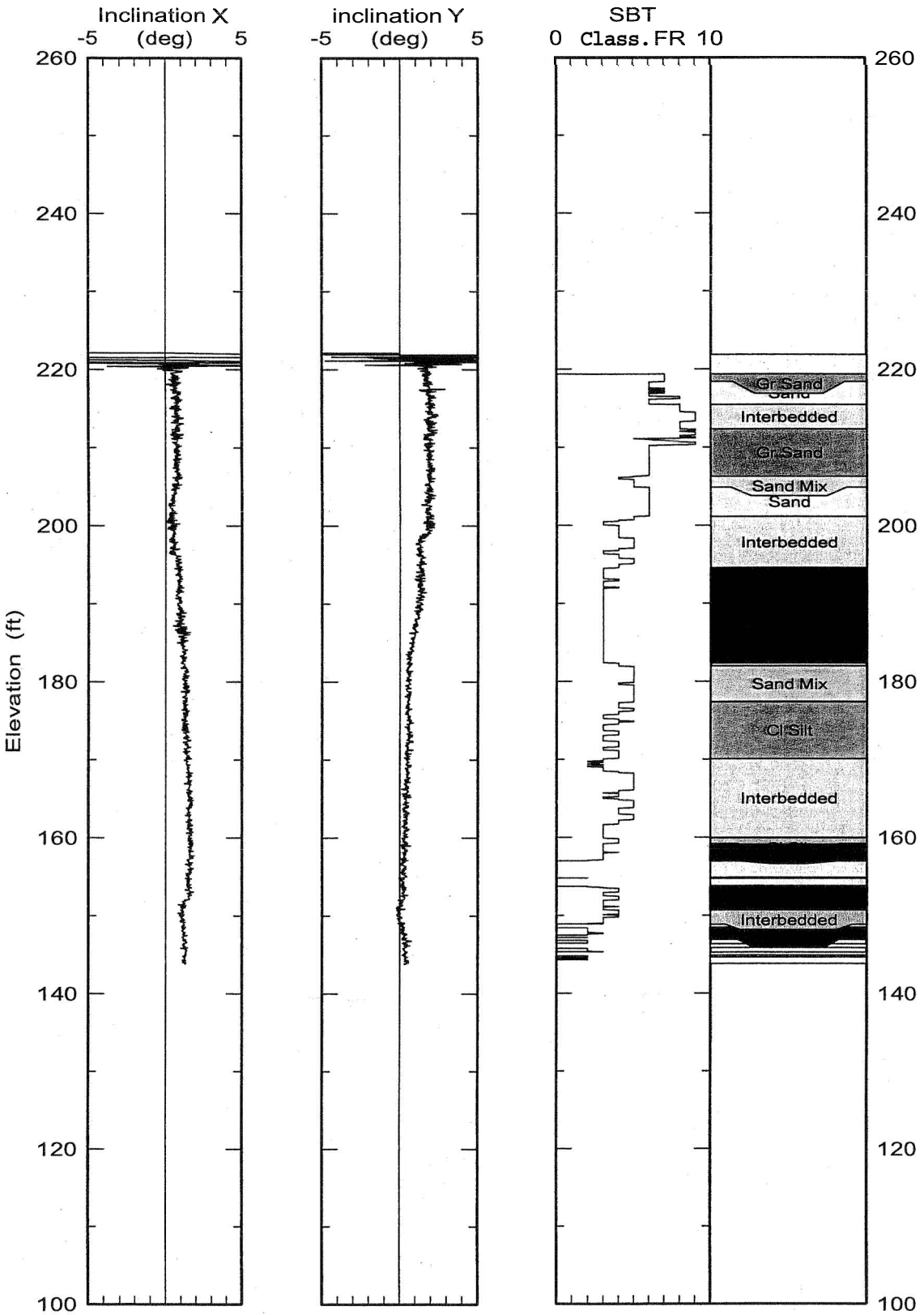

Maximum depth: *78.33* (ft)

Class FR: Friction Ratio Clas

Applied Research Associates, Inc.
South Royalton, VT 05068
802-763-8348
cpt@ned.ara.com
www.ara.com

Date: 07/Sep/2005
Test ID: C-1003
Northing: 7669.31
Easting: 7477.87
Elevation: 219.80

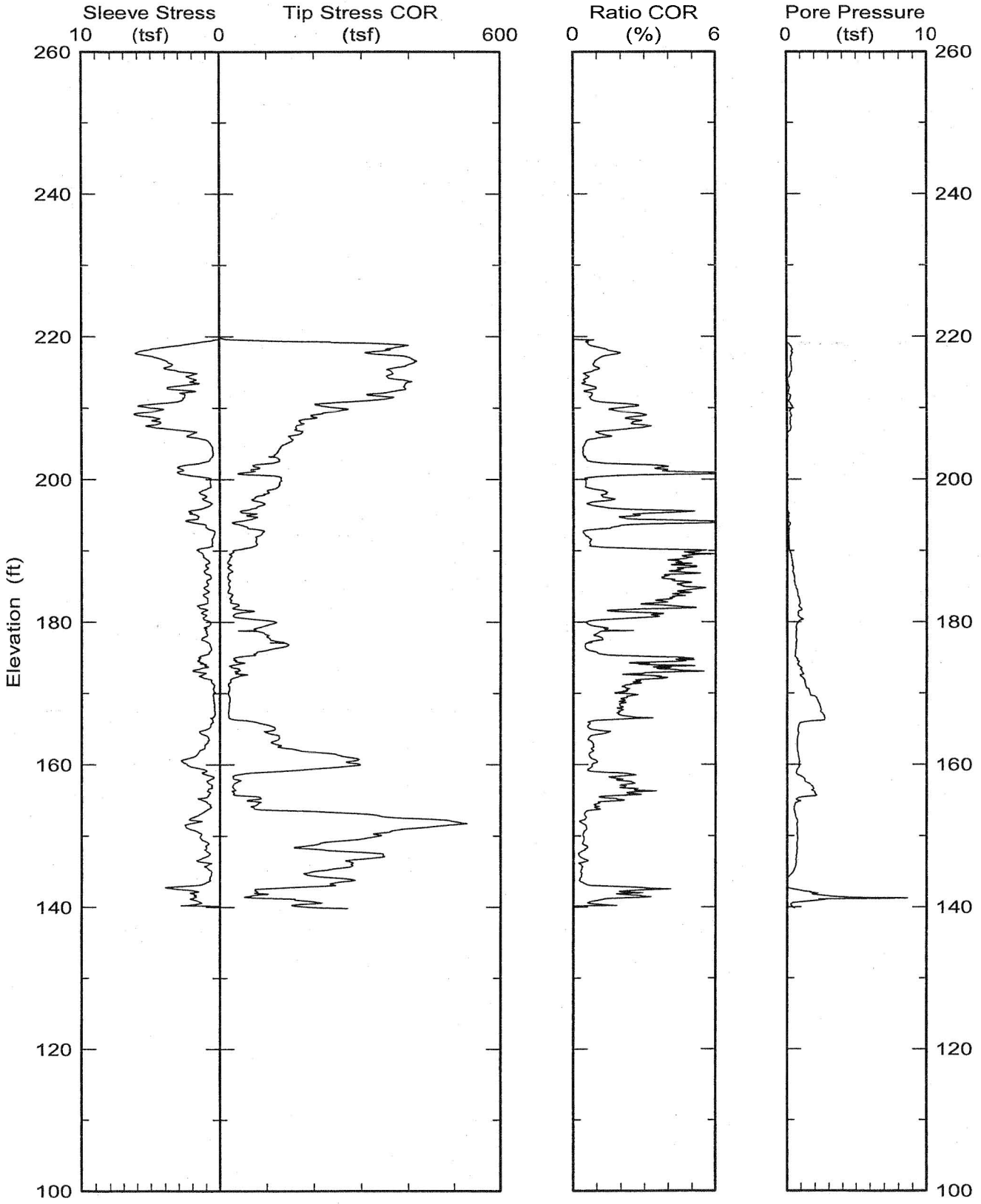

Maximum depth: 79.97 (A)

Applied Research Associates, Inc.
South Royalton, VT 05068
802-763-8348
cpt@ned.ara.com
www.ara.com

Date: 07/Sep/2005
Test ID: C-1003
Northing: 7669.31
Easting: 7477.87
Elevation: 219.80

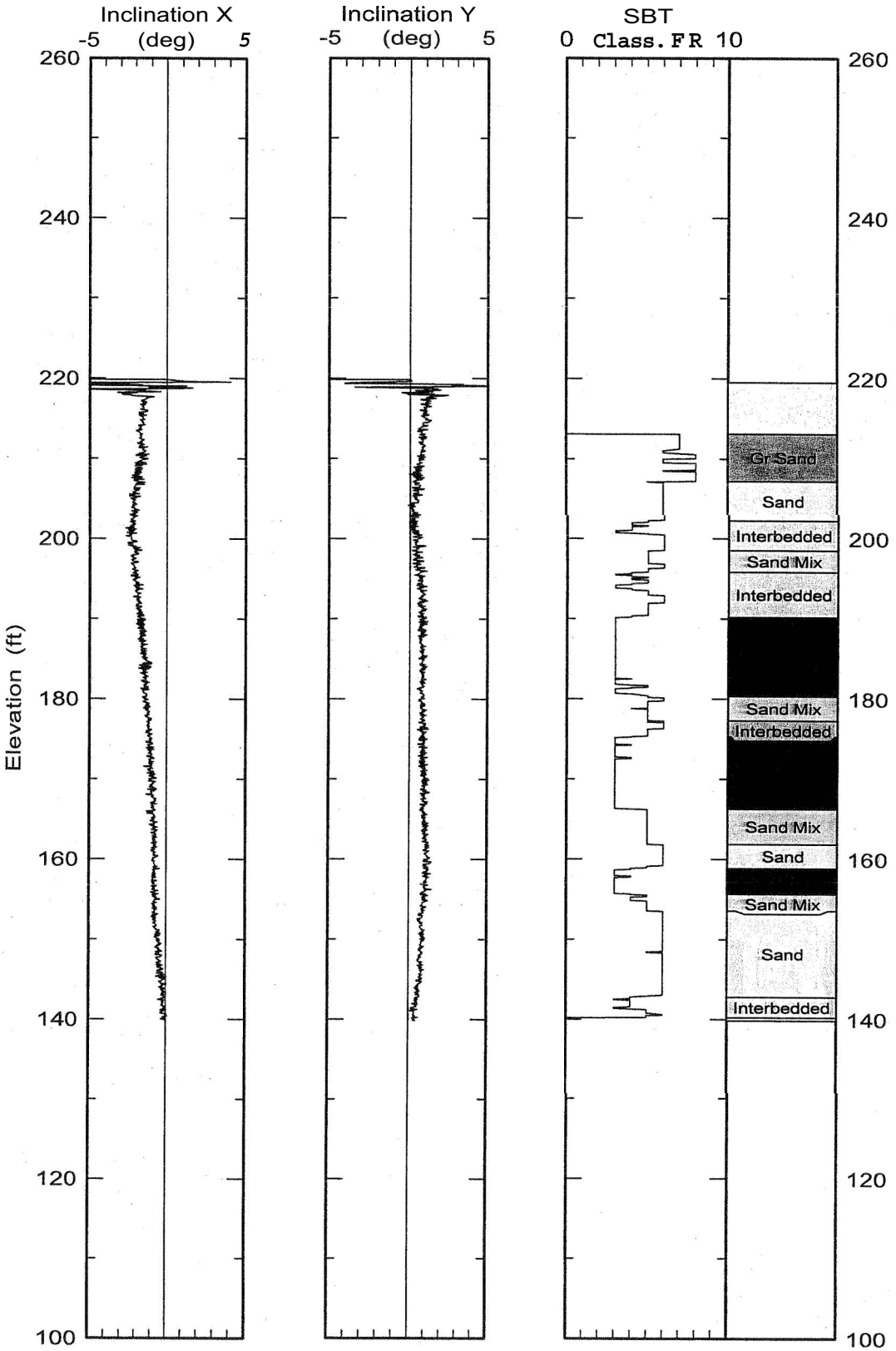

Maximum depth: 79.97 (ft)

Class FR: Friction Ratio Clas

Applied Research Associates, Inc. South Royalton, VT 05068 802-763-8348 cpt@ned.ara.com www.ara.com	Date: 01/Sep/2005 Test ID: C-1004 Northing: 7646.13 Easting: 8361.84 Eievation: 220.82

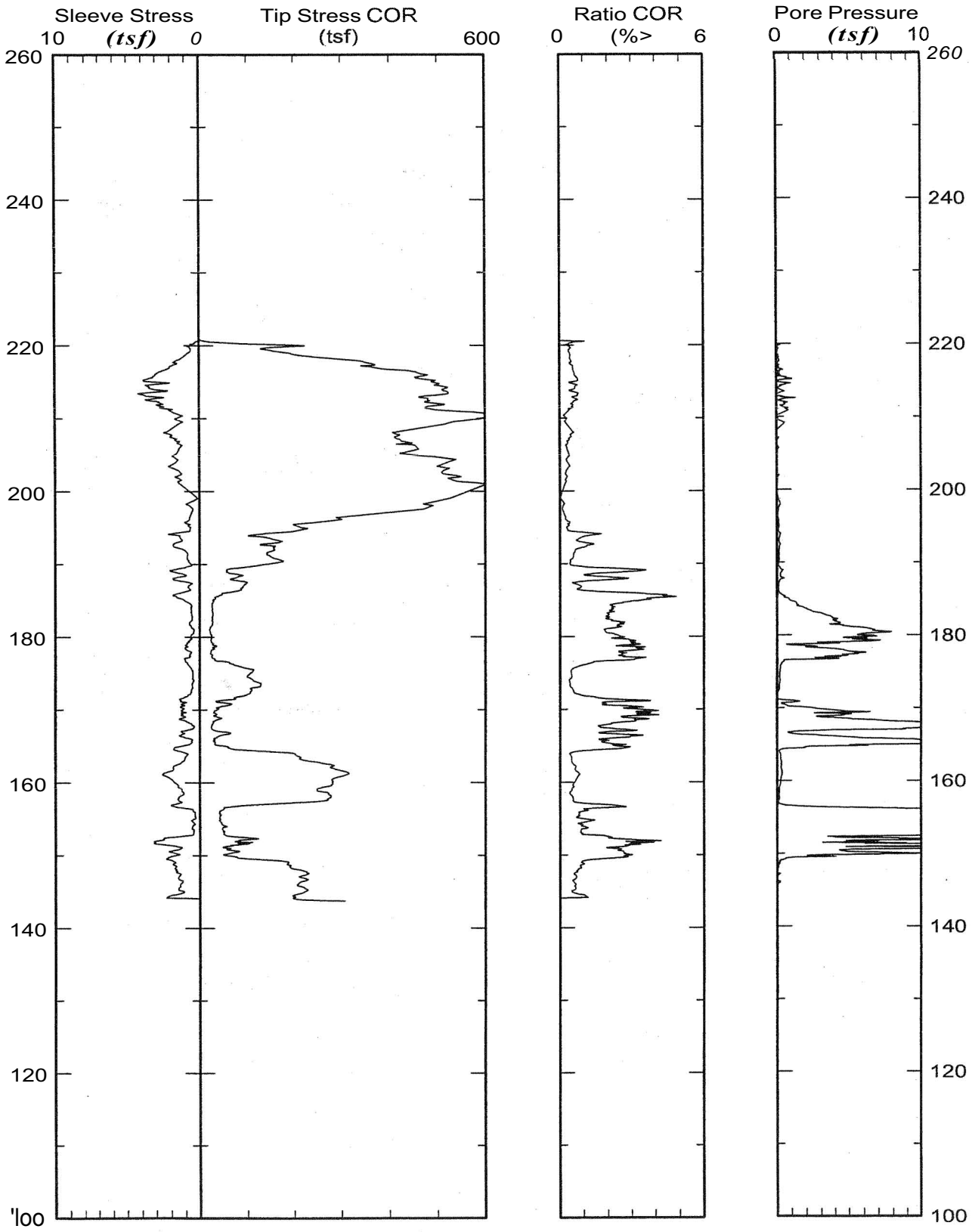

Maximum depth: 77.06 (ft)

Applied Research Associates, Inc.
South Royalton, VT 05068
802-763-8348
cpt@ned.ara.com
www.ara.com

Date: 01/Sep/2005
Test ID: C-1004
Northing: 7646.13
Easting: 8361.84
Elevation: 220.82

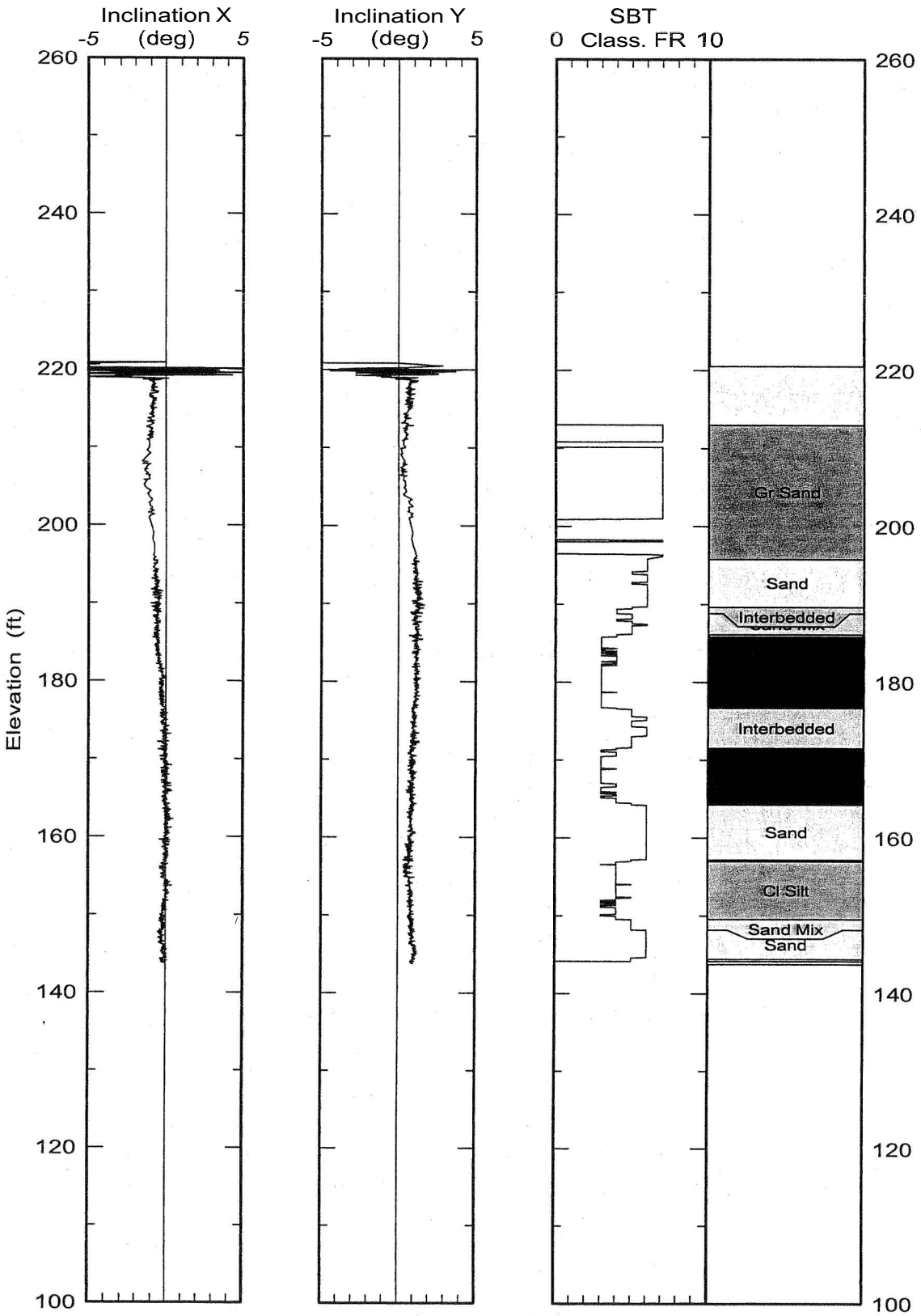

Maximum depth: 77.06 (ft)

Class FR: Friction Ratio Clas

Test ID: C-1004
File: 201S0501C.ECP

Applied Research Associates, Inc.
South Royalton, VT 05068
802-763-8348
cpt@ned.ara.com
www.ara.com

Date: 08/Sep/2005
Test ID: C-1005
Northing: 7995.26
Easting: 8174.60
Elevation: 223.81

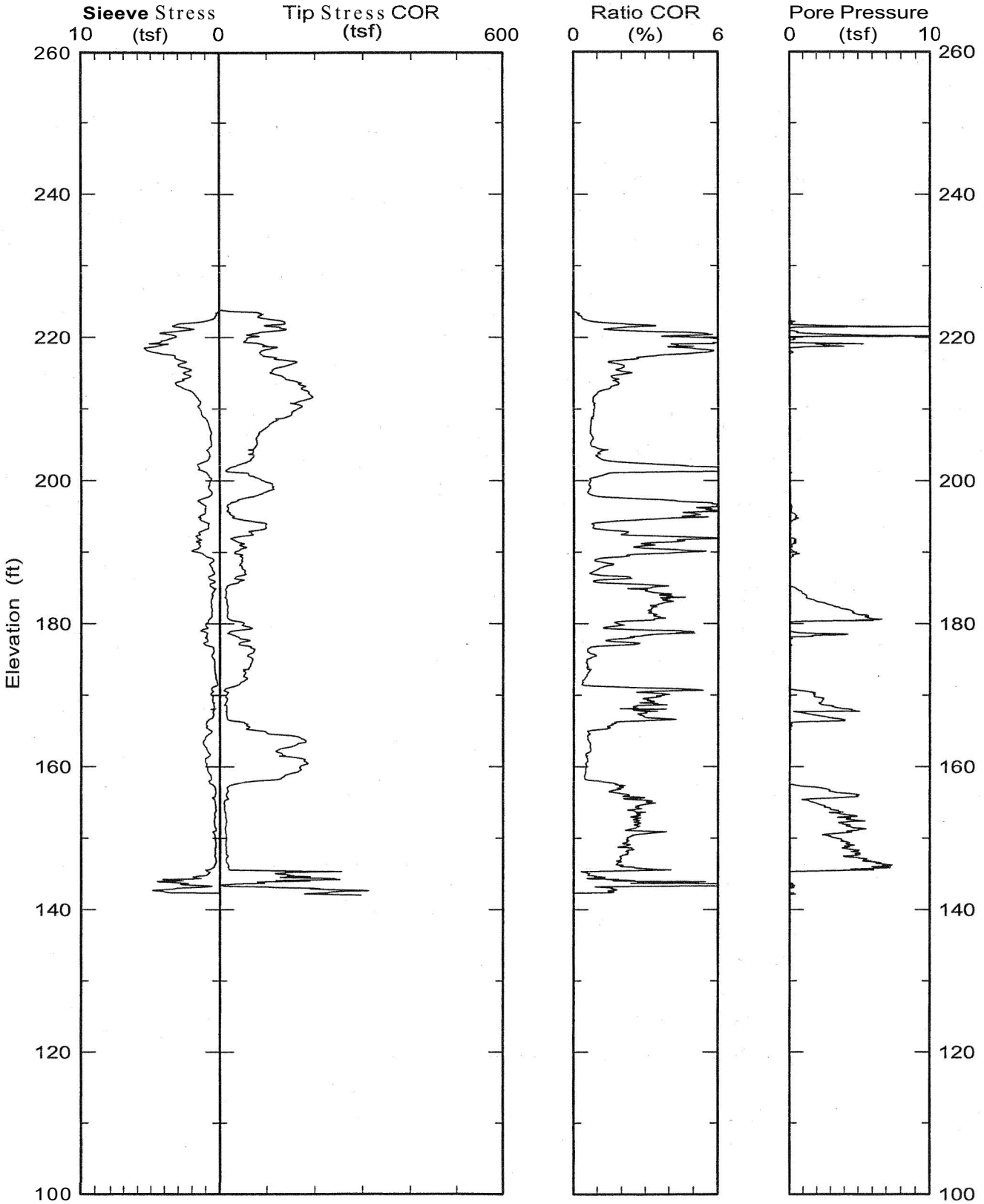

Maximum depth: 81.80 **(R)**

Applied Research Associates, Inc.
South Royalton, VT 05068
802-763-8348
cpt@ned.ara.com
www.ara.com

Date: 08/Sep/2005
Test ID: C-1005
Northing: 7995.26
Easting: 8174.60
Elevation: 223.81

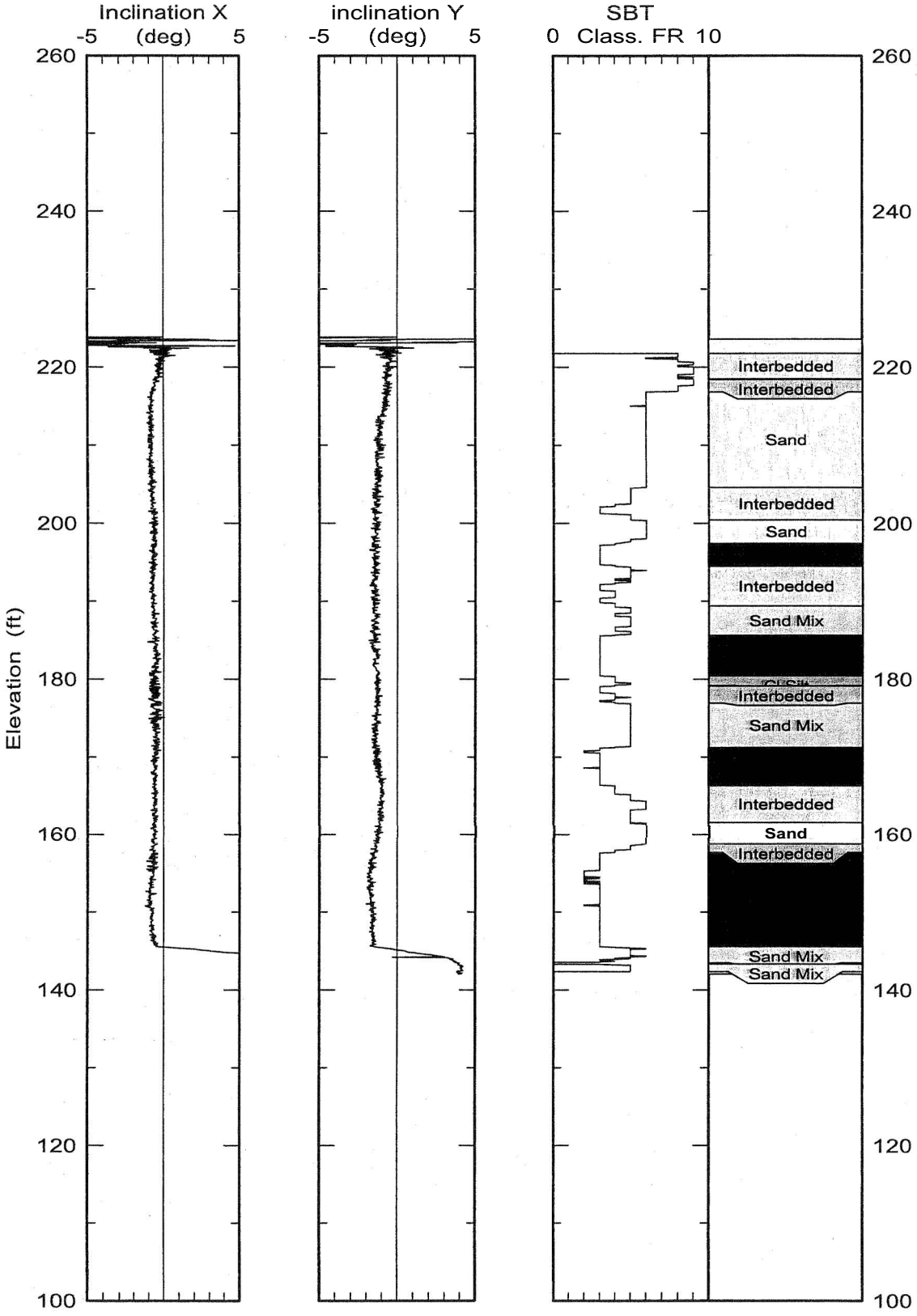

Maximum depth: 81.80 (ft)

Class FR: Friction **Ratio** Clas

Applied Research Associates, Inc.
South Royalton, VT 05068
802-763-8348
cpt@ned.ara.com
www.ara.com

Date: 01/Sep/2005
Test ID: C-1006

Northing: 8001.46
Easting: 7261.58
Elevation: 222.80

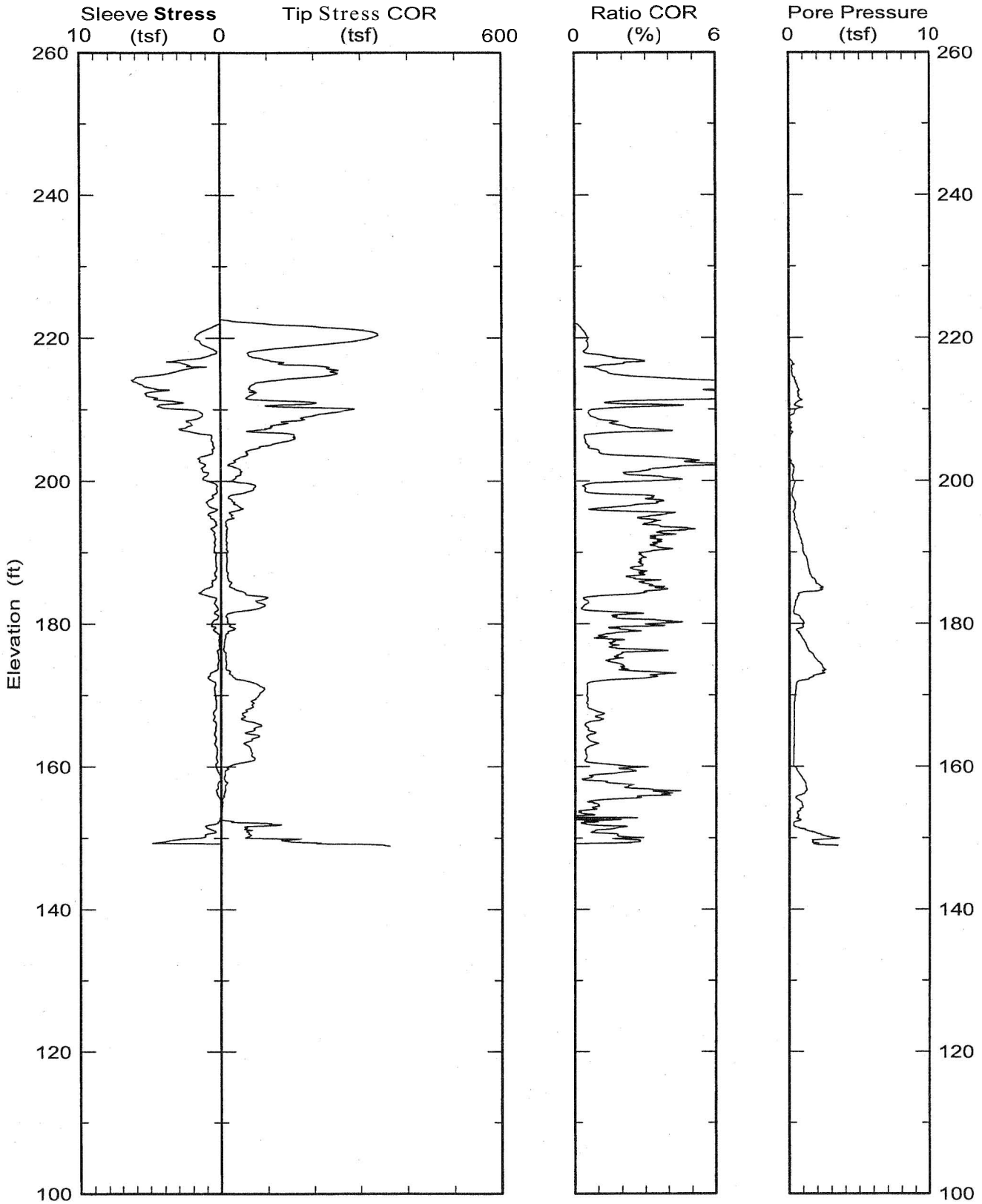

Maximum depth: 73.91 (ft)

Applied Research Associates, Inc.
South Royalton, VT 05068
802-763-8348
cpt@ned.ara.com
www.ara.com

Date: 01/Sep/2005
Test ID: C-1006

Northing: 8001.46
Easting: 7261.58
Elevation: 222.80

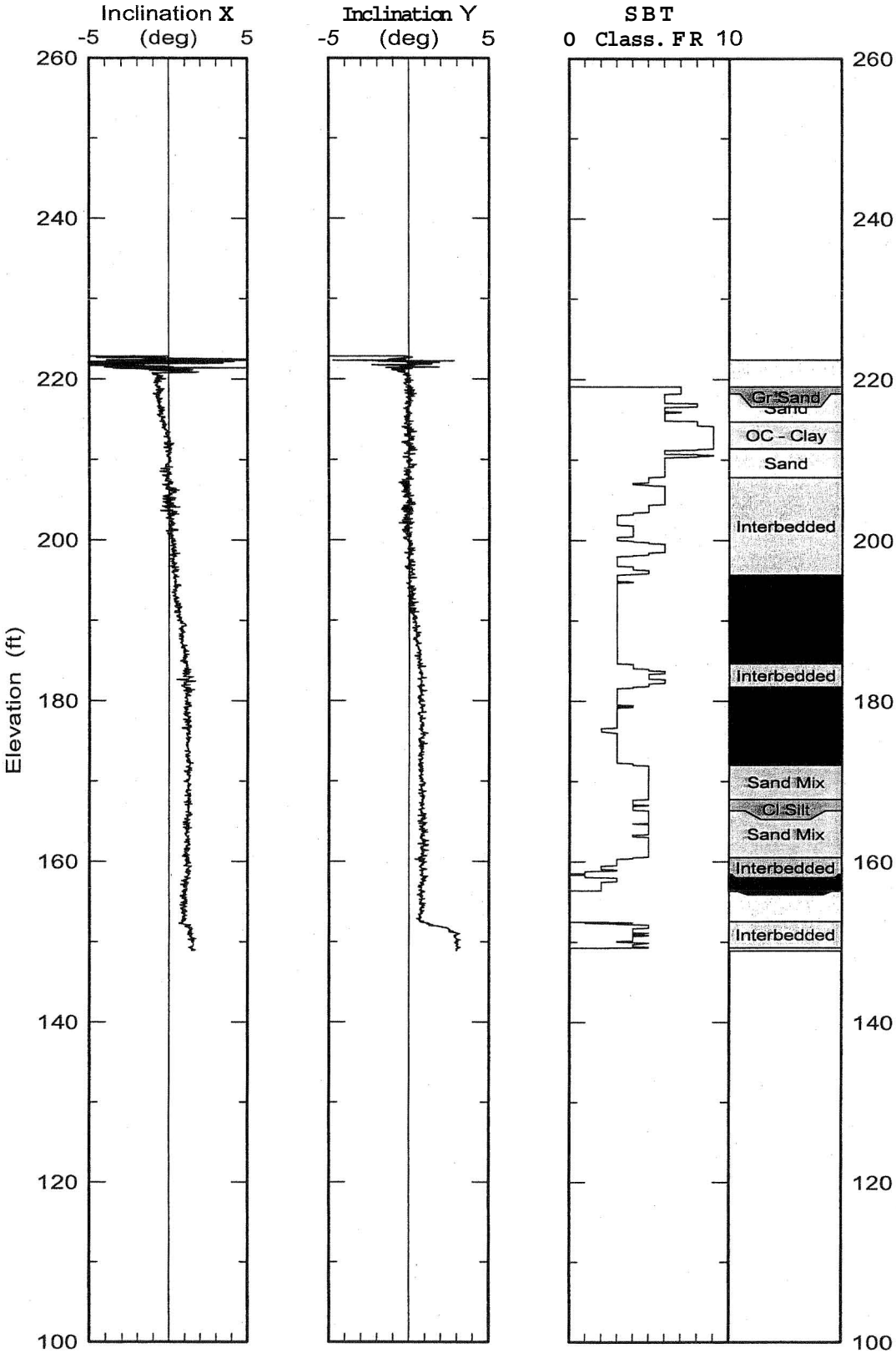

Maximum depth: 73.91 (ft)

Class FR: Friction Ratio Clas

Test ID: C-1006

Applied Research Associates, Inc.
South Royalton, VT 05068
802-763-8348
cpt@ned.ara.com
www.ara.com

Date: 02/Sep/2005
Test ID: C-1007

Northing: 8270.62
Easting: 8055.05
Elevation: 222.81

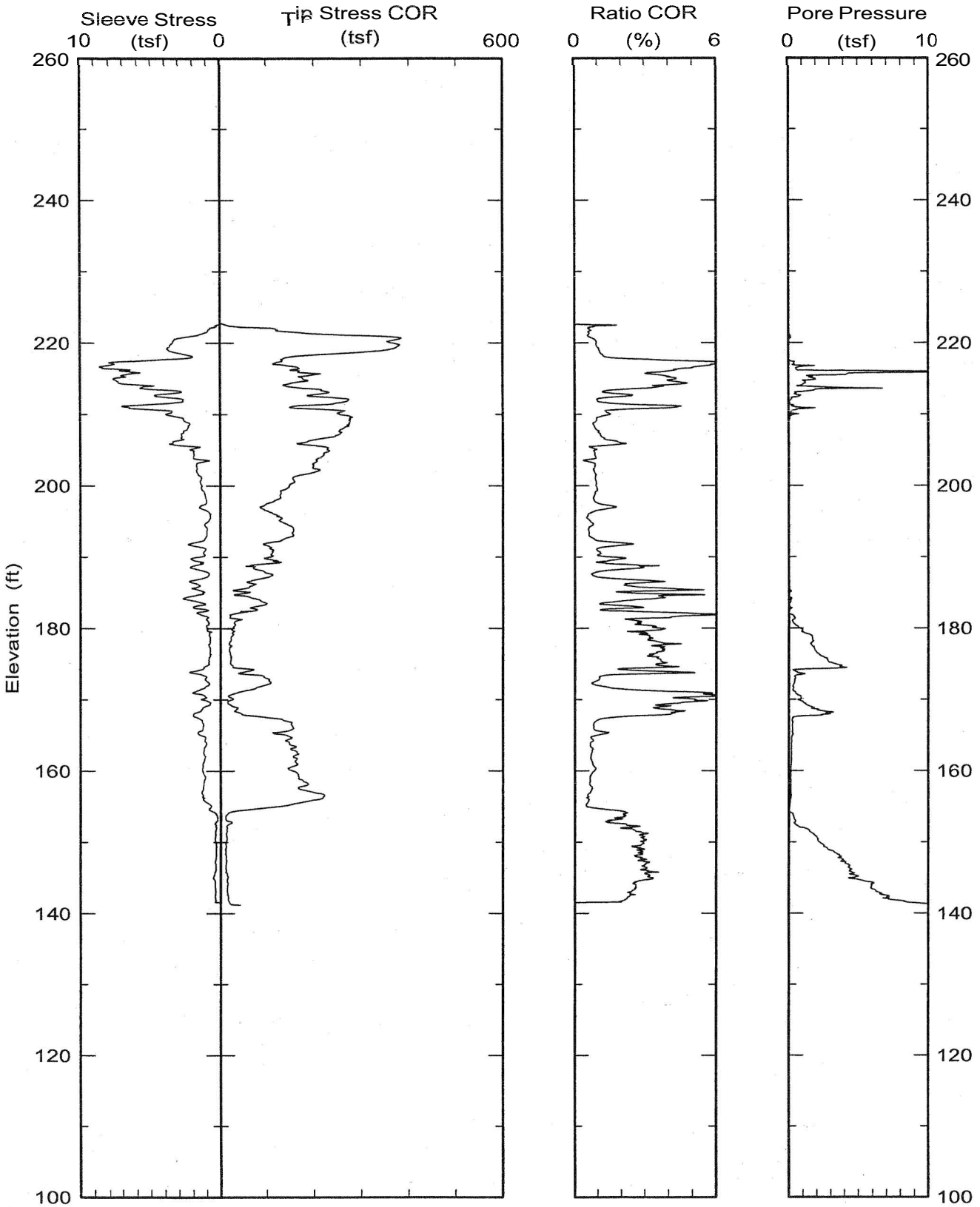

Maximum **depth:** 81.62 (A)

Applied Research Associates, Inc.
South Royalton, VT 05068
802-763-8348
cpt@ned.ara.com
www.ara.com

Date: 02/Sep/2005
Test ID: C-1007
Northing: 8270.62
Easting: 8055.05
Elevation: 222.81

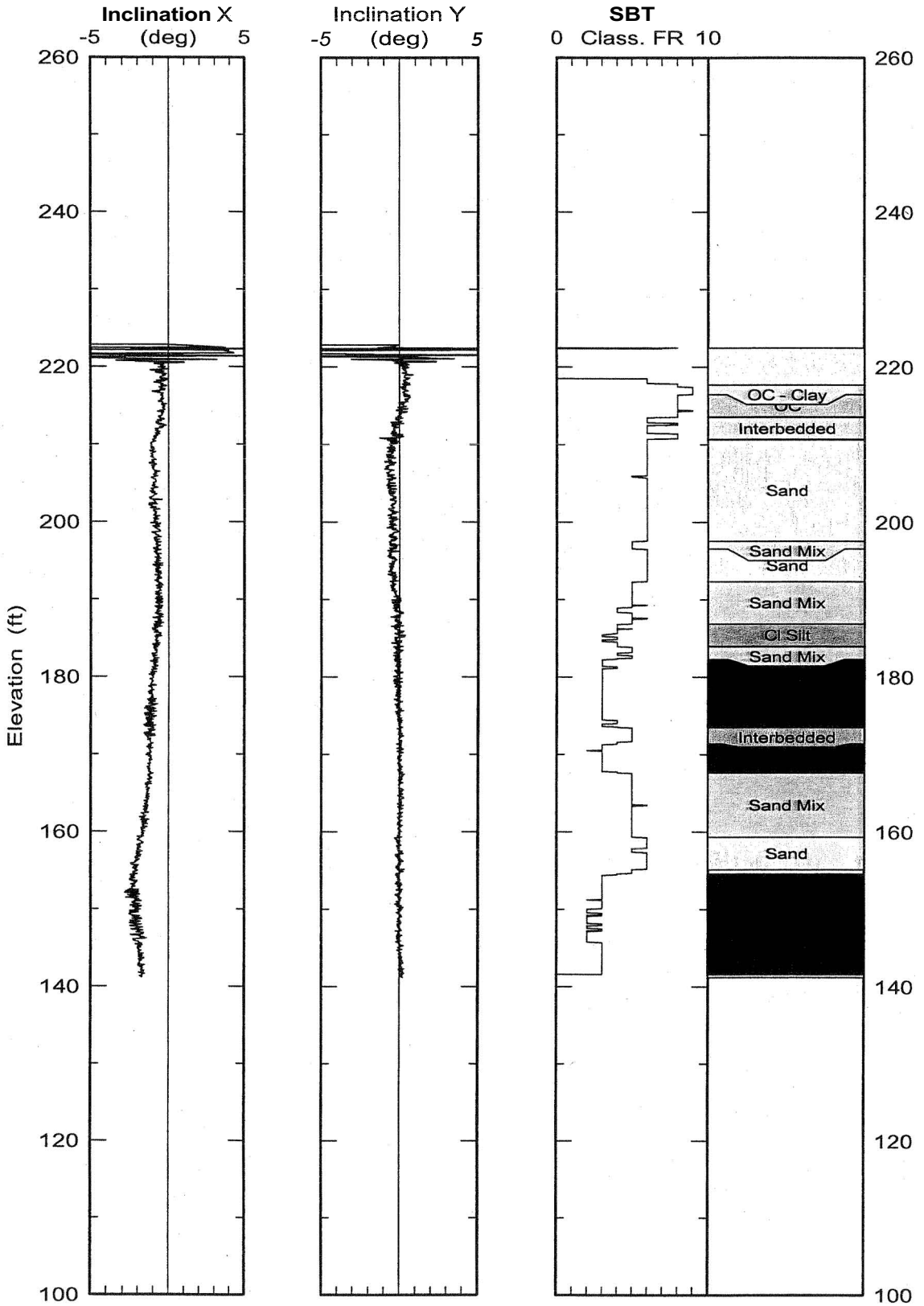

Maximum depth: 81.62 **(R)**

Class FR: Friction Ratio Clas

Applied Research Associates, Inc.
South Royalton, VT 05068
802-763-8348
cpt@ned.ara.com
www.ara.com

Date: 02/Sep/2005
Test ID: C-1008
Northing: 8268.48
Easting: 6930.89
Elevation: 221.30

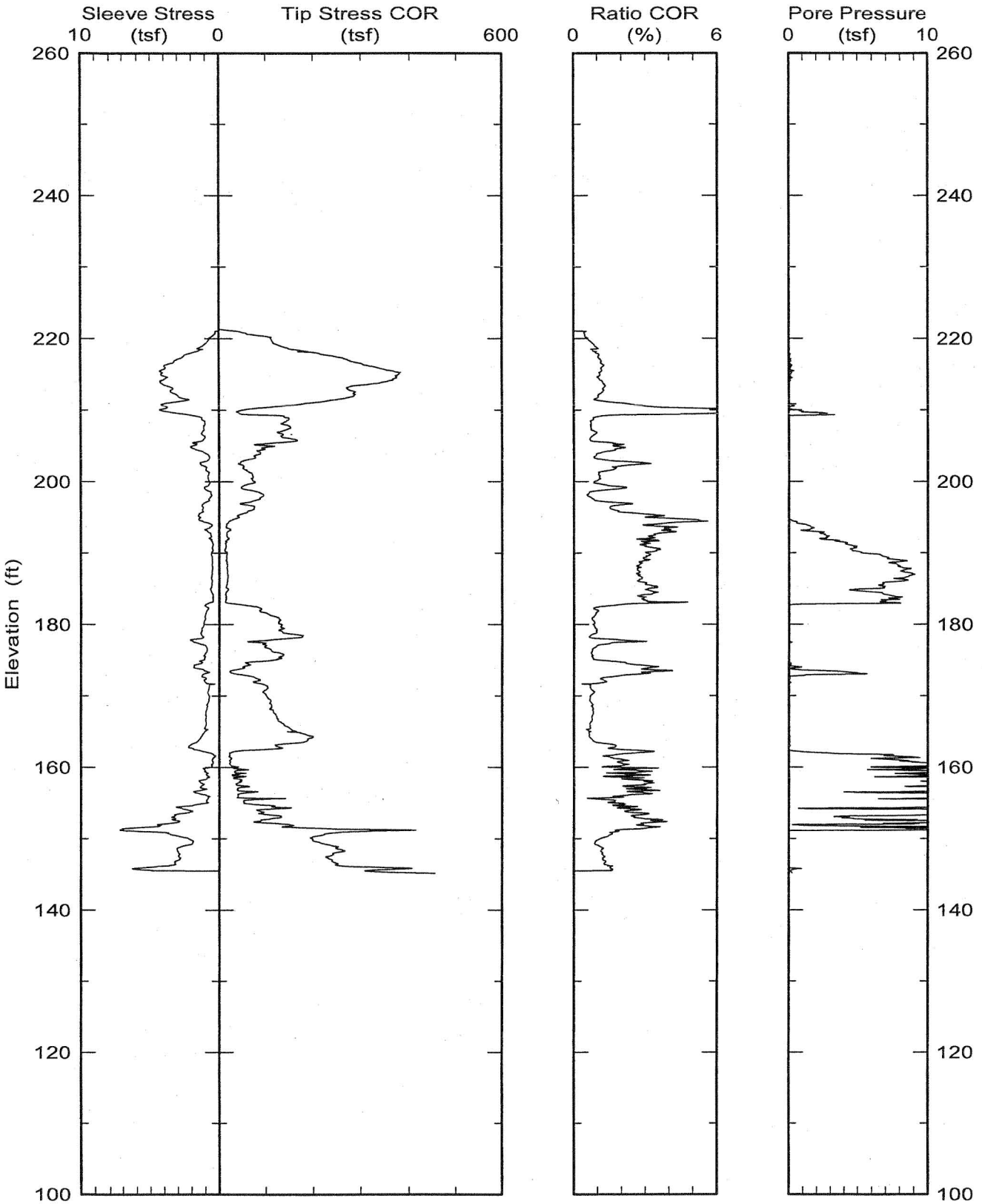

Maximum depth: 76.14 (ft)

Applied Research Associates, Inc.
South Royalton, VT 05068
802-763-8348
cpt@ned.ara.com
www.ara.com

Date: 02/Sep/2005
Test ID: C-1008
Northing: 8268.48
Easting: 6930.89
Elevation: 221.30

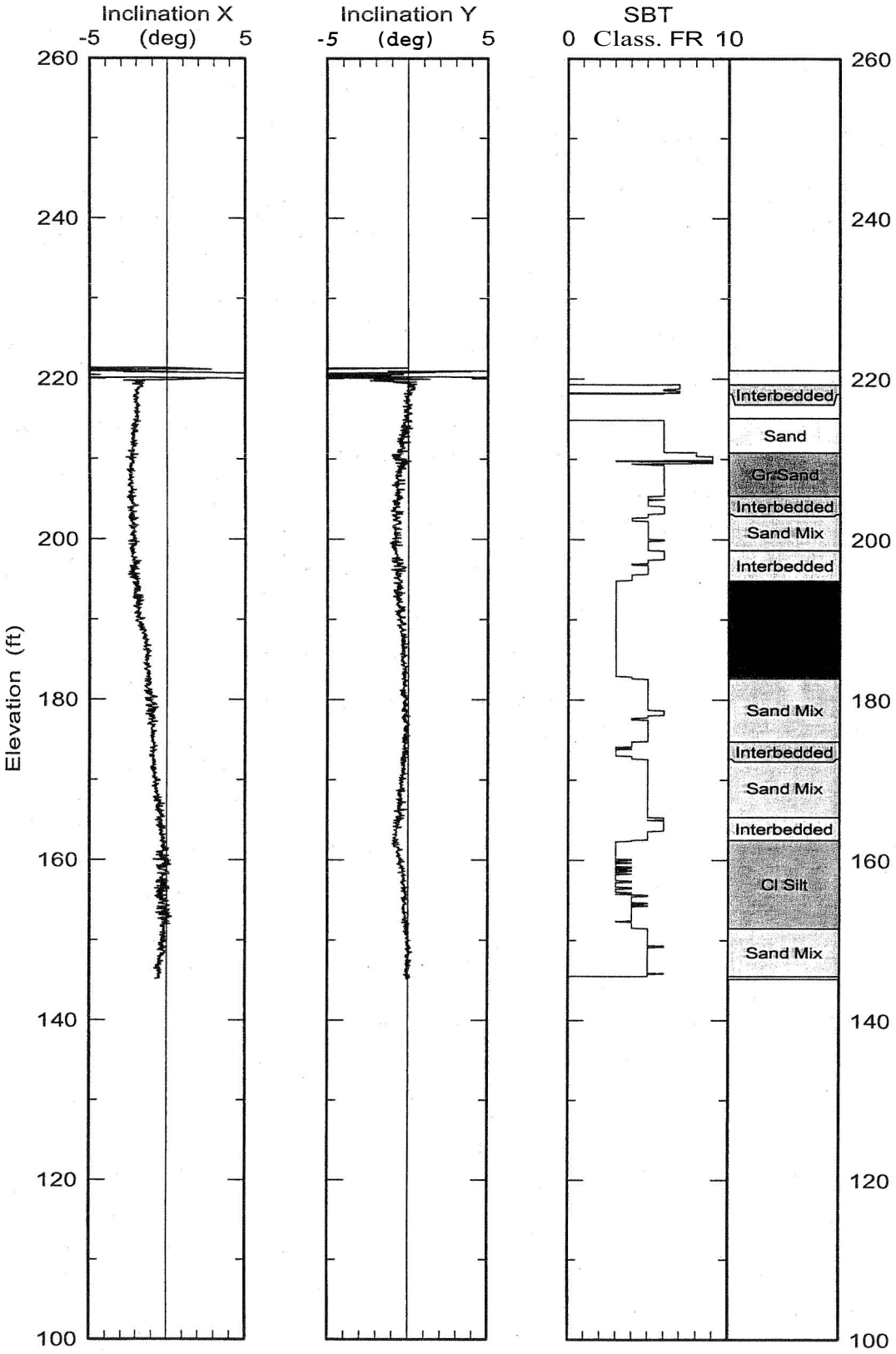

Maximum depth: 76.14 (ft)

Class FR: Friction Ratio Clas

Applied Research Associates, Inc.
South Royalton, VT 05068
802-763-8348
cpt@ned.ara.com
www.ara.com

Date: 07/Sep/2005
Test ID: C-1009

Northing: 5979.62
Easting: 6798.49
Elevation: 218.93

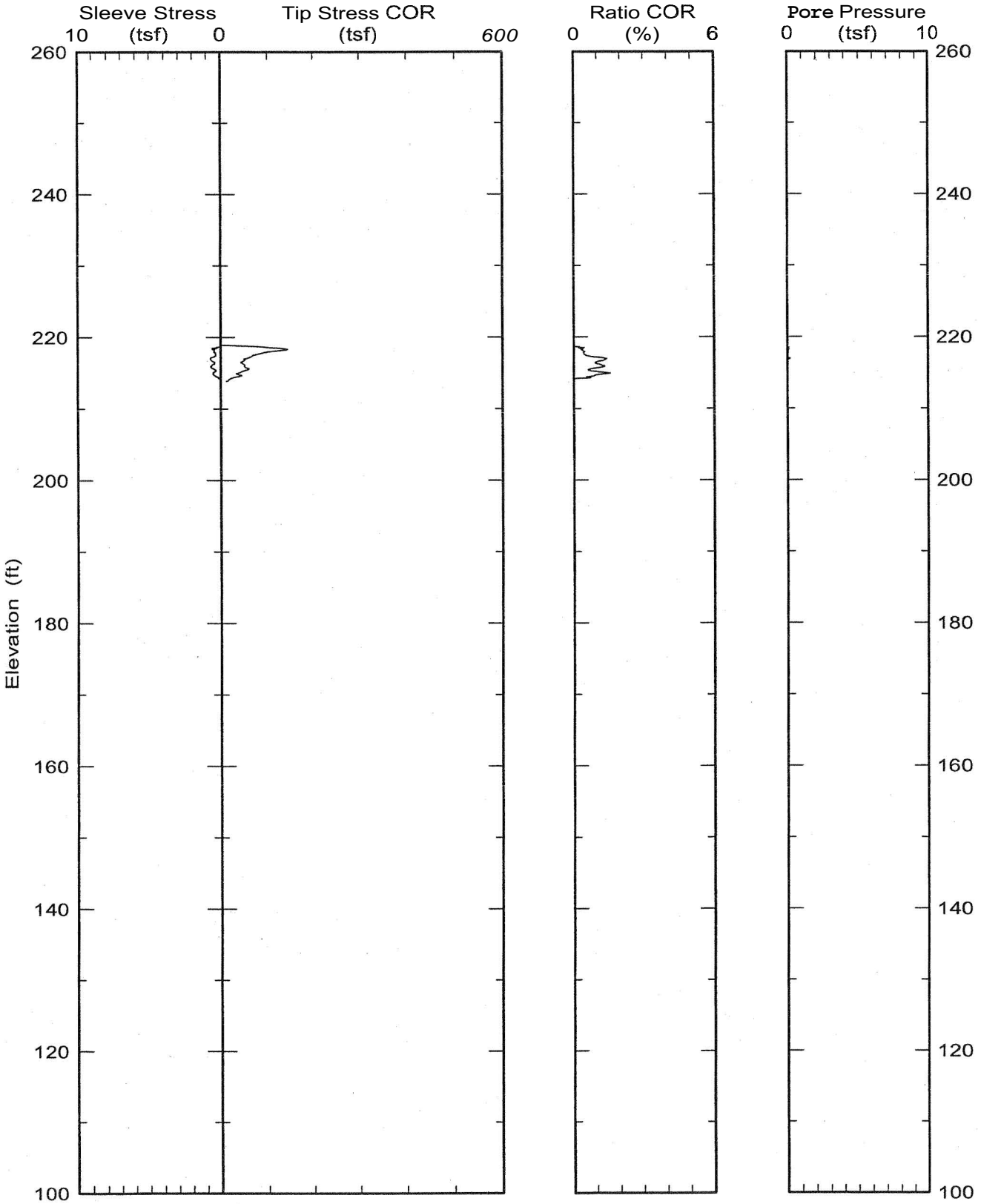

Maximum depth: 5.09 (ft)

Applied Research Associates, Inc. South Royalton, VT 05068 802-763-8348 cpt@ned.ara.com www.ara.com	Date: 07/Sep/2005 Test ID: C-1009 Northing: 5979.62 Easting: 6798.49 Elevation: 218.93

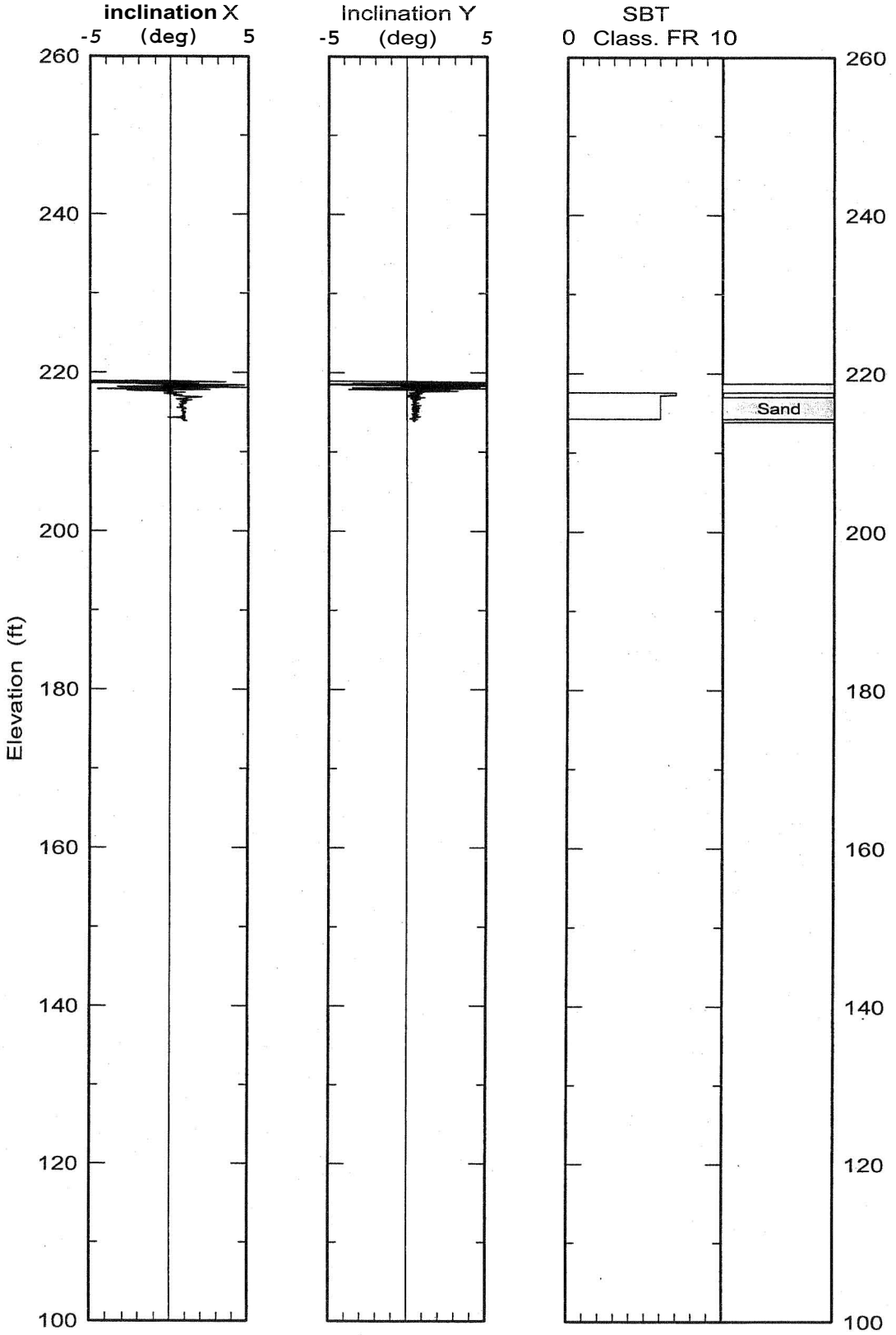

Maximum depth: 5.09 (ft)

Class FR: Friction **Ratio** Clas

Test ID: C-1009

Applied Research Associates, Inc.
South Royalton, VT 05068
802-763-8348
cpt@ned.ara.com
www.ara.com

Date: 07/Sep/2005
Test ID: C-1009A
Northing: 5979.62
Easting: 6798.49
Elevation: 218.93

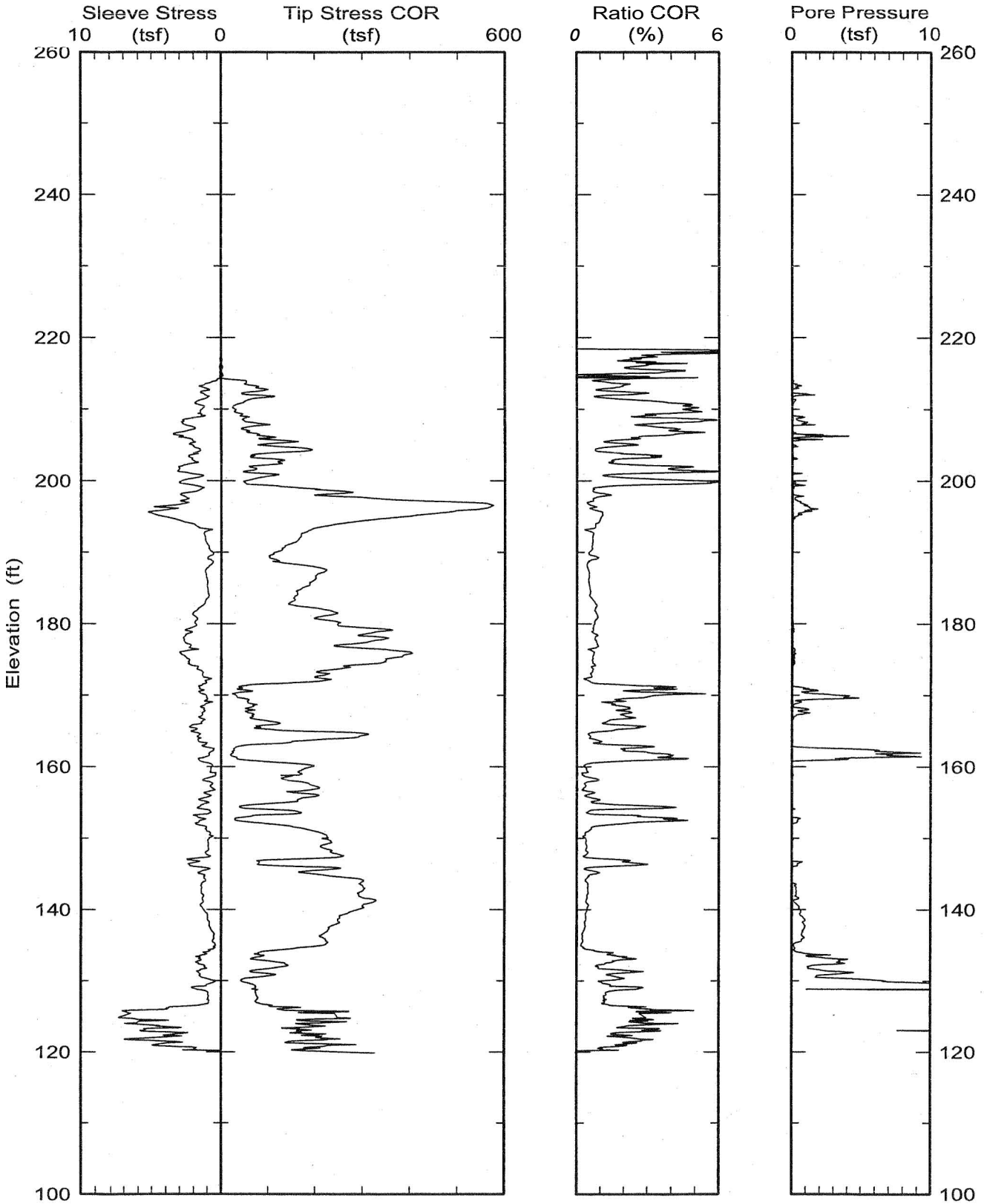

Maximum **depth:** 99.08 (ft)

Applied Research Associates, Inc.
South Royalton, VT 05068
802-763-8348
cpt@ned.ara.com
www.ara.com

Date: 07/Sep/2005
Test ID: C-1009A
Northing: 5979.62
Easting: 6798.49
Elevation: 218.93

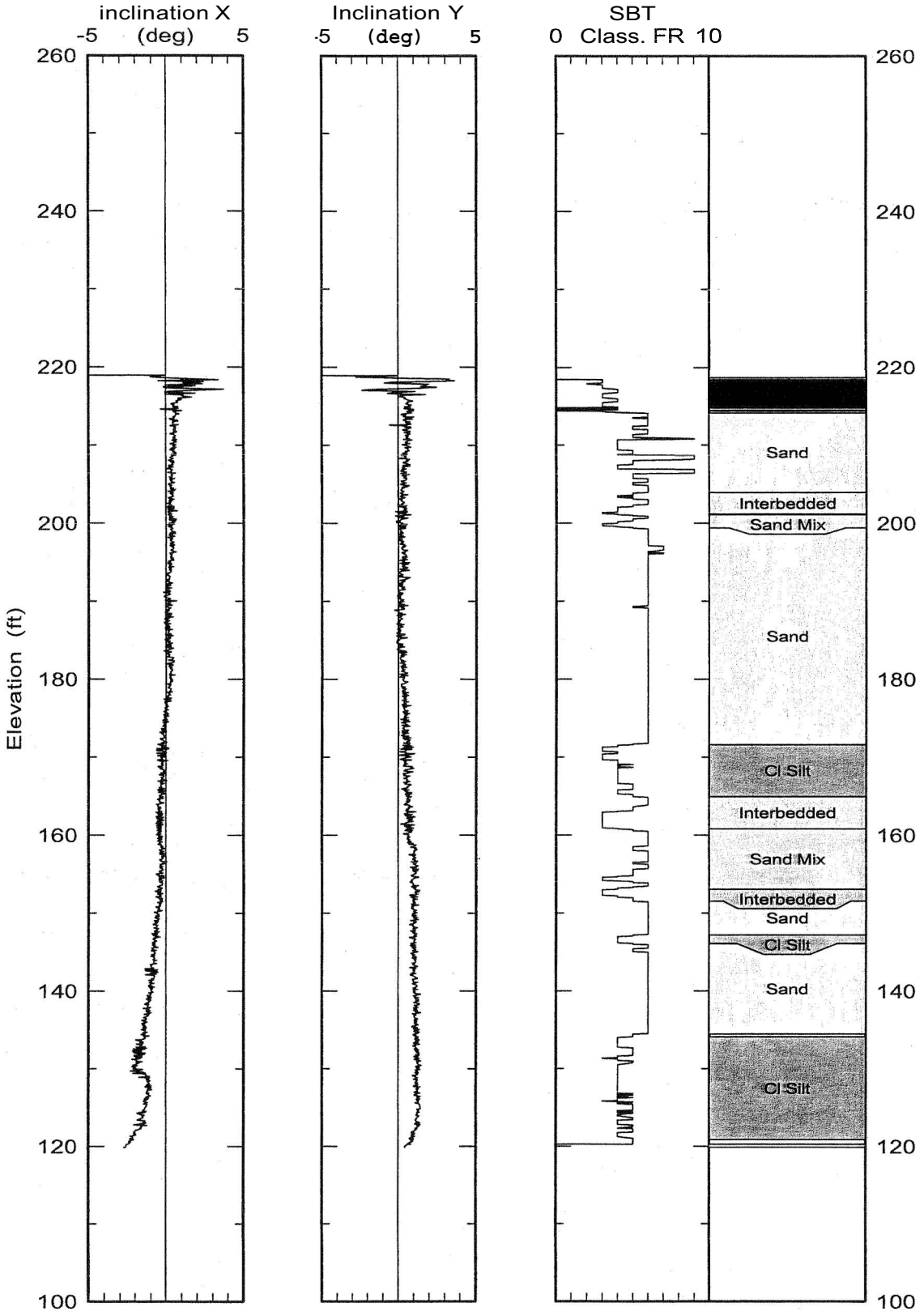

Maximum depth: 99.08 (ft)

Class FR: Friction Ratio Clas

Applied Research Associates, Inc.
South Royalton, VT 05068
802-763-8348
cpt@ned.ara.com
www.ara.com

Date: 08/Sep/2005
Test ID: C-1010
Northing: 6008.34
Easting: 7754.15
Elevation: 219.06

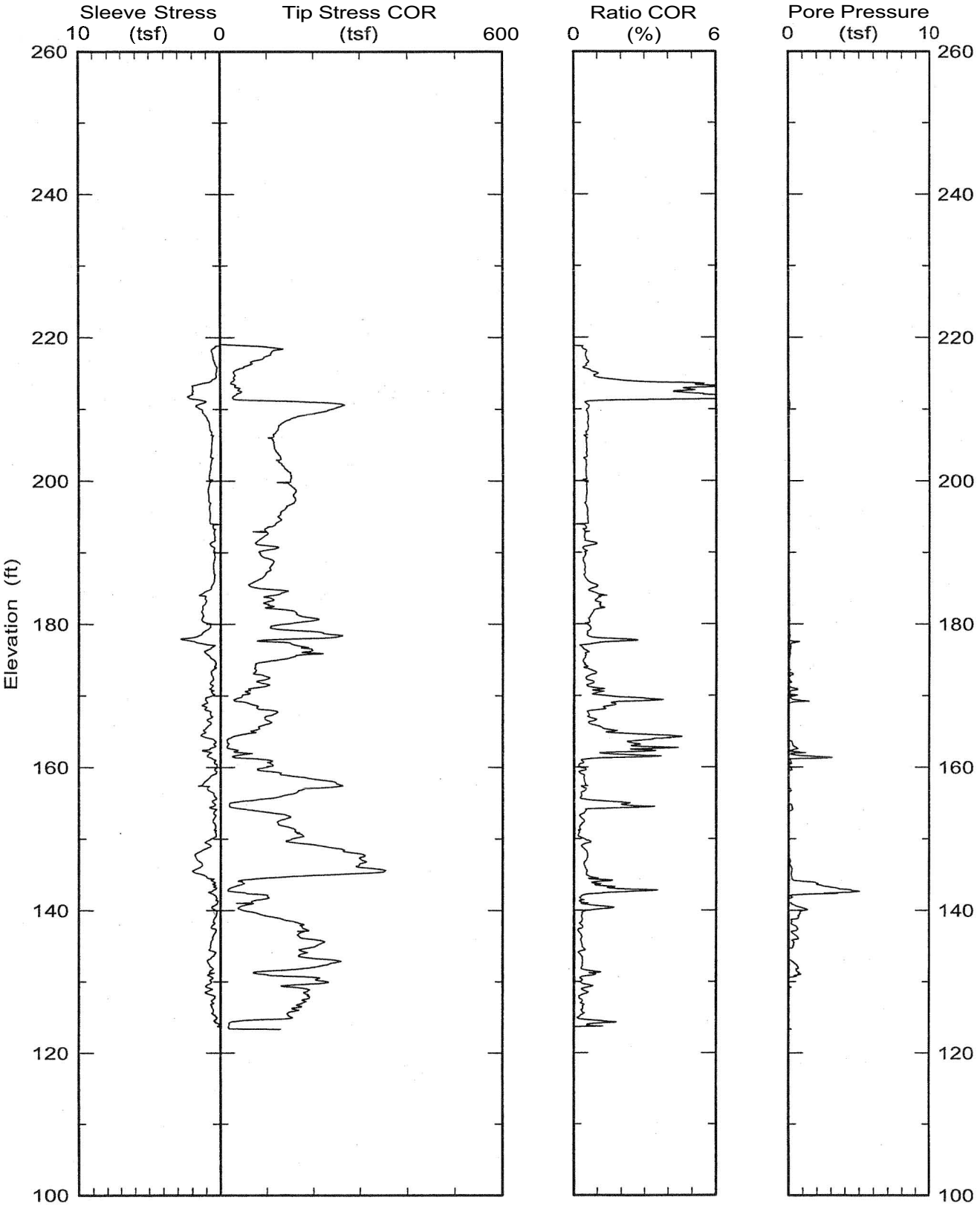

Maximum depth: 95.74 **(R)**

Applied Research Associates, Inc.
South Royalton, VT 05068
802-763-8348
cpt@ned.ara.com
www.ara.com

Date: 08/Sep/2005
Test ID: C-1010
Northing: 6008.34
Easting: 7754.15
Elevation: 219.06

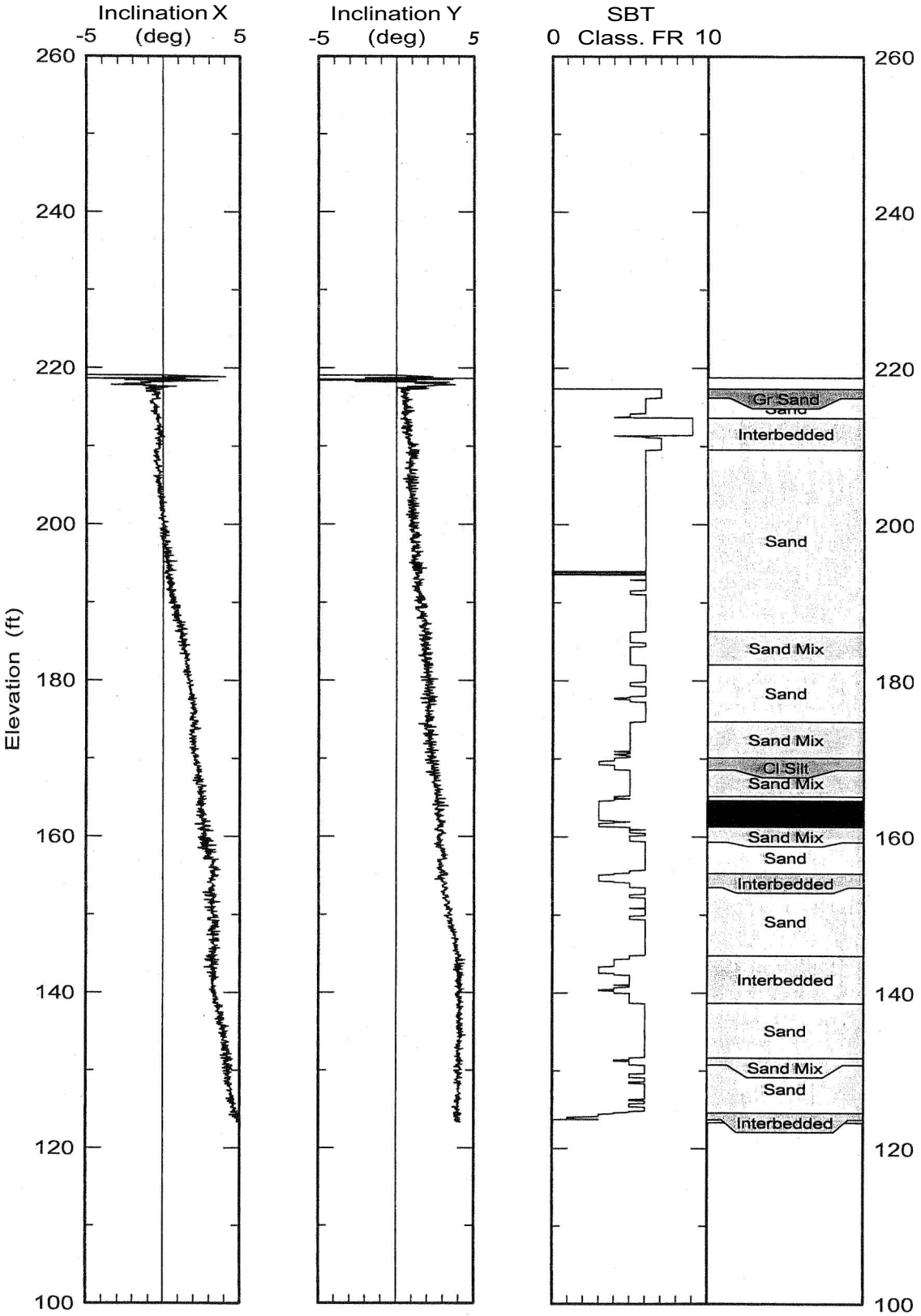

Maximum depth: 95.74 **(R)**

Class FR: Friction Ratio Clas

Test ID: C-1010
File: 208S0502C.ECP

APPENDIX B

SEISMIC DATA

C-1003 APPLIED RESEARCH ASSOCIATES, INC. 07/Sep/2005

Shear Wave Speeds

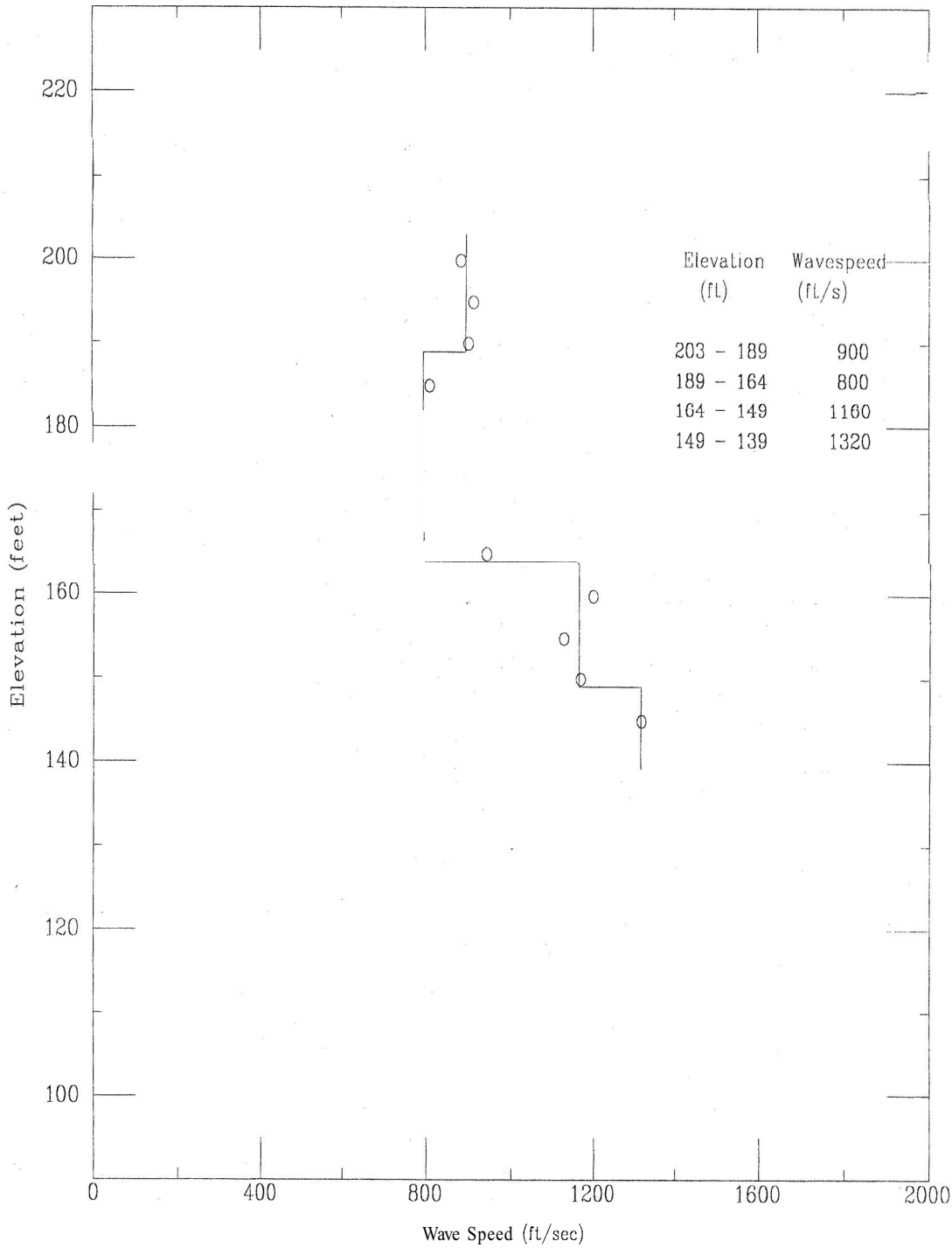

File 207s0506

C-- 1003 APPLIED RESEARCH ASSOCIATES, INC. 07/Sep/2005

Shear Wave Time of Peak

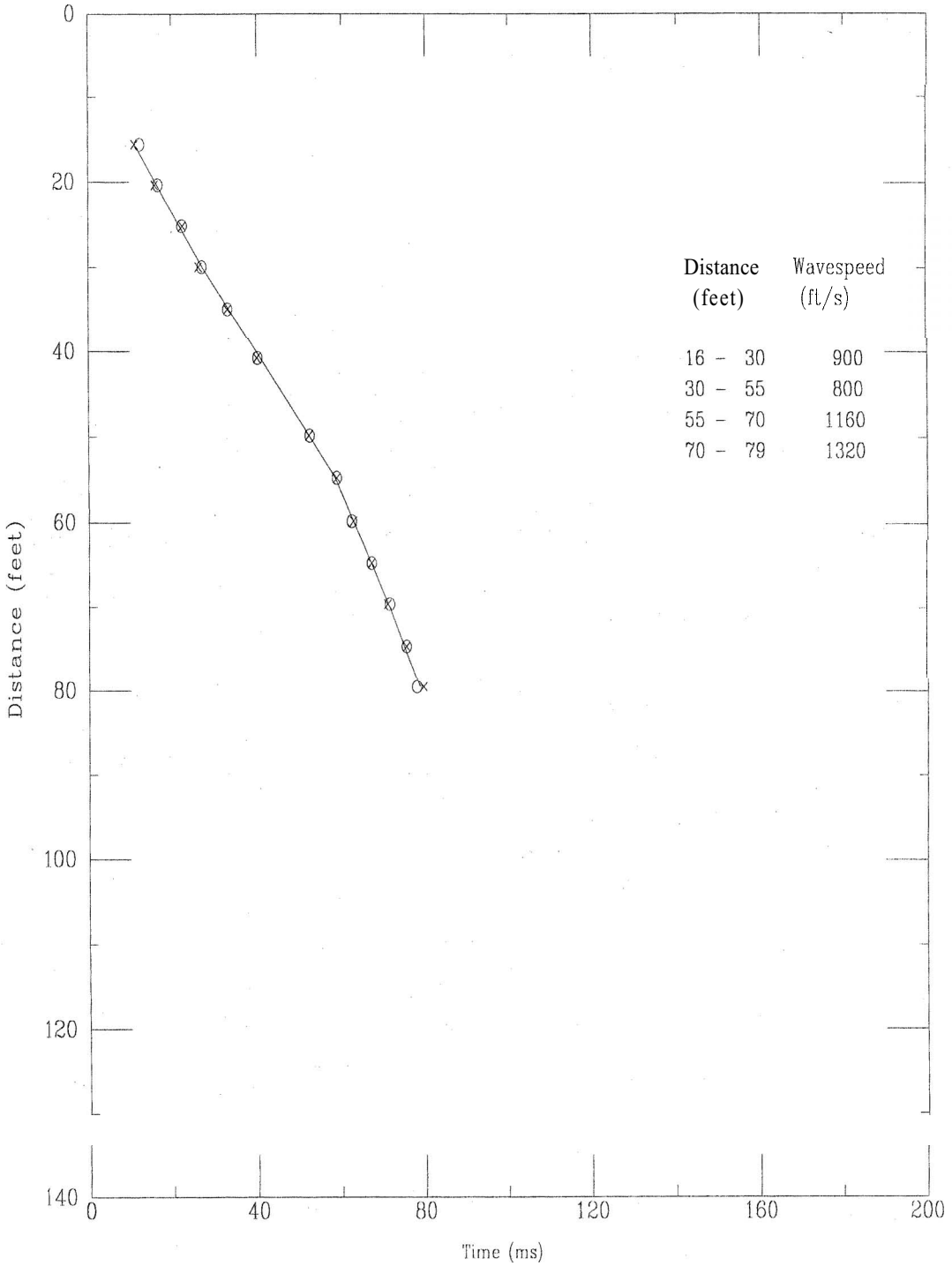

File 207s0506

Applied Research Associates, Inc.
C-1003

S Wave
07/Sep/2005

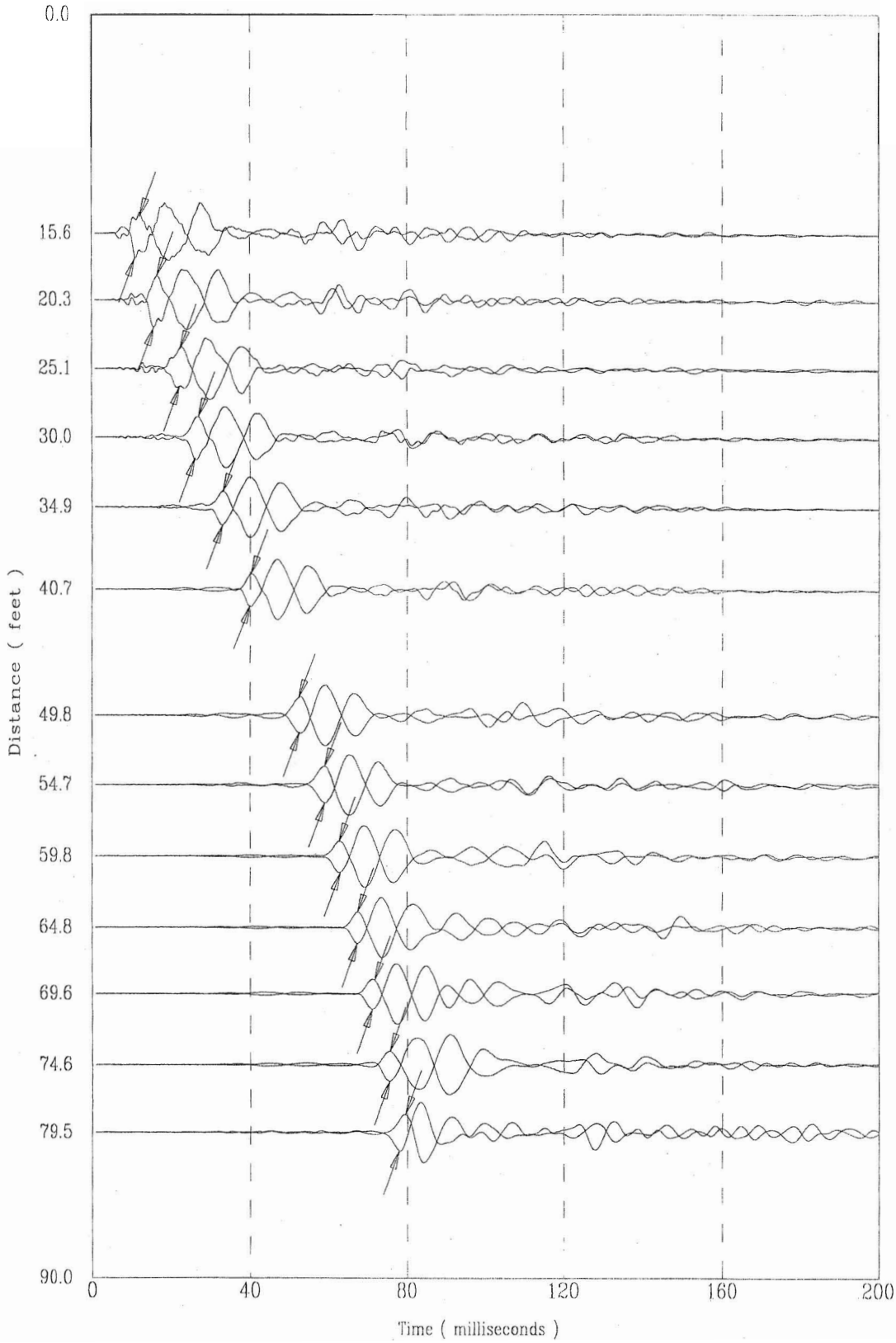

File 207s0506

C- 1005 APPLIED RESEARCH ASSOCIATES, INC 08/Sep/2005

Shear Wave Speeds

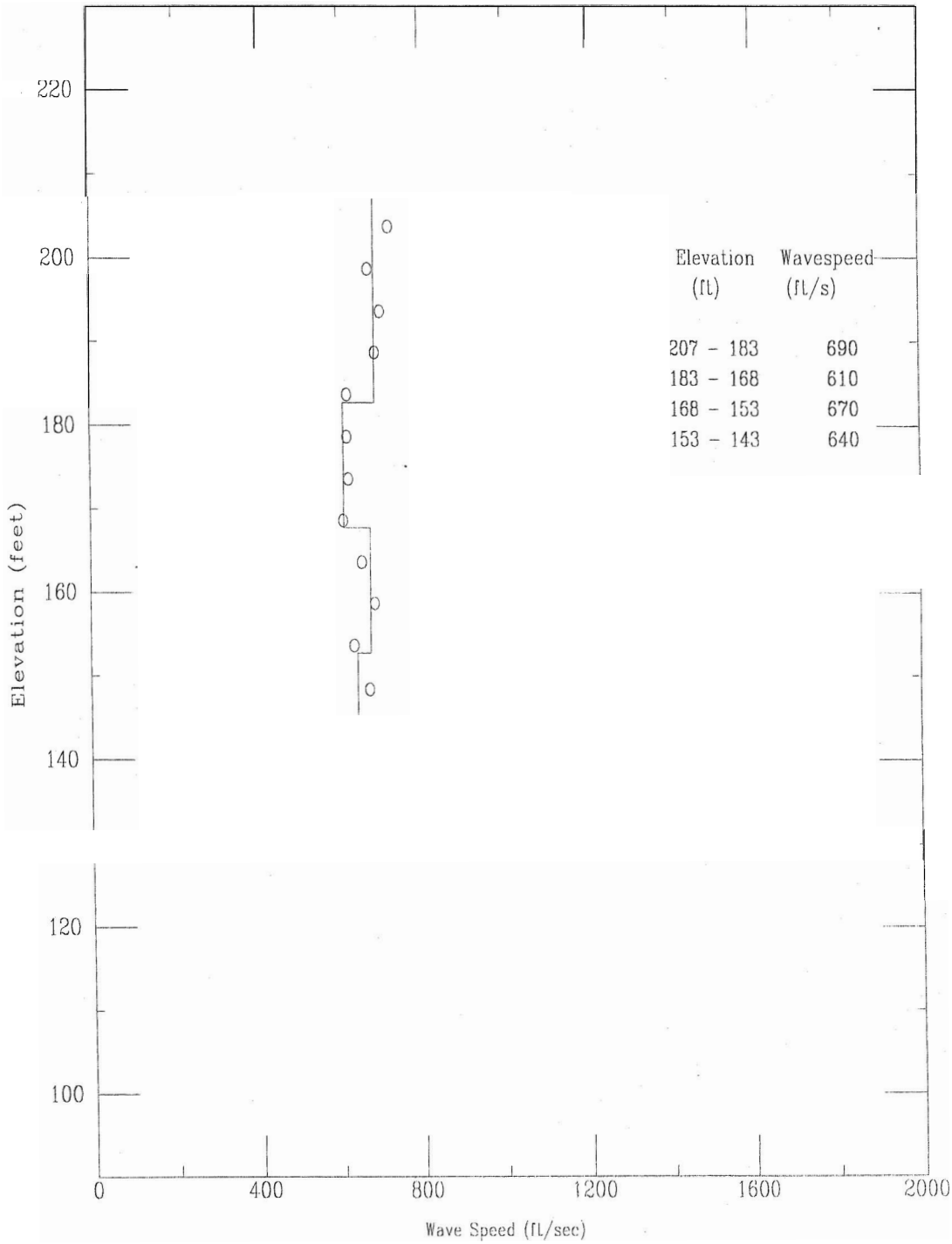

File 208s0501

C-1005 APPLIED RESEARCH ASSOCIATES, INC. 08/Sep/2005

Shear Wave Time of Peak

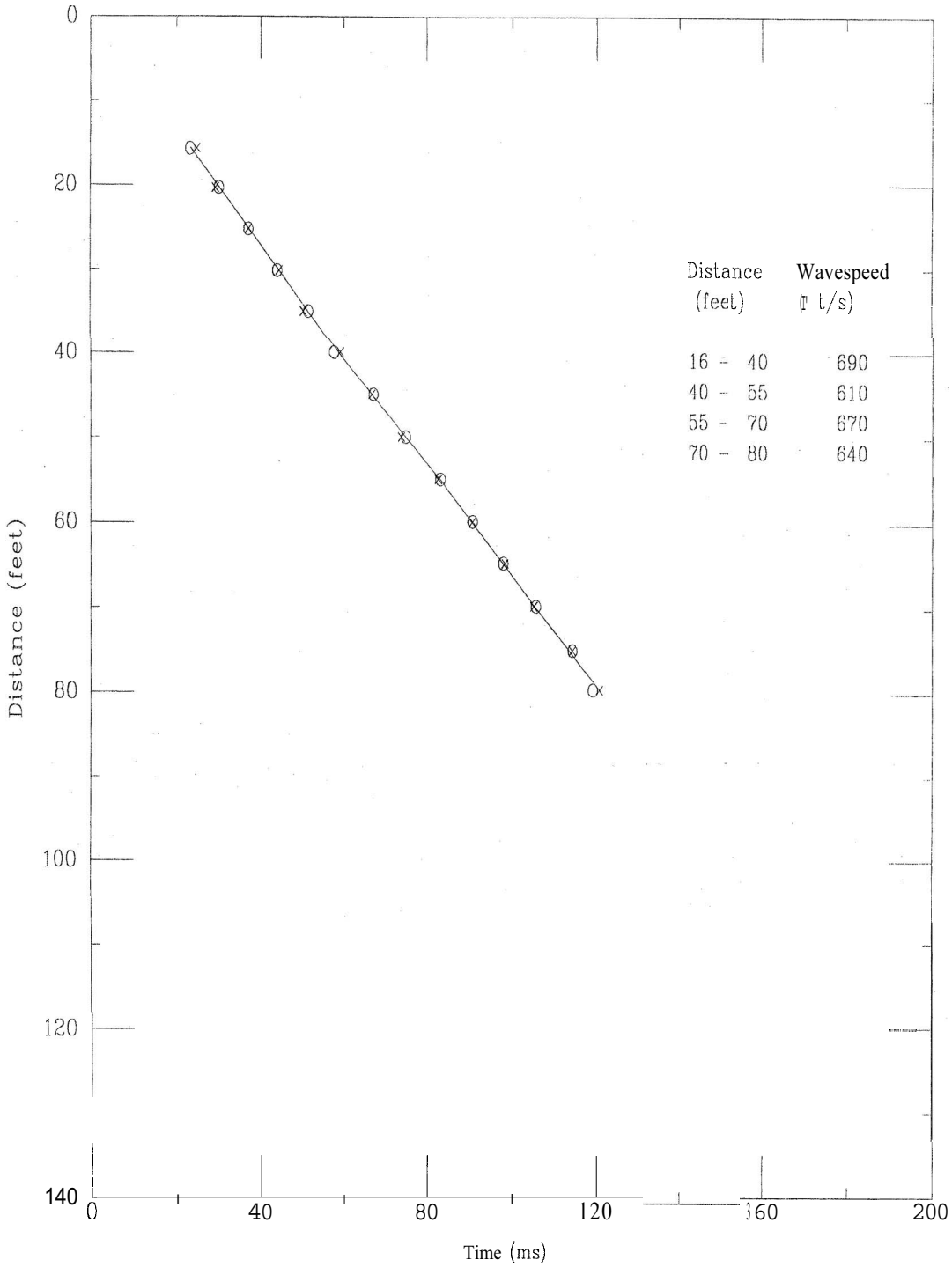

File 208s0501

Applied Research Associales, Inc.
C-1005

S Wave
08/Sep/2005

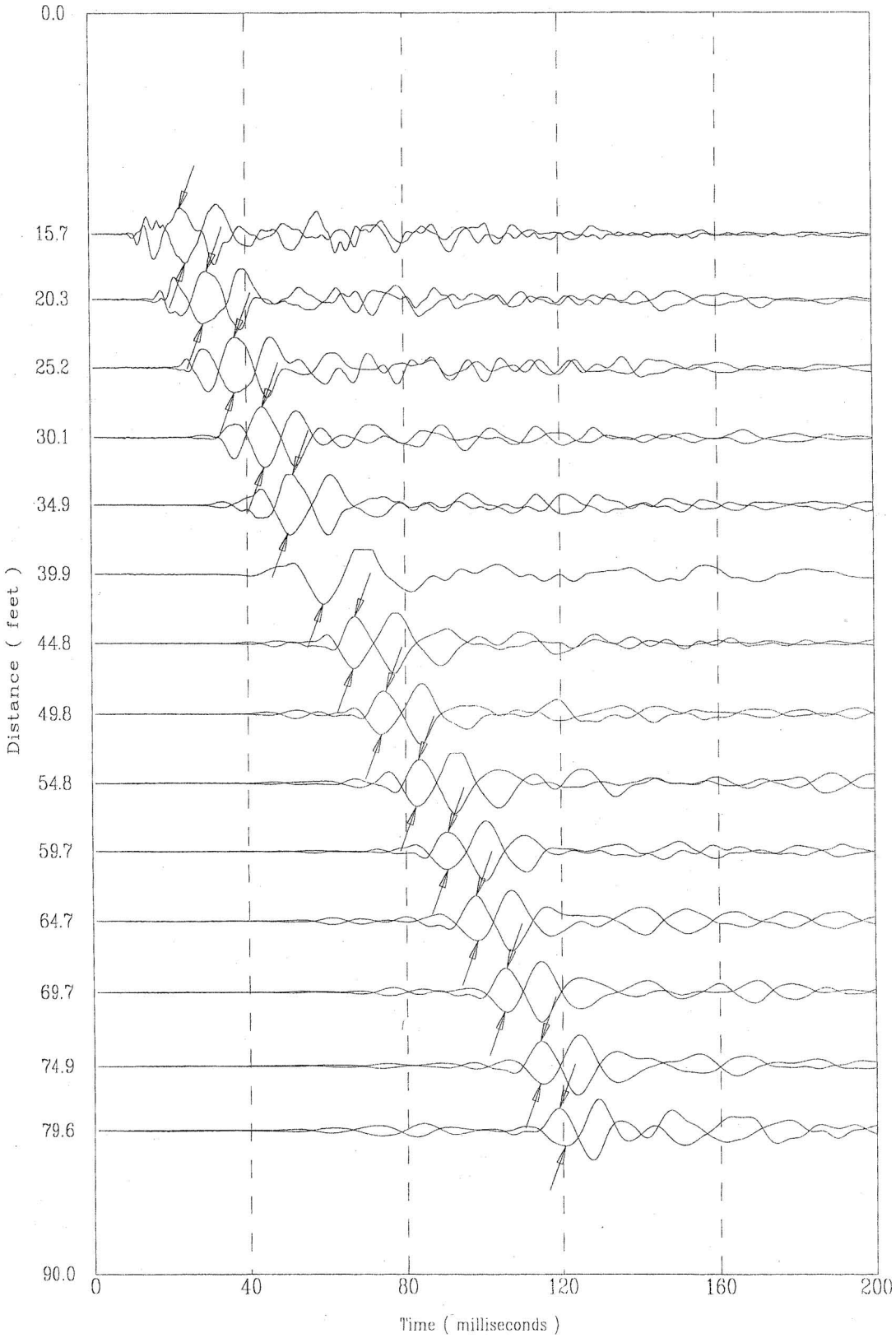

File: 208s0501

Shear Wave Speeds

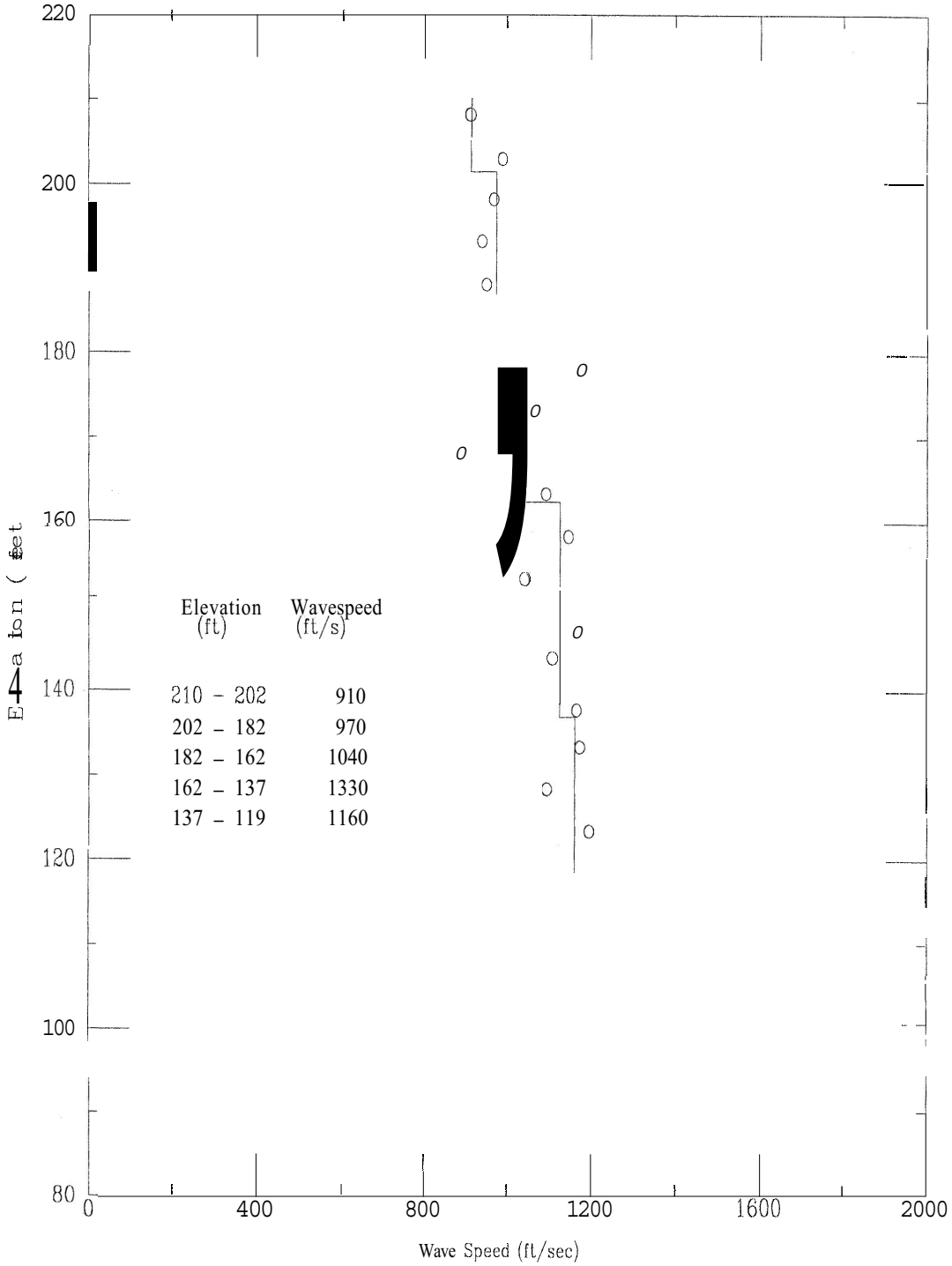

File 207s0505

C-1009 APPLIED RESEARCH ASSOCIATES, INC. 07/Sep/2005

Shear Wave Time of Peak

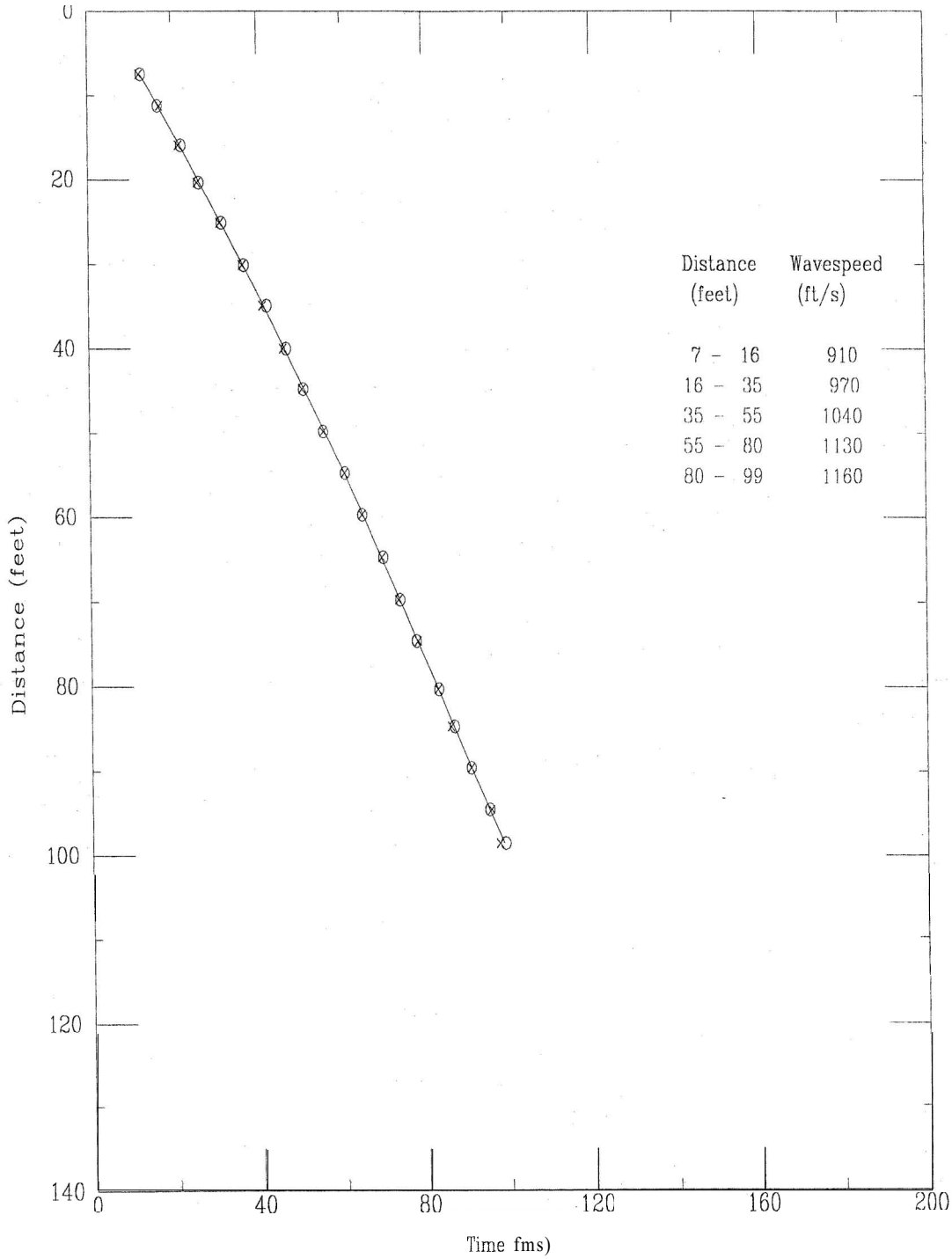

File 207s0505

Applied Research Associates, Inc.
C-1009

S Wave
07/Sep/2005

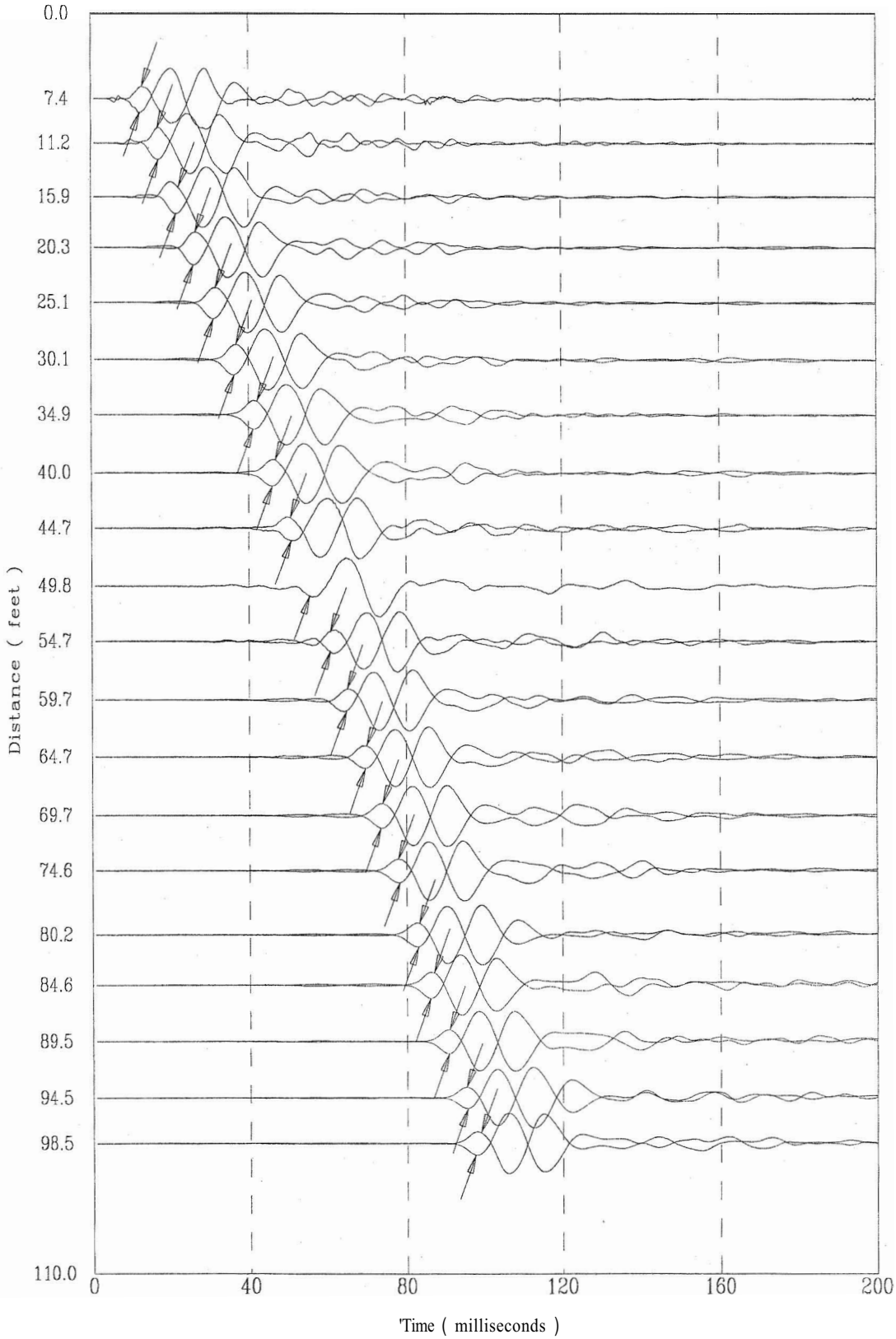

File 207s0505

APPENDIX C

PORE PRESSURE DISSIPATION DATA

MACTEC C-1003

Applied Research Associates, inc. 207S0506D.68

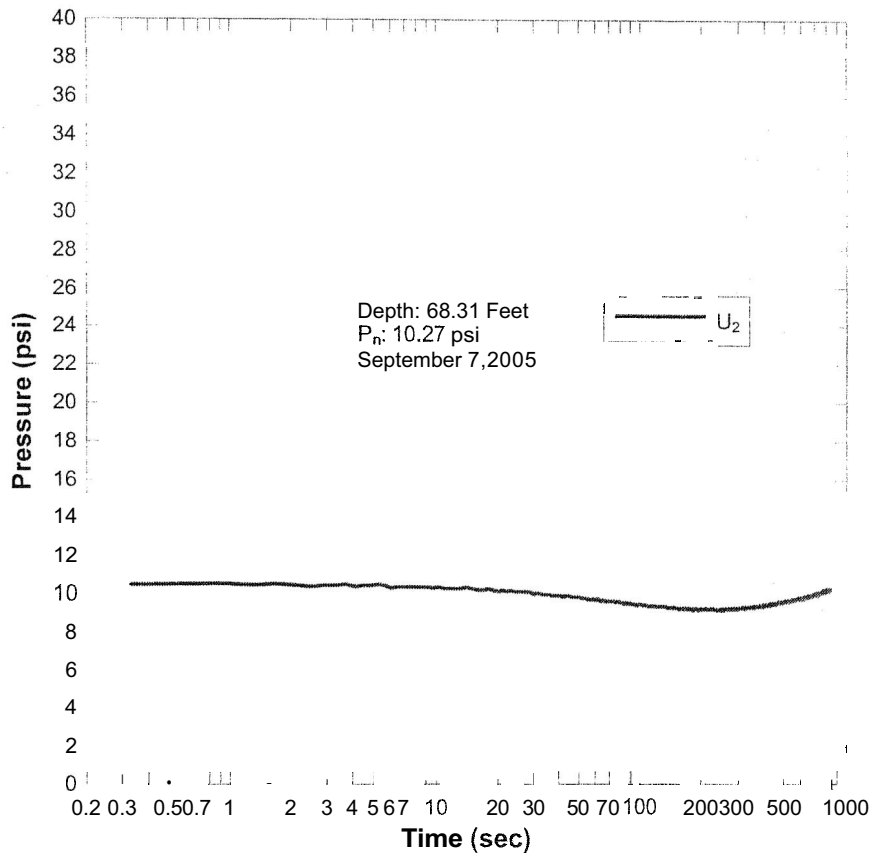

MACTEC C-1003

Applied Research Associates, inc. 207S0506D.79

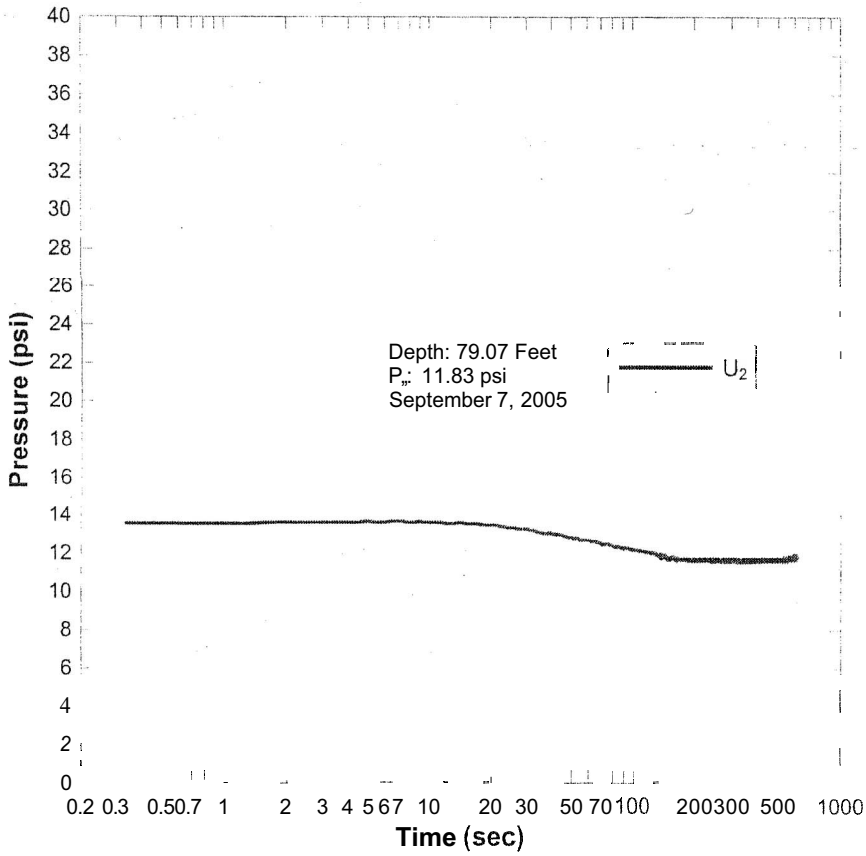

MACTEC C-1004

Applied Research Associates, Inc. 201S0501D.66

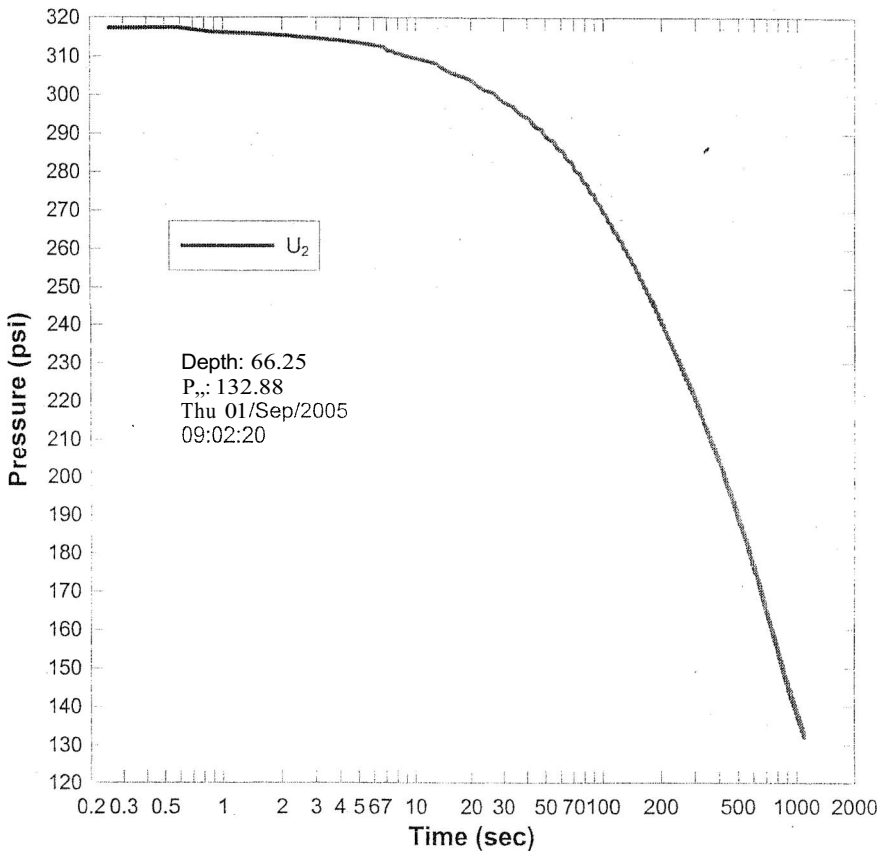

MACTEC C-1005

Applied Research Associates, Inc. 208S0501D.56

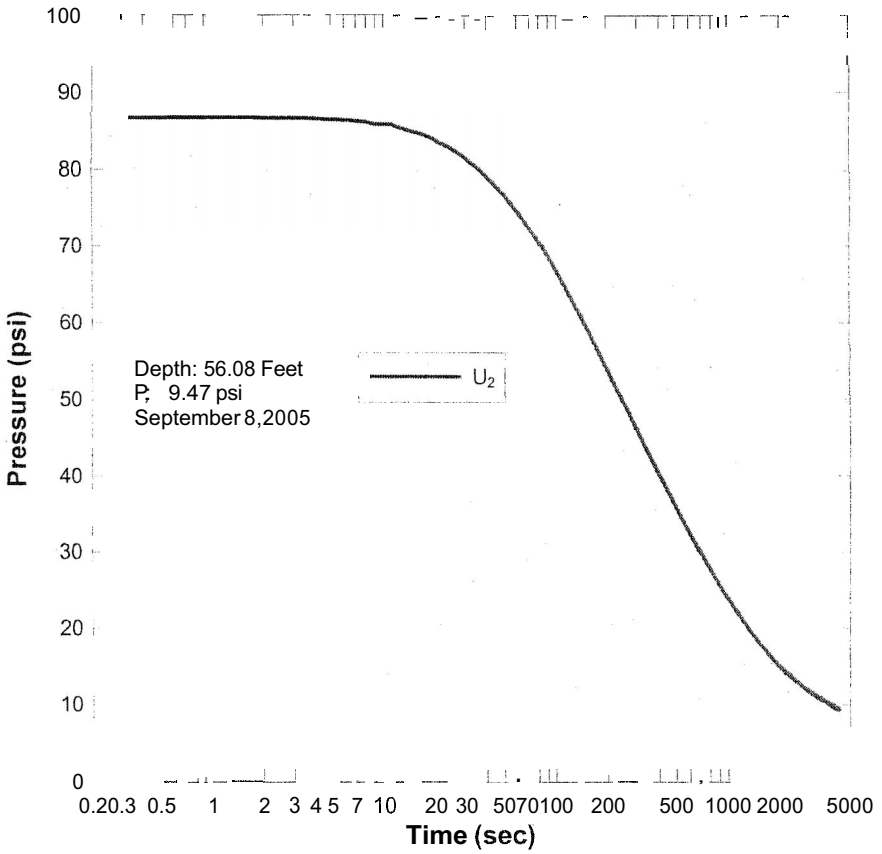

MACTEC C-1005

Applied Research Associates, Inc. 208S0501D.82

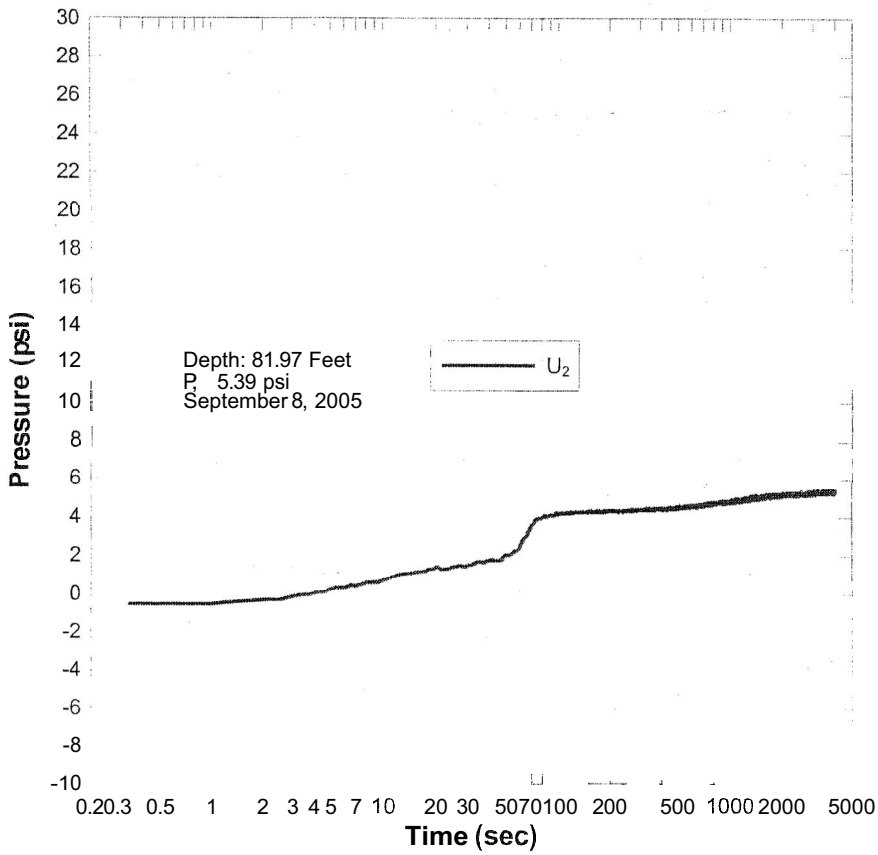

MACTEC C-1005

Applied Research Associates, Inc. 208S0501D.73

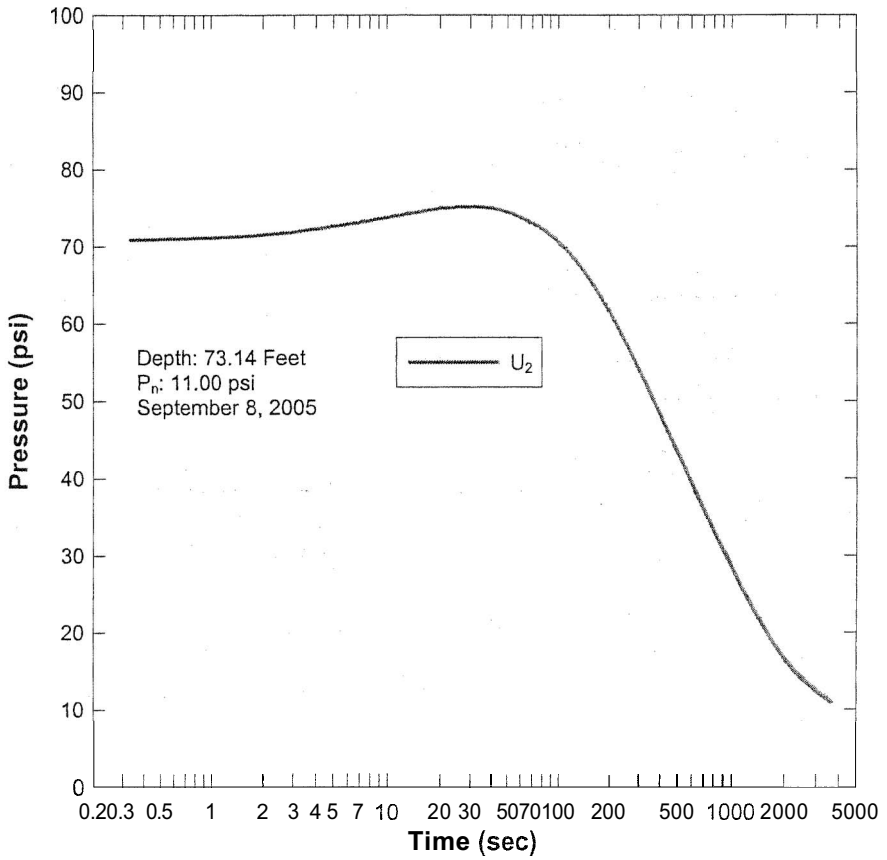

MACTEC **C-1009**

Applied Research Associates, Inc. **207S0505D.60**

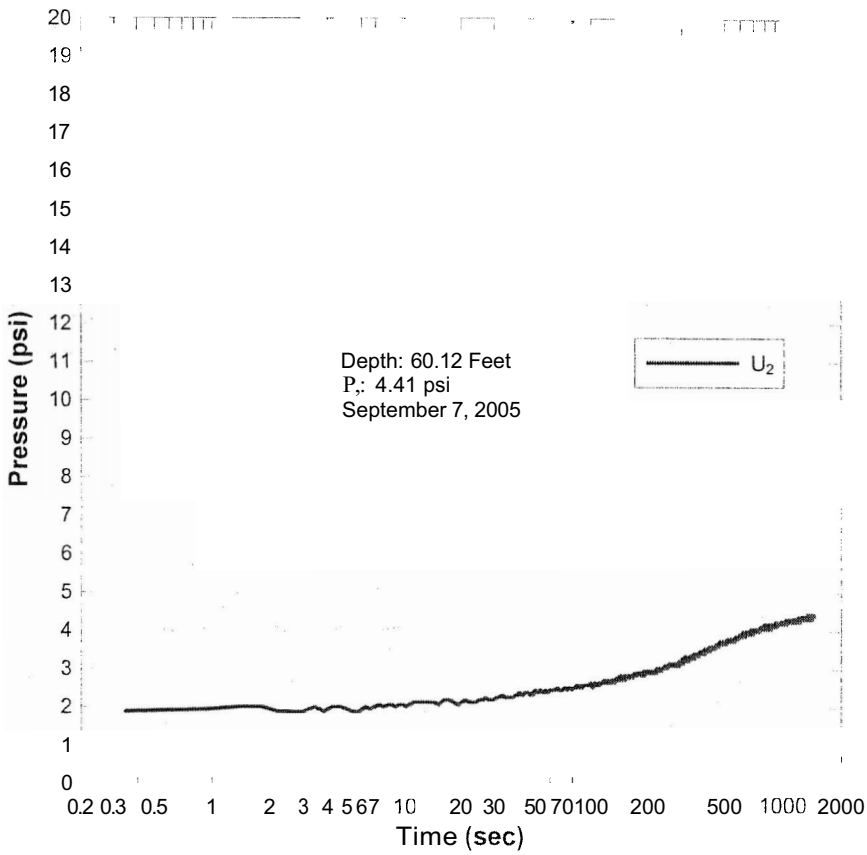

MACTEC **C-1009**

Applied Research Associates, Inc. **207S0505D.77**

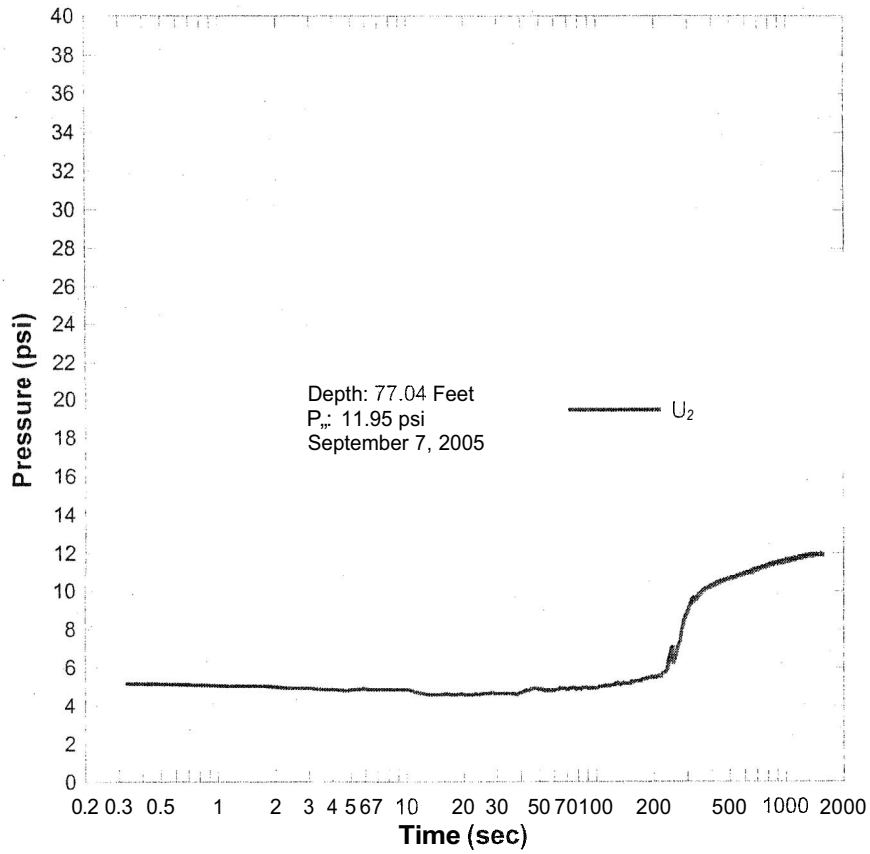

MACTEC C-1009

Applied Research Associates, Inc. 207S0505D.90

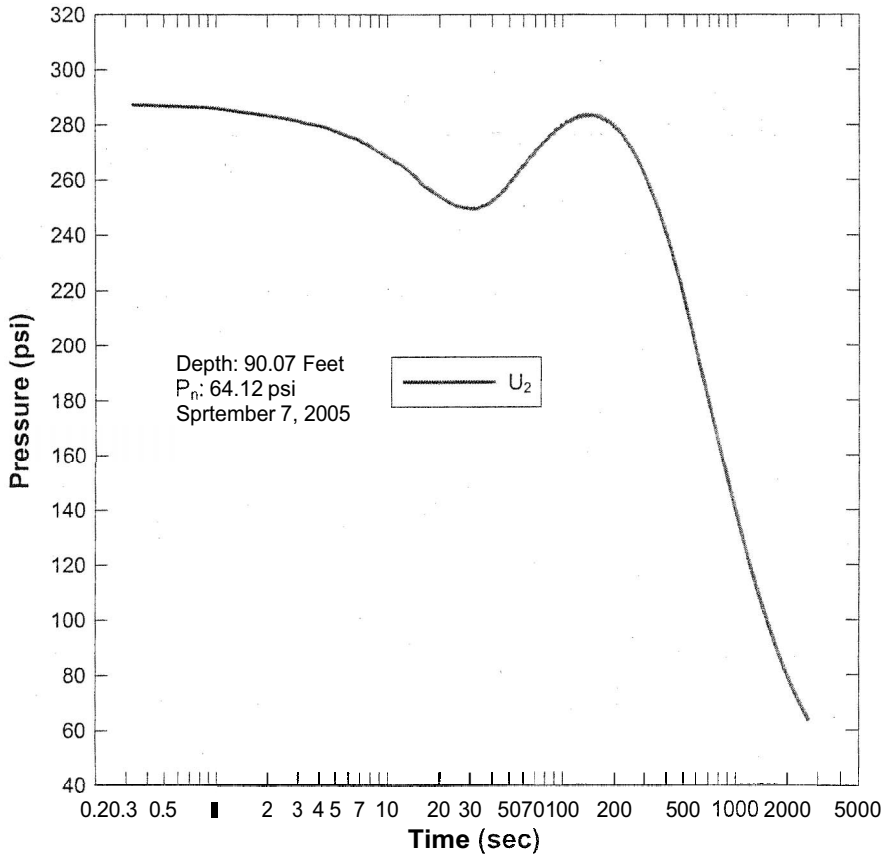

MACTEC **C-1009**

Applied Research Associates, Inc. **207S0505D.99**

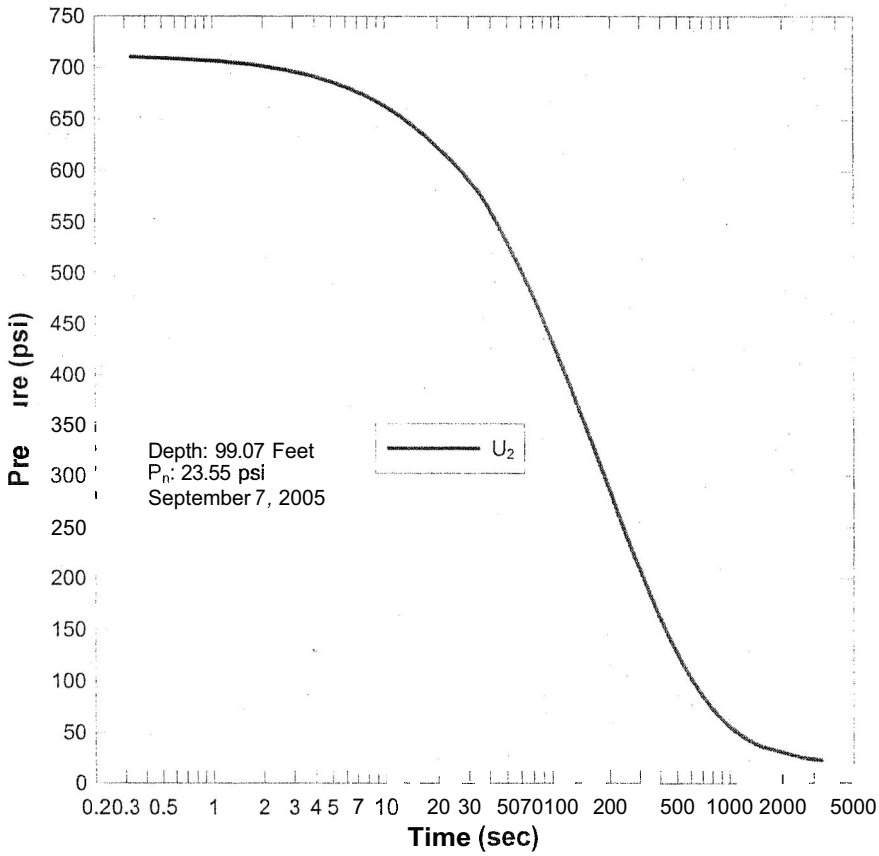

MACTEC

APPENDIX C

REPORT OF
BOREHOLE GEOPHYSICS
By GEOVISION Geophysical Services

GEOVision
geophysical services

VOGTLE ELECTRIC GENERATING PLANT, BOREHOLES B-1002, B-1002A, B-1003, B-1004 AND C-1005A BOREHOLE GEOPHYSICS

December 19, 2005
Report 5492-01 rev a
Volume 4 sf 2 *

* NOTE: VOLUME 2 OF THIS REPORT IS A CDROM CONTAINING THIS REPORT WITH APPENDICES AND DATA IN ELECTRONIC FORMAT.

VOGTLE ELECTRIC GENERATING PLANT, BOREHOLES B-1002, B-1002A, B-1003, B-1004 AND C-1005A BOREHOLE GEOPHYSICS

Prepared for

MACTEC, Inc
396 Plasters Avenue
Atlanta, Georgia 30342
(404) 873-4761
Job 6141-05-0227

Prepared by

GEOVision Geophysical Services
1151 Pomona Road, Unit P
Corona, California 92882
(951) 549-1234
Project 5492

December 19, 2005
Report 5492-01 rev a
Volume 1 of 2

TABLE OF CONTENTS

INTRODUCTION 9

SCOPE OF WORK 10

INSTRUMENTATION 11

Suspension Instrumentation 11

Caliper / Natural Gamma Instrumentation 13

Resistivity / Spontaneous Potential Instrumentation 15

Boring Deviation Instrumentation 16

MEASUREMENT PROCEDURES 17

Suspension Measurement Procedures 17

Caliper / Natural Gamma Measurement Procedures 17

Resistivity / Spontaneous Potential Measurement Procedures 19

Boring Deviation Measurement Procedures 20

DATA ANALYSIS 22

Suspension Analysis 22

Caliper / Natural Gamma Analysis 24

Resistivity / Spontaneous Potential Analysis 24

Boring Deviation Analysis 25

RESULTS 25

Suspension Results 25

Caliper / Natural Gamma Results 26

Resistivity / Spontaneous Potential Results 26

Boring Deviation Results 26

SUMMARY 27

Discussion of Suspension Results 27

Discussion of Caliper / Natural Gamma Results 28

Discussion of Resistivity / Spontaneous Potential Results 28

Discussion of Boring Deviation Results 29

Quality Assurance 29

Suspension Data Reliability 30

FIGURES

Figure 1. Example Calibration Curve for Caliper Probe 18

Figure 2. Concept illustration of long P-S logging system 31

Figure 3. Concept illustration of short P-S logging system 32

Figure 4. Example of filtered (1400 Hz lowpass) record 33

Figure 5. Example of unfiltered record 34

Figure 6. Borings B-1002 and B-1002A, Suspension R1-R2 P- and S_H-wave velocities 35

Figure 7. Boring B-1003, Suspension R1-R2 P- and S_H-wave velocities 37

Figure 8. Boring B-1003, Deviation Projection 38

Figure 9. Boring B-1004, Suspension R1-R2 P- and S_H-wave velocities 43

Figure 10. Boring C-1005A, Suspension R1-R2 P- and S_H-wave velocities 45

TABLES

Table 1. Boring locations and logging dates 10

Table 2. Logging dates and depth ranges 21

Table 3. Boring Bottom Depths and Start / Stop Depth Errors 22

Table 4. Borings B-1002 and B-1002A, Suspension R1-R2 depths and P- and SH-wave velocities 36

Table 5. Boring B-1003, Suspension R1-R2 depths and P- and S_H-wave velocities 39

Table 6. Boring B-1004, Suspension R1-R2 depths and P- and S_H-wave velocities 44

Table 7. Boring C-1005A, Suspension R1-R2 depths and P- and S_H-wave velocities .. 46

APPENDICES

APPENDIX A: Suspension velocity measurement quality assurance suspension source to receiver analysis results 47

APPENDIX A FIGURES

Figure A-1. Borings B-1002 and B-1002A, R1 - R2 high resolution analysis and S-R1 quality assurance analysis P- and SH-wave data 48

Figure A-2. Boring B-1003, R1 - R2 high resolution analysis and S-R1 quality assurance analysis P- and S_H-wave data 50

Figure A-3. Boring B-1004, R1 - R2 high resolution analysis and S-R1 quality assurance analysis P- and S_H-wave data 55

Figure A-4. Boring C-1005A, R1 - R2 high resolution analysis and S-R1 quality assurance analysis P- and S_H-wave data 57

APPENDIX A TABLES

Table A-1. Borings B-1002 and B-1002A, R1 - R2 high resolution analysis and S-R1 quality assurance analysis P- and S_H-wave data 49

Table A-2. Boring B-1003, R1 - R2 high resolution analysis and S-R1 quality assurance analysis P- and S_H-wave data 51

Table A-3. Boring B-1004, R1 - R2 high resolution analysis and S-R1 quality assurance analysis P- and S_H-wave data 56

Table A-4. Boring C-1005A, R1 - R2 high resolution analysis and S-R1 quality assurance analysis P- and S_H-wave data 58

APPENDIX B: OYO Model 170 suspension velocity logging system NIST traceable calibration procedure 59

APPENDIX C: OYO Model 170 suspension velocity logging field measurement procedure..... 64

APPENDIX D: OYO Model 170 suspension velocity logging field data sheets 73

Boring B-1002 Run 1 Suspension velocity logging field data sheets..... 74

Boring B-1002 Run 2 Suspension velocity logging field data sheets..... 80

Boring B-1002A Suspension velocity logging field data sheets..... 83

Boring B-1003 Run 1 Suspension velocity logging field data sheets..... 87

Boring B-1003 Run 2 Suspension velocity logging field data sheets..... 106

Boring B-1003 Run 3 Suspension velocity logging field data sheets..... 114

Boring B-1004 Suspension velocity logging field data sheets 119

Boring C-1005A Suspension velocity logging field data sheets..... 124

APPENDIX E: Geophysical logging field data sheets..... 127

Boring B-1002, B-1002A Caliper, natural gamma, resistivity and spontaneous potential logs 128

Boring B-1003 Caliper, natural gamma, resistivity and spontaneous potential logs 133

Boring B-1004 Caliper, natural gamma, resistivity and spontaneous potential logs 150

APPENDIX F: Boring geophysical logging field data sheets 155

Boring B-1002 Boring geophysical logging field data sheets..... 156

Boring B-1003 Boring geophysical logging field data sheets..... 158

Boring B-1003 Boring geophysical logging field data sheets..... 160

Boring B-1003 Deep Boring geophysical logging field data sheets 162

Boring B-1004 Boring geophysical logging field data sheets..... 166

INTRODUCTION

Boring geophysical measurements were collected in five uncased borings located at the Vogtle Electric Generating Plant Advanced Light Water Reactor, located south of Augusta, Georgia. Suspension logging data acquisition was performed between September 22 and November 11, 2005 by Rob Steller of GEOVision. The work was performed under subcontract with MACTEC, Inc., with Matt Cooke serving as the point of contact for MACTEC.

This report describes the field measurements, data analysis, and results of this work.

SCOPE OF WORK

This report presents the results of boring geophysical measurements collected between September 22 and November 11, 2005, in five uncased borings, as detailed below. The purpose of these studies was to supplement stratigraphic information obtained during MACTEC's soil sampling program and to acquire shear wave velocities and compressional wave velocities as a function of depth, as a component of the Vogtle Electric Generating Plant Advanced Light Water Reactor Early Site Permit Project.

BORING DESIGNATION	DATES LOGGED	ELEVATION	COORDINATES	
			NORTHING	EASTING
B-1002	9/22/05, 9/23/05	221.98	7998.524	6985.474
B-1002A	10/05/05	222.27	7985.618	6986.068
B-1003	10/03/05, 10/22/05, 11/10/05, 11/11/05	223.21	7974.364	7889.853
B-1004	10/04/05	249.78	7985.411	6131.444
C-1005A	10/06/05	223.66	7989.752	8179.263

Table 1. Boring locations and logging dates

The OYO Model 170 Suspension Logging Recorder and Suspension Logging Probe were used to obtain in-situ horizontal shear and compressional wave velocity measurements at 1.6 or 3.3 ft intervals. The acquired data was analyzed and a profile of velocity versus depth was produced for both compressional and horizontally polarized shear waves.

A detailed reference for the velocity measurement techniques used in this study is:

> Guidelines for Determining Design Basis Ground Motions, Report TR-102293, Electric Power Research Institute, Palo Alto, California, November 1993, Sections 7 and 8.

INSTRUMENTATION

Suspension Instrumentation

Suspension soil velocity measurements were performed using the Model 170 suspension logging system, S/N 19029, manufactured by OYO Corporation. This system directly determines the average velocity of a 3.3 ft high segment of the soil column surrounding the boring of interest by measuring the elapsed time between arrivals of a wave propagating upward through the soil column. The receivers that detect the wave, and the source that generates the wave, are moved as a unit in the boring producing relatively constant amplitude signals at all depths.

The suspension system probe consists of a combined reversible polarity solenoid horizontal shear-wave source (S_H) and compressional-wave source (P), joined to two biaxial receivers by a flexible isolation cylinder, as shown in Figure 1. The separation of the two receivers is 3.3 ft, allowing average wave velocity in the region between the receivers to be determined by inversion of the wave travel time between the two receivers. Initial runs were performed in B-1002 using a shorter 19 ft probe configuration on September 22, 2005, but due to observed high amplitude signals, and the possibility of saturation of the receivers by those high amplitude signals, the longer 22 ft configuration was used for all subsequent measurements. Throughout the text, dimensions for the longer 22 ft configuration, as shown in Figure 1, will be given, followed by dimensions for the shorter configuration, as shown in Figure 2, enclosed in parenthesis. The total length of the probe as used in these surveys is 22 (19) ft, with the center point of the receiver pair 15.4 (12.1) ft above the bottom end of the probe.

The probe receives control signals from, and sends the amplified receiver signals to, instrumentation on the surface via an armored 4 conductor cable. The cable is wound onto the drum of a winch and is used to support the probe. Cable travel is measured to provide probe depth data, using a 3.28 ft diameter sheave fitted with a digital rotary encoder.

The entire probe is suspended by the cable and centered in the boring by nylon "whiskers", therefore, source motion is not coupled directly to the boring walls; rather, the source motion

creates a horizontally propagating impulsive pressure wave in the fluid filling the boring and surrounding the source. This pressure wave is converted to P and S_H-waves in the surrounding soil and rock as it passes through the casing and grout annulus and impinges upon the wall of the boring. These waves propagate through the soil and rock surrounding the boring, in turn causing a pressure wave to be generated in the fluid surrounding the receivers as the soil waves pass their location. Separation of the P and S_H-waves at the receivers is performed using the following steps:

1. Orientation of the horizontal receivers is maintained parallel to the axis of the source, maximizing the amplitude of the recorded S_H -wave signals.
2. At each depth, S_H-wave signals are recorded with the source actuated in opposite directions, producing S_H-wave signals of opposite polarity, providing a characteristic S_H-wave signature distinct from the P-wave signal.
3. The 10.4 (7.02) ft separation of source and receiver 1 permits the P-wave signal to pass and damp significantly before the slower S_H-wave signal arrives at the receiver. In faster soils or rock, the isolation cylinder is extended to allow greater separation of the P- and S_H-wave signals.
4. In saturated soils, the received P-wave signal is typically of much higher frequency than the received S_H-wave signal, permitting additional separation of the two signals by low pass filtering.
5. Direct arrival of the original pressure pulse in the fluid is not detected at the receivers because the wavelength of the pressure pulse in fluid is significantly greater than the dimension of the fluid annulus surrounding the probe (meter versus centimeter scale), preventing significant energy transmission through the fluid medium.

In operation, a distinct, repeatable pattern of impulses is generated at each depth as follows:

1. The source is fired in one direction producing dominantly horizontal shear with some vertical compression, and the signals from the horizontal receivers situated parallel to the axis of motion of the source are recorded.
2. The source is fired again in the opposite direction and the horizontal receiver signals are recorded.
3. The source is fired again and the vertical receiver signals are recorded. The repeated source pattern facilitates the picking of the P and S_H-wave arrivals; reversal of the source changes the polarity of the S_H-wave pattern but not the P-wave pattern.

The data from each receiver during each source activation is recorded as a different channel on the recording system. The Model 170 has six channels (two simultaneous recording channels), each with a 12 bit 1024 sample record. The recorded data is displayed on a CRT display and on paper tape output as six channels with a common time scale. Data is stored on 3.5 inch floppy diskettes for further processing. Up to 8 sampling sequences can be summed to improve the signal to noise ratio of the signals.

Review of the displayed data on the CRT or paper tape allows the operator to set the gains, filters, delay time, pulse length (energy), sample rate, and summing number to optimize the quality of the data before recording. Verification of the calibration of the Model 170 digital recorder is performed every twelve months using a NIST traceable frequency source and counter, as outlined in Appendix B.

Caliper / Natural Gamma Instrumentation

Caliper and natural gamma data were collected using a Model 3ACS 3-leg caliper probe, S/N 2915, manufactured by Robertson Geologging, Ltd. With the short arm configuration used in these surveys, the probe permits measurement of boring diameters between 1.6 - 12 in., concurrent with measurement of natural gamma emission from the boring walls. The probe is 6.82 ft long, and 1.5 inches in diameter.

This probe is useful in the following studies:

- Measurement of boring diameter and volume
- Location of hard and soft formations
- Location of fissures, caving, pinching and casing damage
- Bed boundary identification
- Strata correlation between borings

The probe receives control signals from, and sends the digitized measurement values to, a Robertson Micrologger II, S/N 5310, on the surface via an armored 4 conductor cable. The cable is wound onto the drum of a winch and is used to support the probe. Cable travel is measured to provide probe depth data, using a 3.28 ft diameter sheave fitted with a digital rotary encoder. The probe and depth data are transmitted by USB link from the Micrologger unit to a laptop computer where it is displayed and stored on hard disk.

The caliper consists of three arms, each with a toothed quadrant at their base, pivoted in the lower probe body. A toothed rack engages with each quadrant, thus constraining the arms to move together. Linear movement of the rack is converted to opening and closing of the arms. Springs hold the arms open in the operating position. A motor drive is provided to retract the arms, allowing the probe to be lowered into the boring. The rack is coupled to a potentiometer which converts movement into a voltage sensed by the probe's microprocessor.

Natural gamma measurements rely upon small quantities of radioactive material contained in all rocks to emit gamma radiation as they decay. Trace amounts of Uranium and Thorium are present in a few minerals, where potassium-bearing minerals such as feldspar, mica and clays will include traces of a radioactive isotope of Potassium. These emit gamma radiation as they decay with an extremely long half-life. This radiation is detected by scintillation - the production of a tiny flash of light when gamma rays strike a crystal of sodium iodide. The light is converted into an electrical pulse by a photomultiplier tube. Pulses above a threshold value of 60 KeV are counted by the probe's microprocessor. The measurement is useful because the radioactive elements are concentrated in certain rock types e.g. clay or shales, and depleted in others e.g. sandstone or coal.

Resistivity / Spontaneous Potential Instrumentation

Resistivity, spontaneous potential and natural gamma data were collected using a Model ELXG electric log probe, S/N 3040, manufactured by Robertson Geologging, Ltd. This probe measures Single Point Resistance (SPR), short normal resistivity (16”), long normal resistivity (64”), Spontaneous Potential (SP) and natural gamma. The probe is 8.20 ft long, and 1.73 inches in diameter.

This probe is useful in the following studies:

- Bed boundary identification
- Strata correlation between borings
- Strata geometry and type (shale indication)

The probe receives control signals from, and sends the digitized measurement values to, a Robertson Micrologger II, S/N 5310, on the surface via an armored 4 conductor cable. The cable is wound onto the drum of a winch and is used to support the probe. Cable travel is measured to provide probe depth data, using a 3.28 ft diameter sheave fitted with a digital rotary encoder. The probe and depth data are transmitted by USB link from the Micrologger unit to a laptop computer where it is displayed and stored on hard disk.

The resistivity section of the probe operates by driving an alternating current into the formation from the central SPR/DRIVE electrode. The current returns via the logging cable armor. To ensure adequate penetration of the formation the logging cable is insulated for approximately 30 feet from the cablehead. Voltages are measured between the 16" and 64" electrodes and the remote earth connection at surface, as noted below:

- Single Point Resistance (SPR): The current flowing to the cable armor is measured along with the voltage at the SPR electrode. The voltage divided by current gives resistance.

- Spontaneous Potential (SP): This is the DC bias of the 16" electrode with respect to the voltage return at the surface (ground stake).

Data quality depends upon good grounding at the surface. This is achieved with a metal stake driven into the mud-pit.

Natural gamma data was collected during the caliper data run, so this function, though present in this probe, was not used during these logging runs.

Boring Deviation Instrumentation

Boring deviation data were collected using a Model HIRAT High Resolution Acoustic Televiewer probe, S/N 5174, manufactured by Robertson Geologging, Ltd. This probe is generally used to acquire acoustic images of the boring wall, but may also be used to collect boring deviation data. The probe is 7.58 ft long, and 1.9 inches in diameter, and is fitted with upper and lower four-arm centralizers.

This probe is useful in the following studies:

- Measurement of boring diameter and volume
- Location of hard and soft formations
- Location of fissures, caving, pinching and casing damage
- Bed boundary identification
- Strata correlation between borings

The probe receives control signals from, and sends the digitized measurement values to, a Robertson Micrologger II, S/N 5310, on the surface via an armored 4 conductor cable. The cable is wound onto the drum of a winch and is used to support the probe. Cable travel is measured to provide probe depth data, using a 3.28 ft diameter sheave fitted with a digital rotary encoder. The probe and depth data are transmitted by USB link from the Micrologger unit to a laptop computer where it is displayed and stored on hard disk.

MEASUREMENT PROCEDURES

Suspension Measurement Procedures

All five borings were logged as uncased borings, filled with bentonite or polymer based drilling mud. Measurements followed the GEOVision standard field procedures, as presented in Appendix C. Prior to use, the measuring sheave and rotary encoder function were checked using a steel tape by Jay Fagan of MACTEC. In each boring, the probe was positioned with the mid-point of the receiver spacing at grade, and the electronic depth counters were set to zero. The probe was lowered to the bottom of the boring, and then returned to the surface, stopping at 1.6 ft or 3.3 ft intervals to collect data, as summarized in Table 2, below.

At each measurement depth the measurement sequence of two opposite horizontal records and one vertical record was performed, and the gains were adjusted as required. The data from each depth was printed on paper tape, checked, and recorded on diskette before moving to the next depth.

Upon completion of the measurements, the probe zero depth indication at grade was verified prior to removal from the boring.

Caliper / Natural Gamma Measurement Procedures

Caliper and natural gamma data were collected in Borings B-1002, B-1003 and B-1004. No caliper or natural gamma data was collected in C-1005A. No caliper data was collected in B-1002A either, however, natural gamma data for the shallow (dry) sections of B-1002 and B-1004 were collected through the PVC casing, as summarized in Table 2, below. With the preceding two exceptions, the borings were logged as uncased borings, filled with bentonite or polymer based drilling mud.

Prior to use, the caliper tool was calibrated, using the supplied three point calibration jig, which is a circular plate with a series of holes in the top surface into which the tips of the caliper arms fit. This has circles of diameters from 2" to 12", as verified using a NIST traceable caliper by

Jay Fagan of MACTEC. Alternatively, it is possible to use pipe sections of known internal diameter. The calibration jig is placed over a bucket with the probe standing upright with its nose section passing through the jig's central hole. The caliper probe arms are opened under program control, and the tips of the arms are placed in the holes marked with the required diameter. the value of the current calibration point, as stamped on the jig, is entered via the control computer. The system counts for 15 seconds to make an average of the response. The procedure is repeated for the second and third required openings.

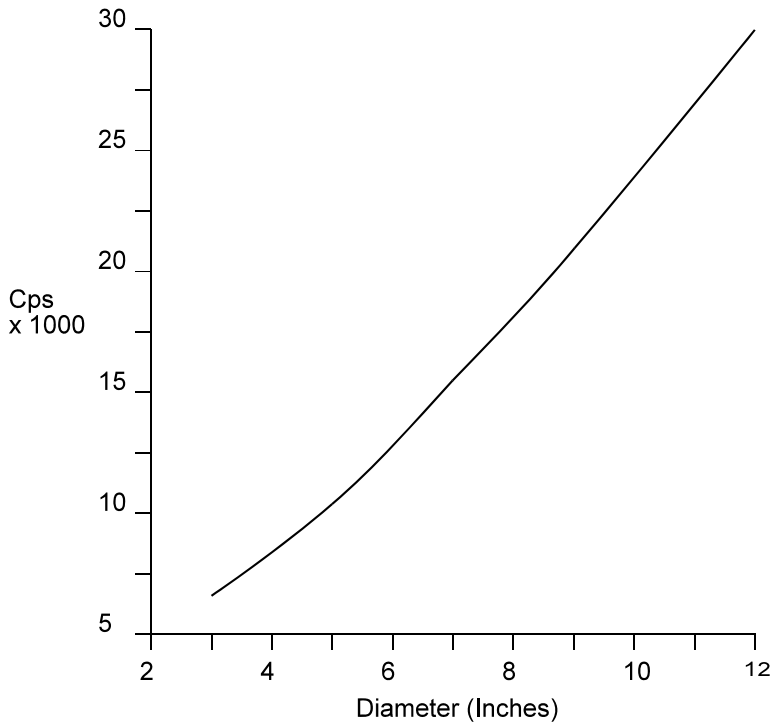

Figure 1. Example Calibration Curve for Caliper Probe

The computation and generation of the calibration coefficient file is entirely automatic. The calibration file is simply the set of coefficients of a quadratic curve which fits the three data points. Figure 1 shows the response of a caliper probe using data gathered during calibration. In addition, the caliper calibration is effectively checked at the end of each run by measuring the inside diameter of the casing at the top of the boring. Natural gamma was not calibrated in the field, as it is a qualitative measurement, not a quantitative value, and is used only to assist in picking transitions between stratigraphic units.

In each boring, the probe was positioned with the top of the probe at grade, and the electronic depth counter was set to 6.82 ft, the specified length of the probe, as verified with a tape measure. The probe was lowered to the bottom of the boring, where the caliper legs were opened, and data collection begun. The probe was then returned to the surface at 9.8 ft/sec, collecting data continuously at 0.033 ft spacing, as summarized in Table 2, below.

Upon completion of the measurements, the probe zero depth indication at grade was verified prior to removal from the boring, as summarized in Table 3, below.

Resistivity / Spontaneous Potential Measurement Procedures

Resistivity and spontaneous potential data were collected in Borings B-1002, B-1003 and B-1004. No resistivity or spontaneous potential data was collected in B-1002A or C-1005A.

After attaching the probe to the logging cable, the probe head was insulated by wrapping all exposed metal of the cablehead and probe with self-amalgamating insulation tape. The 30 ft insulating sleeve on the logging cable was checked for any damage, and repaired with self-amalgamating insulation tape as needed.

The reference ground stake was driven firmly into the mud pit, and connected to the ground socket on the winch switch box.

This sonde measures real units downhole, so there is no calibration procedure to be followed for these channels.

In each boring, the probe was positioned with the top of the probe at grade, and the electronic depth counter was set to 8.2 ft, the specified length of the probe, as verified with a tape measure. The probe was lowered to the bottom of the boring, where data collection was begun. The probe was then returned to the surface at 16.4 ft/sec, collecting data continuously at 0.033 ft spacing, as summarized in Table 2, below. The natural gamma data collected in this log is redundant with

the data collected in the caliper / natural gamma log, so the slower 9.8 ft/sec speed used to optimize natural gamma data resolution was not employed for this log.

When the uninsulated section of the logging cable left the boring fluid, or entered steel casing, the log was terminated, as the sonde does not function under these conditions.

Upon completion of the measurements, the probe zero depth indication at grade was verified prior to removal from the boring, as summarized in Table 3, below.

Boring Deviation Measurement Procedures

Boring deviation data was collected only in B-1003, to a depth of 1072.8 ft. The deeper section of B-1003 was not logged with this tool due to the significant voids and fractures observed on the caliper log of that section. It was decided that the risk of probe loss was too great to justify attempting such a log. Data was collected in a bentonite based drilling mud.

Prior to use, the deviation probe tiltmeters and compass function were checked by hanging from the drill rig and by comparison with a Brunton surveyors' compass.

The probe was positioned with the tip of the probe at grade, and the electronic depth counter was set to 0.0 ft. The probe was lowered to the bottom of the boring, and data collection begun. The probe was then returned to the surface at 9.8 ft/sec, collecting data continuously at 0.033 ft spacing, as summarized in Table 2, below.

Upon completion of the measurements, the probe zero depth indication at grade was verified prior to removal from the boring, as summarized in Table 3, below.

BORING NUMBER	TOOL AND RUN NUMBER	DEPTH RANGE (FEET)	OPEN HOLE (FEET)	DEPTH TO BOTTOM OF CASING (FEET)	SAMPLE INTERVAL (FEET)	DATE LOGGED
B-1002	SUSPENSION 1	88.6 – 242.8	258	88.5	1.6	9/22/05
B-1002	CALIPER 1	0 – 254.8	258	88.5	0.033	9/22/05
B-1002	ELOG 1	86.3 – 256.5	258	88.5	0.033	9/23/05
B-1002	SUSPENSION 2	1.64 - 54.1	70	NO CASING	1.6	9/23/05
B-1002	ELOG 2	3.3 – 69.9	70	NO CASING	0.033	9/23/05
B-1002A	SUSPENSION 1	49.2 – 68.9	85	NO CASING	1.6	10/5/05
B-1003	SUSPENSION 1	64.0 – 157.5	1074	88.0	1.6	10/3/05
B-1003	SUSPENSION 1	157.5 – 1033.5	1074	88.0	3.3	10/3/05
B-1003	SUSPENSION 1	1033.5 – 1061.4	1074	88.0	1.6	10/3/05
B-1003	CALIPER 1	0 – 1076.3	1074	88.0	0.033	10/3/05
B-1003	ELOG 1	DATA LOST	1074	88.0	0.033	10/3/05
B-1003	DEVIATION 1	0 – 1072.8	1074	88.0	0.033	10/3/05
B-1003	ELOG 2	82.9 – 1062.1	1065	88.0	0.033	10/22/05
B-1003	SUSPENSION 2	1053.2 – 1309.1	1324	1054	1.6	11/10/05
B-1003	CALIPER 2	1051.7 – 1324.2	1324	1054	0.033	11/10/05
B-1003	ELOG 3	1050.1 – 1324.0	1324	1054	0.033	11/10/05
B-1003	SUSPENSION 3	1302.5 – 1327.1	1338	1054	1.6	11/11/05
B-1004	SUSPENSION 1	134.5 – 285.8	302	135	1.6	10/4/05
B-1004	CALIPER 1	0 – 303.4	302	135	0.033	10/4/05
B-1004	ELOG 1	118.2 – 303.4	302	135	0.033	10/4/05
C-1005A	SUSPENSION 1	3.3 – 32.8	48	NO CASING	1.6	10/6/05

Table 2. Logging dates and depth ranges

BORING NUMBER	TOOL AND RUN NUMBER	TOOL HIT BOTTOM (FT)	DRILLER DEPTH (FT)	START DEPTH (FT)	END DEPTH (FT)	DEPTH BUST (FT)
B-1002	SUSPENSION 1	254.9	260	0.0	0.07	0.07
B-1002	CALIPER 1	254.8	260	6.82	6.89	0.07
B-1002	ELOG 1	256.5	260	8.20	8.20	0.0
B-1002	SUSPENSION 2	69.5	70	0.0	0.0	0.0
B-1002	ELOG 2	69.9	70	8.20	8.20	0.0
B-1002A	SUSPENSION 1	84.3	105	0.0	0.0	0.0
B-1003	SUSPENSION 1	1076.8	1074	6.56	5.94	-0.38
B-1003	CALIPER 1	1079.1	1074	6.82	6.61	-0.22
B-1003	ELOG 1	1078.4	1074	8.20	8.07	-0.13
B-1003	DEVIATION 1	1072.8	1074	0.0	0.3	0.3
B-1003	ELOG 2	1062.1	1060	8.20	8.02	-0.18
B-1003	SUSPENSION 2	1324.5	1324	172.08	171.82	-0.26
B-1003	CALIPER 2	1324.2	1324	172.34	172.01	-0.33
B-1003	ELOG 3	1324.2	1324	173.72	173.23	-0.49
B-1003	SUSPENSION 3	1342.5	1338	168.5	168.0	-0.5
B-1004	SUSPENSION 1	301.2	302	0.0	0.0	0.0
B-1004	CALIPER 1	304.1	302	6.82	6.80	-0.02
B-1004	ELOG 1	304.1	302	8.20	8.20	0.0
C-1005A	SUSPENSION 1	48.2	90	0.0	0.0	0.0

Table 3. Boring Bottom Depths and Start / Stop Depth Errors

DATA ANALYSIS

Suspension Analysis

Using the proprietary OYO program PSLOG.EXE version 1.0, included in volume 2 of 2 (CDR) of this report, the recorded digital waveforms were analyzed to locate the most prominent first minima, first maxima, or first break on the vertical axis records, indicating the arrival of P-wave energy. The difference in travel time between receiver 1 and receiver 2 (R1-R2) arrivals was used to calculate the P-wave velocity for that 3.3 ft segment of the soil column. When observable, P-wave arrivals on the horizontal axis records were used to verify the velocities determined from the vertical axis data. The time picks were then transferred into an EXCEL template (EXCEL version 2003 SP2) to complete the velocity calculations based upon the arrival

time picks made in PSLOG. The PSLOG pick files and the EXCEL analysis files are included in the boring specific directories on volume 2 of 2 (CDR) of this report.

The P-wave velocity over the 10.4 (7.02) ft interval from source to receiver 1 (S-R1) was also picked using PSLOG, and calculated and plotted in EXCEL, for quality assurance of the velocity derived from the travel time between receivers. In this analysis, the depth values as recorded were increased by 6.79 (5.15) ft to correspond to the mid-point of the 10.4 (7.02) ft S-R1 interval, as illustrated in Figure 1. Travel times were obtained by picking the first break of the P-wave signal at receiver 1 and subtracting 3.0 milliseconds, the calculated and experimentally verified delay from source trigger pulse (beginning of record) to source impact. This delay corresponds to the duration of acceleration of the solenoid before impact.

As with the P-wave records, using PSLOG, the recorded digital waveforms were analyzed to locate the presence of clear S_H-wave pulses, as indicated by the presence of opposite polarity pulses on each pair of horizontal records. Ideally, the S_H-wave signals from the 'normal' and 'reverse' source pulses are very nearly inverted images of each other. Digital FFT - IFFT lowpass filtering was used to remove the higher frequency P-wave signal from the S_H-wave signal. Different filter cutoffs were used to separate P- and S_H-waves at different depths, ranging from 600 Hz in the slowest zones to 4000 Hz in the regions of highest velocity. At each depth, the filter frequency was selected to be at least twice the fundamental frequency of the S_H-wave signal being filtered.

Generally, the first maxima were picked for the 'normal' signals and the first minima for the 'reverse' signals, although other points on the waveform were used if the first pulse was distorted. The absolute arrival time of the 'normal' and 'reverse' signals may vary by +/- 0.2 milliseconds, due to differences in the actuation time of the solenoid source caused by constant mechanical bias in the source or by boring inclination. This variation does not affect the R1-R2 velocity determinations, as the differential time is measured between arrivals of waves created by the same source actuation. The final velocity value is the average of the values obtained from the 'normal' and 'reverse' source actuations.

As with the P-wave data, S_H-wave velocity calculated from the travel time over the 10.4 ft interval from source to receiver 1 was calculated and plotted for verification of the velocity

derived from the travel time between receivers. In this analysis, the depth values were increased by 6.79 (5.15) ft to correspond to the mid-point of the 10.4 (7.02) ft S-R1 interval. Travel times were obtained by picking the first break of the S_H-wave signal at the near receiver and subtracting 3.0 milliseconds, the calculated and experimentally verified delay from the beginning of the record at the source trigger pulse to source impact.

These data and analysis were reviewed by John Diehl as a component of GEOVision's in-house QA-QC program, and by Dr. Richard Lee, as an independent expert review.

Figure 2 shows an example of R1 - R2 measurements on a sample filtered suspension record. In Figure 2, the time difference over the 3.3 ft interval of 1.88 milliseconds for the horizontal signals is equivalent to an S_H-wave velocity of 1745 ft/sec. Whenever possible, time differences were determined from several phase points on the S_H-waveform records to verify the data obtained from the first arrival of the S_H-wave pulse. Figure 3 displays the same record before filtering of the S_H-waveform record with a 1400 Hz FFT - IFFT digital lowpass filter, illustrating the presence of higher frequency P-wave energy at the beginning of the record, and distortion of the lower frequency S_H-wave by residual P-wave signal.

Caliper / Natural Gamma Analysis

No analysis is required with the caliper or natural gamma data. The data are converted to LAS format and transmitted to the client.

Resistivity / Spontaneous Potential Analysis

No analysis is required with the resistivity or spontaneous potential data. The data are converted to LAS format and transmitted to the client.

Boring Deviation Analysis

The collected Acoustic Televiewer data was processed with Robertson Geologging's RGLDIP program, version 6.1, to extract the deviation data and produce an ASCII file and plots of deviation data.

RESULTS

Suspension Results

Suspension R1-R2 P- and S_H-wave velocities are plotted in Figures 5 - 8. The suspension velocity data presented in these figures are presented in Tables 3 - 6. The PSLOG and EXCEL analysis files for each boring are included in the boring specific directories on volume 2 of 2 (CDR) of this report, along with the raw and filtered waveforms.

P- and S_H-wave velocity data from R1-R2 analysis and quality assurance analysis of S-R1 data are plotted together in Figures A1 –A4 to aid in visual comparison. It must be noted that R1-R2 data is an average velocity over a 3.3 ft segment of the soil column; S-R1 data is an average over 10.4 (7.02) ft, creating a significant smoothing relative to the R1-R2 plots. S-R1 data are presented in Tables A1 – A4, and included in the EXCEL analysis files for each boring on volume 2 of 2 (CDR) of this report.

Calibration procedures and records for the suspension measurement system are presented in Appendix B.

The GEOVision standard field procedures are reproduced in Appendix C.

The GEOVision standard field log sheets for all borings are reproduced in Appendix D.

Caliper/ Natural Gamma Results

Caliper and natural gamma data is presented in combined log plots with resistivity and spontaneous potential in Appendix E. LAS 2.0 data and Acrobat files for each boring are included in the boring specific sub-directories in the data directory on volume 2 of 2 (CDR) of this report.

Resistivity / Spontaneous Potential Results

Resistivity and spontaneous potential data is presented in combined log plots with caliper and natural gamma data in Appendix E. LAS 2.0 data and Acrobat files for each boring are included in the boring specific sub-directories in the data directory on volume 2 of 2 (CDR) of this report.

Boring Deviation Results

Boring deviation data is presented graphically in Figure 8. Deviation data is provided in EXCEL and Acrobat formats in the B-1003 sub-directory in the data directory on volume 2 of 2 (CDR) of this report.

SUMMARY

Discussion of Suspension Results

Suspension PS velocity data is ideally collected in an uncased fluid filled boring, drilled with rotary mud (rotary wash) methods. Due to the difficult drilling conditions at this site, some portions of the borings would not stay open above water table, and some significant wash-outs of the borings occurred below water table, as shown in the caliper logs. Despite these washouts, the quality of these data ranged from good to excellent. Each boring is discussed in more detail below.

Suspension PS velocity data quality is judged based upon 5 criteria:

1. Consistent data between receiver to receiver (R1 – R2) and source to receiver (S – R1) data.
2. Consistent relationship between P-wave and S_H -wave (excluding transition to saturated soils)
3. Consistency between data from adjacent depth intervals.
4. Clarity of P-wave and S_H-wave onset, as well as damping of later oscillations.
5. Consistency of profile between adjacent borings, if available.

B-1002, B-1002A: These data show excellent correlation between R1 – R2 and S – R1 data, as well as excellent correlation between P-wave and S_H-wave velocities, with the exception of a region between 30 and 40 ft, which appears to be a perched water table. P-wave and S_H-wave onsets are generally clear, and later oscillations are well damped. This is an excellent data set.

B-1003: These data show excellent correlation between R1 – R2 and S – R1 data, as well as excellent correlation between P-wave and S_H-wave velocities. P-wave and S_H-wave onsets are clear, and later oscillations are well damped. The data from this boring is in very close agreement with the velocities obtained in B-1002. This is an exceptional data set.

B-1004: These data show excellent correlation between R1 – R2 and S – R1 data, as well as excellent correlation between P-wave and S_H-wave velocities. P-wave and S_H-wave onsets are clear, and later oscillations are well damped. This is an excellent data set.

C-1005A: These data show good correlation between R1 – R2 and S – R1 data, as well as good correlation between P-wave and S_H-wave velocities. P-wave and S_H-wave onsets are generally clear, though later oscillations are not well damped. The data from this boring is in fair agreement with the velocities obtained in B-1002. This is a fair to good data set.

Discussion of Caliper / Natural Gamma Results

B-1002: This is a excellent data set for the entire depth of the boring, though caliper data is only useful below the bottom of the PVC casing at 88.5 ft.

B-1003: This is a excellent data set for the entire depth of the boring, though caliper data is only useful below the bottom of the PVC casing at 88 ft.

B-1004: This is a excellent data set for the entire depth of the boring, though caliper data is only useful below the bottom of the PVC casing at 135 ft,

C-1005A: No caliper / natural gamma data was collected in this boring.

Discussion of Resistivity / Spontaneous Potential Results

B-1002: These data show good correlation between the different logs below 92 ft. The data is degraded above 128 ft, as the insulated cable moved into the PVC casing at this point on run 1, and the shallower run 2 data was degraded by fluid loss in the uncased boring.

B-1003: These data show good correlation between the different logs below 128 ft. The data is degraded above 128 ft, as the insulated cable moved into the casing at this point on run 2. Also, on run 3, the insulated cable moved into the casing at 1084 ft, degrading the data from this run above this depth.

B-1004: Spontaneous potential measurements did not appear to be successful in this boring, and resistivity data was poor. Despite several different placements of the ground rod, the data continued to be anomalous on four attempts to collect data. The most plausible explanation is due to currents induced in the ground by ground cables from nearby power lines. The resistivity data may still be useful in validating unit boundaries.

C-1005A: No resistivity / spontaneous potential / natural gamma data was collected in this boring.

Discussion of Boring Deviation Results

B-1003: These data show a fairly constant slope of the boring of roughly 1 degree to the east for the entire depth of the boring, placing the 1050 ft depth mark 13 ft east of the boring collar.

Quality Assurance

These boring geophysical measurements were performed using industry-standard or better methods for measurements and analyses. All work was performed under GEOVision quality assurance procedures, which include:

- Use of NIST-traceable calibrations, where applicable, for field and laboratory instrumentation
- Use of standard field data logs

- Use of independent verification of velocity data by comparison of receiver-to-receiver and source-to-receiver velocities
- Independent review of calculations and results by a registered professional engineer, geologist, or geophysicist.

Suspension Data Reliability

P- and S_H-wave velocity measurement using the Suspension Method gives average velocities over a 3.3 ft interval of depth. This high resolution results in the scatter of values shown in the graphs. Individual measurements are very reliable with estimated precision of +/- 5%. Standardized field procedures and quality assurance checks contribute to the reliability of these data.

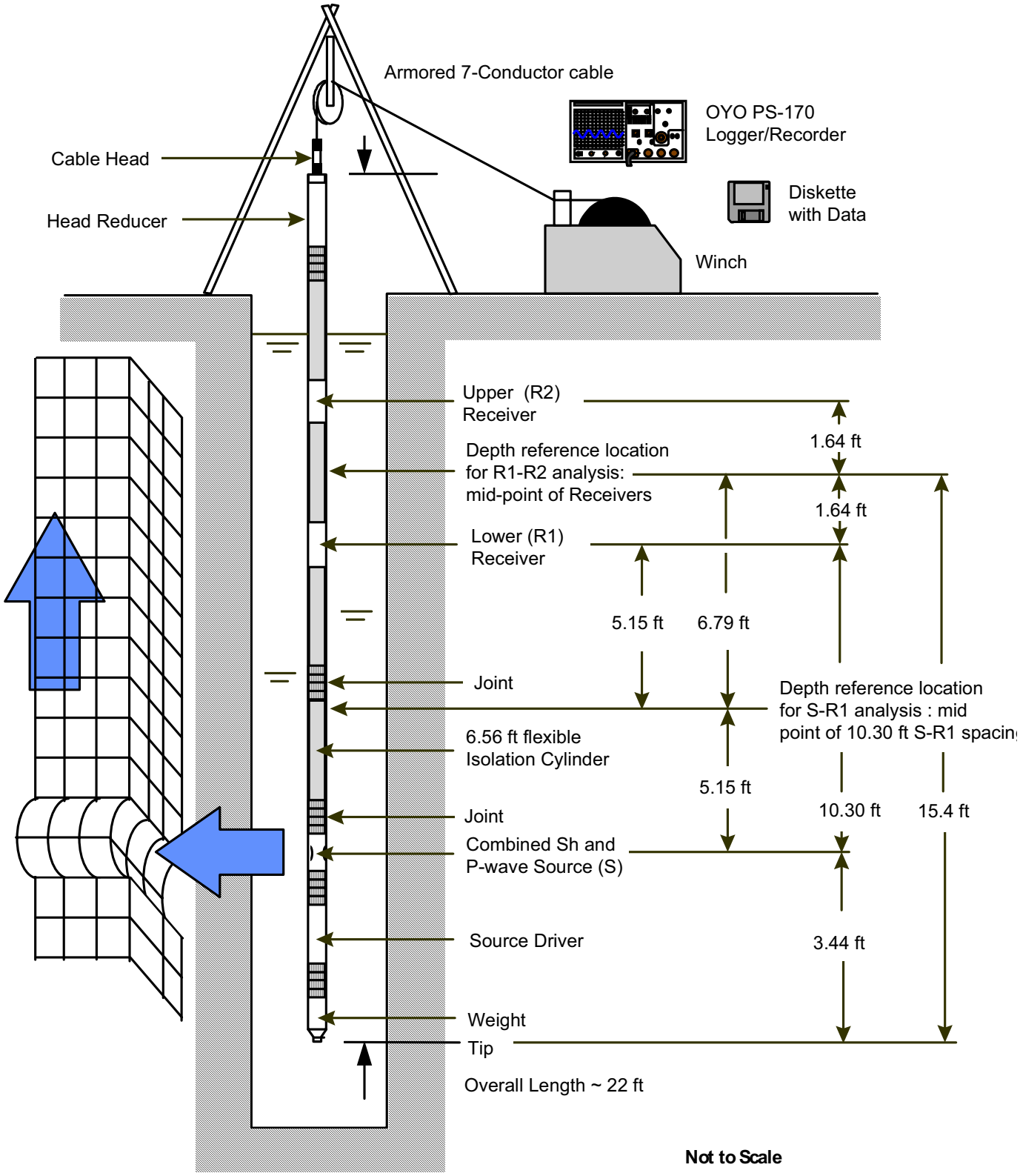

Figure 2. Concept illustration of long P-S logging system

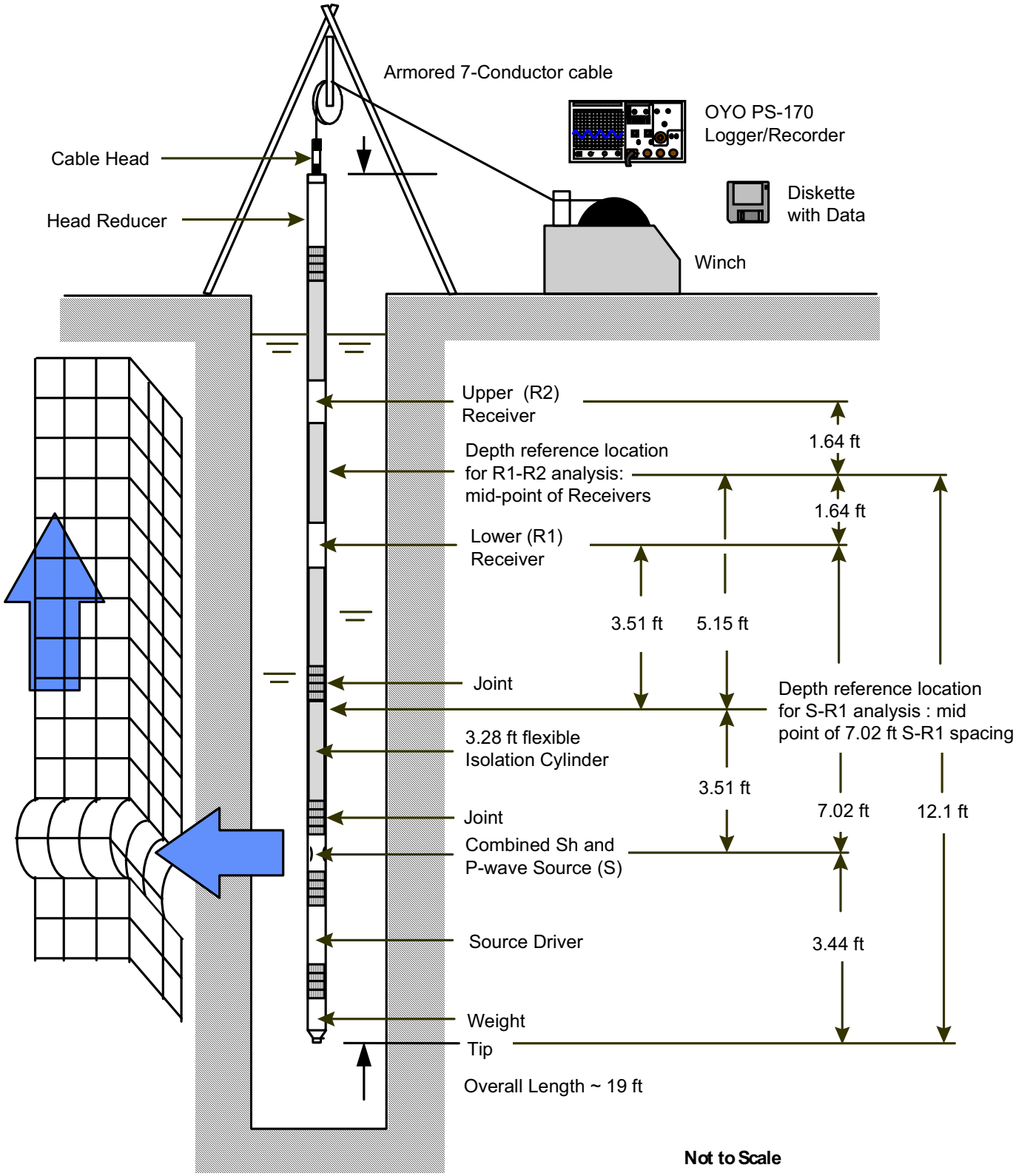

Figure 3. Concept illustration of short P-S logging system

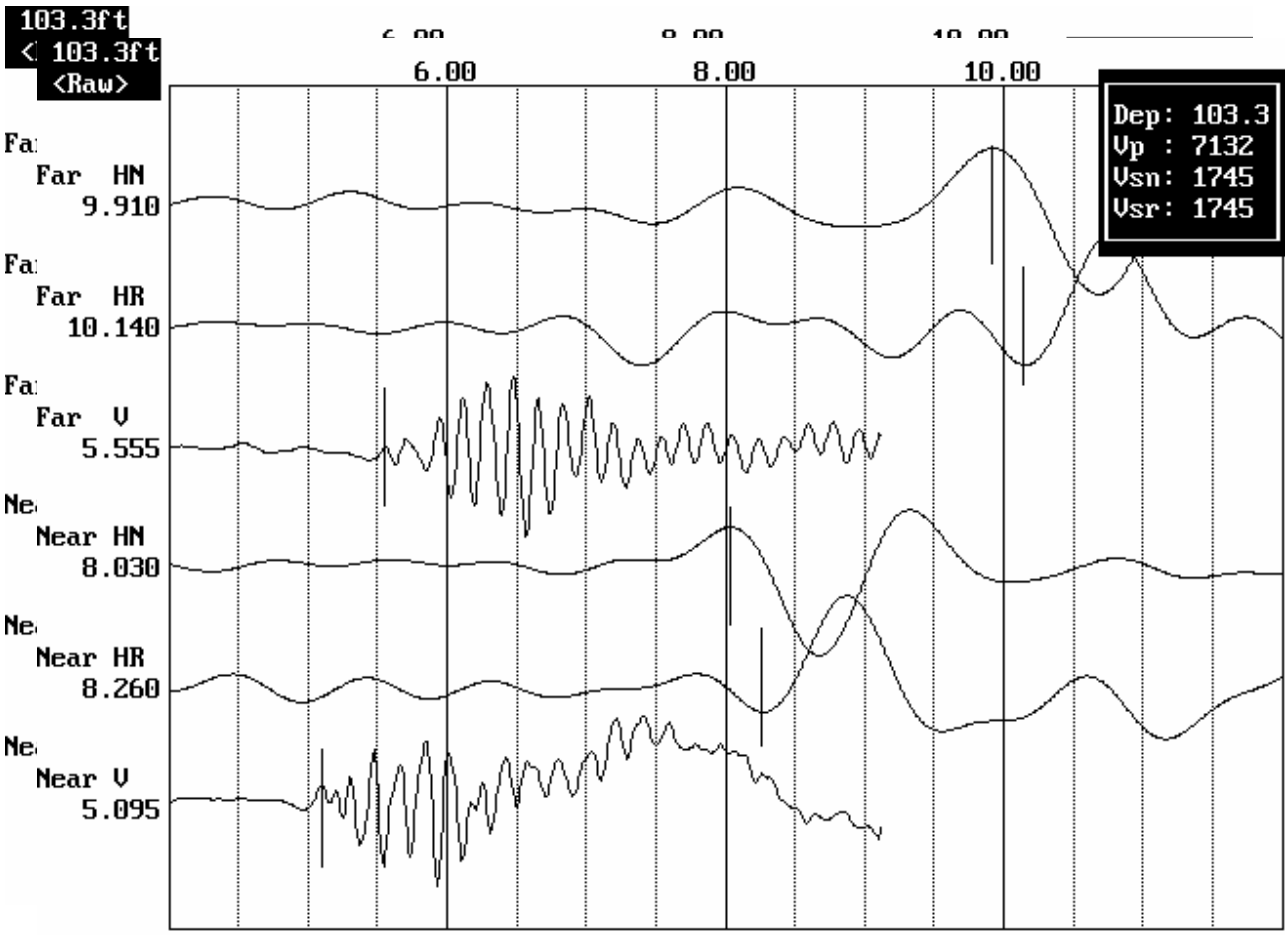

Figure 4. Example of filtered (1400 Hz lowpass) record

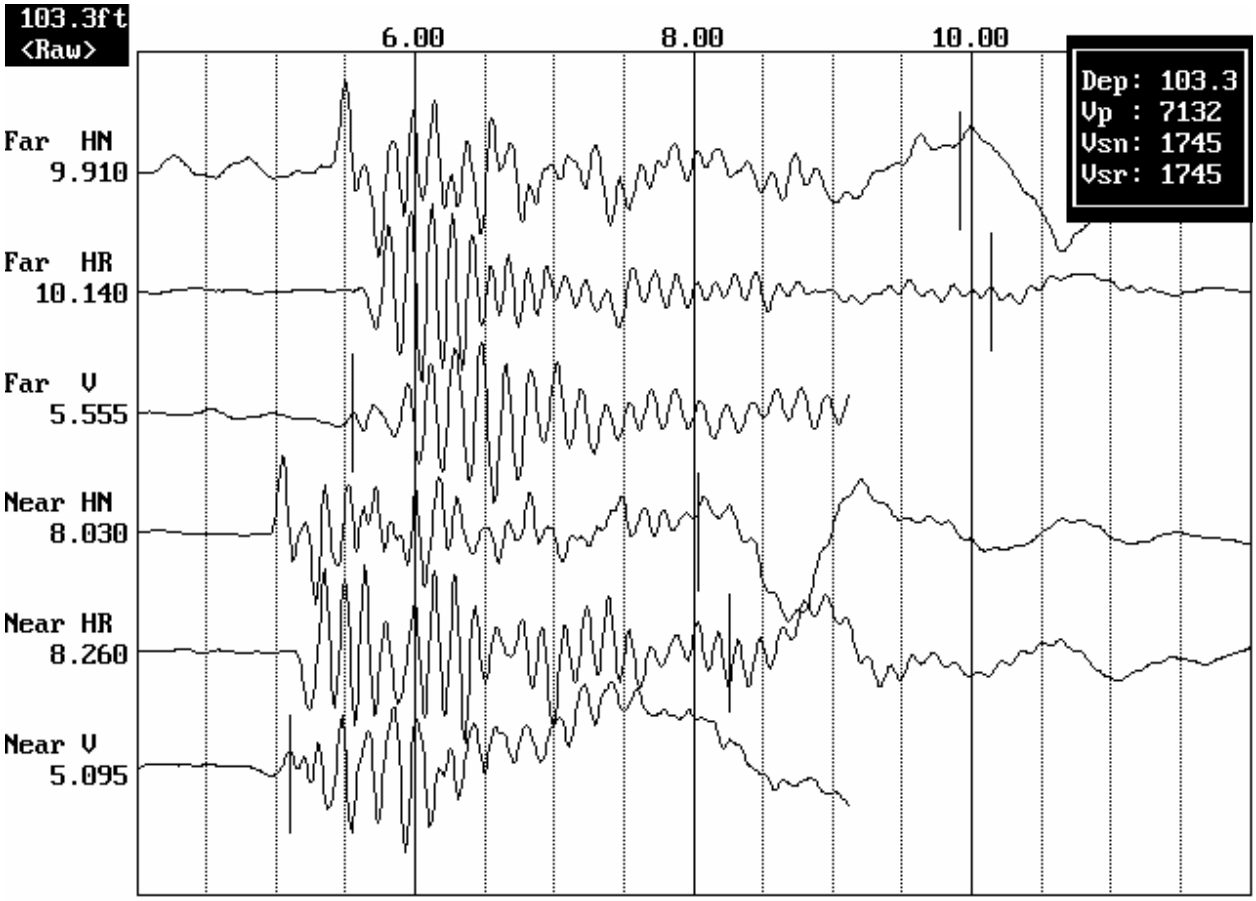

Figure 5. Example of unfiltered record

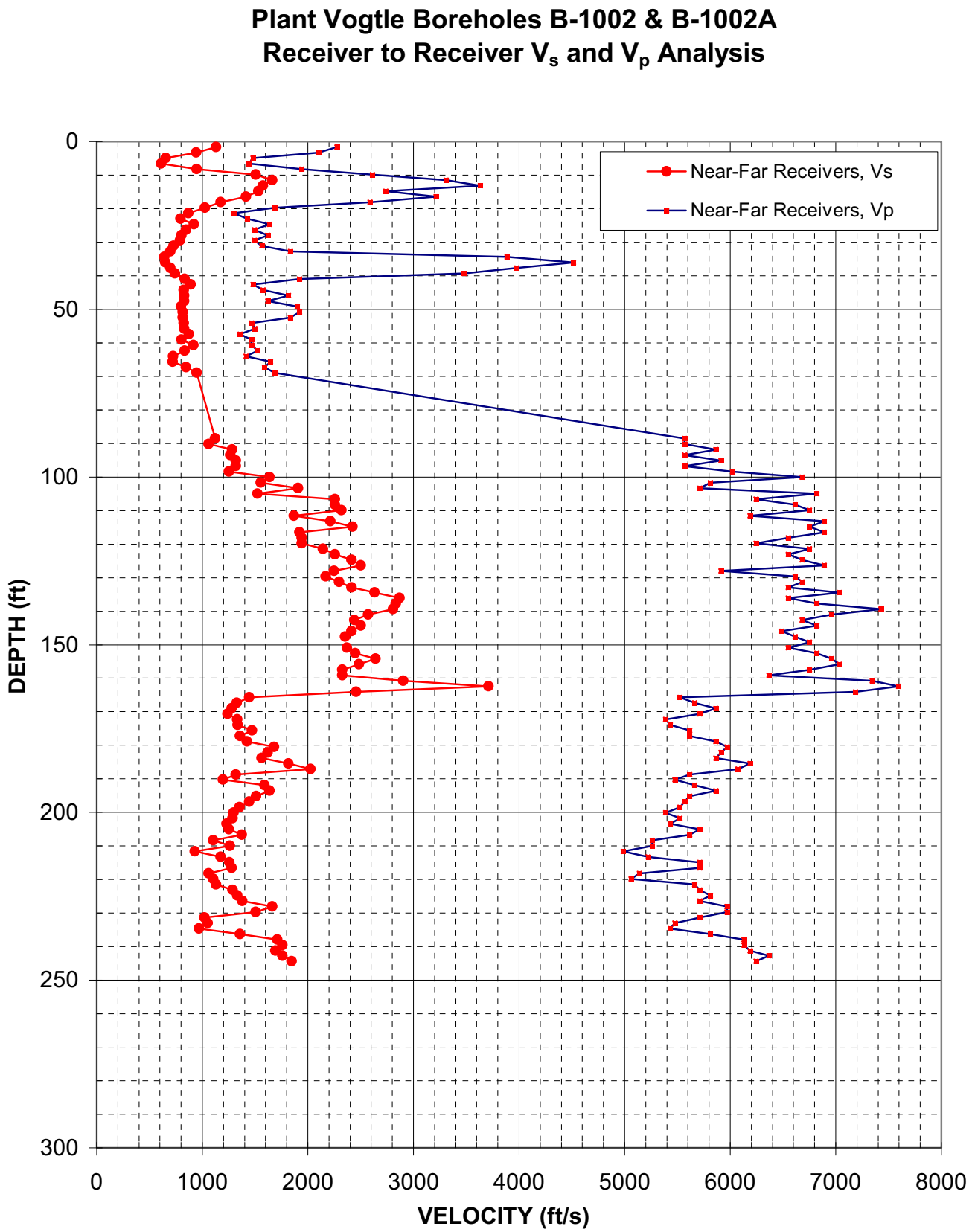

Figure 6. Boring B-1002 and B-1002A, Suspension R1-R2 P- and S_H-wave velocities

Depth (ft)	V_s (ft/sec)	V_p (ft/sec)
1.6	1130	2270
3.3	940	2100
4.9	650	1480
6.6	610	1440
8.2	950	1940
9.8	1510	2610
11.5	1660	3310
13.1	1580	3630
14.8	1530	2740
16.4	1420	3210
18.0	1180	2590
19.7	1030	1690
21.3	870	1300
23.0	800	1430
24.6	920	1640
26.3	850	1490
27.9	810	1620
29.5	790	1490
31.2	730	1560
32.8	700	1840
34.5	640	3890
36.1	650	4520
37.7	700	3980
39.4	740	3480
41.0	840	1920
42.7	890	1480
44.3	830	1580
45.9	830	1820
47.6	830	1620
49.2	800	1900
50.9	820	1920
52.5	820	1840
54.1	830	1470
55.8	830	1500
57.4	870	1360
59.1	810	1470
60.7	920	1470
62.3	840	1530
64.0	730	1420
65.6	720	1650
67.3	850	1590
68.9	950	1690
88.6	1120	5570
90.2	1060	5570
91.9	1290	5860
93.5	1270	5570
95.1	1320	5910
96.8	1320	5570
98.4	1250	6020
100.1	1640	6680

Depth (ft)	V_s (ft/sec)	V_p (ft/sec)
101.7	1550	5810
103.4	1910	5710
105.0	1530	6820
106.6	2260	6250
108.3	2260	6620
109.9	2320	6750
111.6	1870	6190
113.2	2210	6890
114.8	2420	6750
116.5	1920	6890
118.1	1940	6550
119.8	1940	6250
121.4	2140	6750
123.0	2260	6550
124.7	2410	6680
126.3	2500	6890
128.0	2250	5910
129.6	2170	6620
131.2	2300	6680
132.9	2410	6550
134.5	2630	7040
136.2	2870	6550
137.8	2830	6820
139.4	2810	7430
141.1	2570	6960
142.7	2440	6680
144.4	2500	6820
146.0	2410	6490
147.6	2350	6620
149.3	-	6750
150.9	2370	6550
152.6	2450	6820
154.2	2640	6960
155.8	2480	7040
157.5	2330	6750
159.1	2330	6370
160.8	2910	7340
162.4	3710	7590
164.0	2460	7190
165.7	1450	5520
167.3	1330	5660
169.0	1280	5860
170.6	1240	5710
172.2	1330	5390
173.9	1340	5430
175.5	1470	5620
177.2	1360	5620
178.8	1420	5860
180.5	1680	5970
182.1	1620	5910

Depth (ft)	V_s (ft/sec)	V_p (ft/sec)
183.7	1560	5860
185.4	1820	6190
187.0	2030	6080
188.7	1320	5620
190.3	1200	5480
191.9	1590	5660
193.6	1640	5860
195.2	1510	5620
196.9	1450	5570
198.5	1350	5520
200.1	1300	5390
201.8	1290	5520
203.4	1230	5430
205.1	1250	5710
206.7	1380	5620
208.3	1100	5260
210.0	1260	5260
211.6	930	4990
213.3	1170	5220
214.9	1260	5710
216.5	1280	5710
218.2	1060	5140
219.8	1110	5060
221.5	1130	5660
223.1	1290	5710
224.7	1330	5810
226.4	1380	5710
228.0	1660	5970
229.7	1510	5970
231.3	1020	5710
232.9	1050	5480
234.6	970	5430
236.2	1360	5810
237.9	1710	6130
239.5	1760	6130
241.1	1700	6190
242.8	1760	6370
244.4	1850	6250

Table 4. Boring B-1002 and B-1002A, Suspension R1-R2 depths and P- and S_H-wave velocities

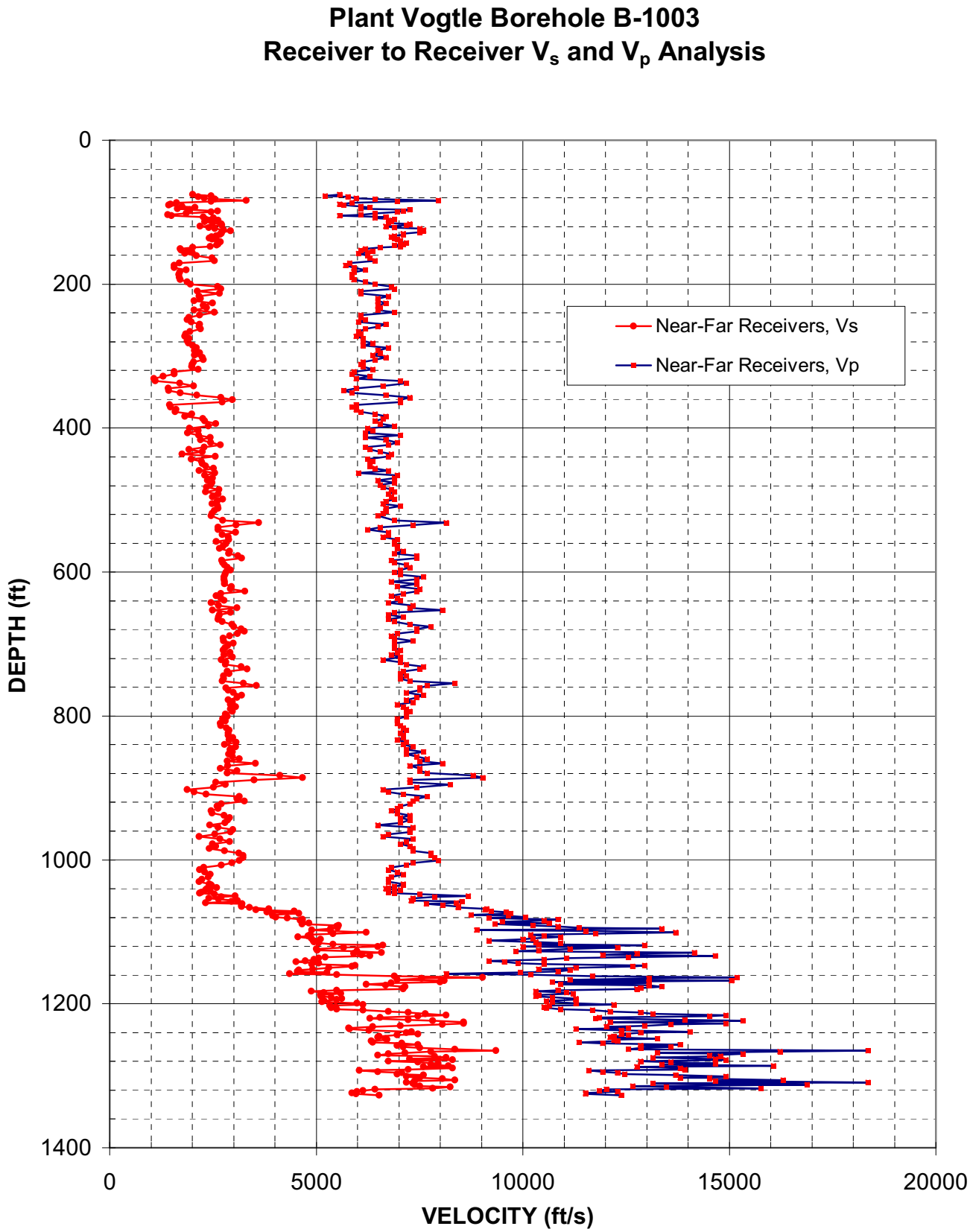

Figure 7. Boring B-1003, Suspension R1-R2 P- and S_H-wave velocities

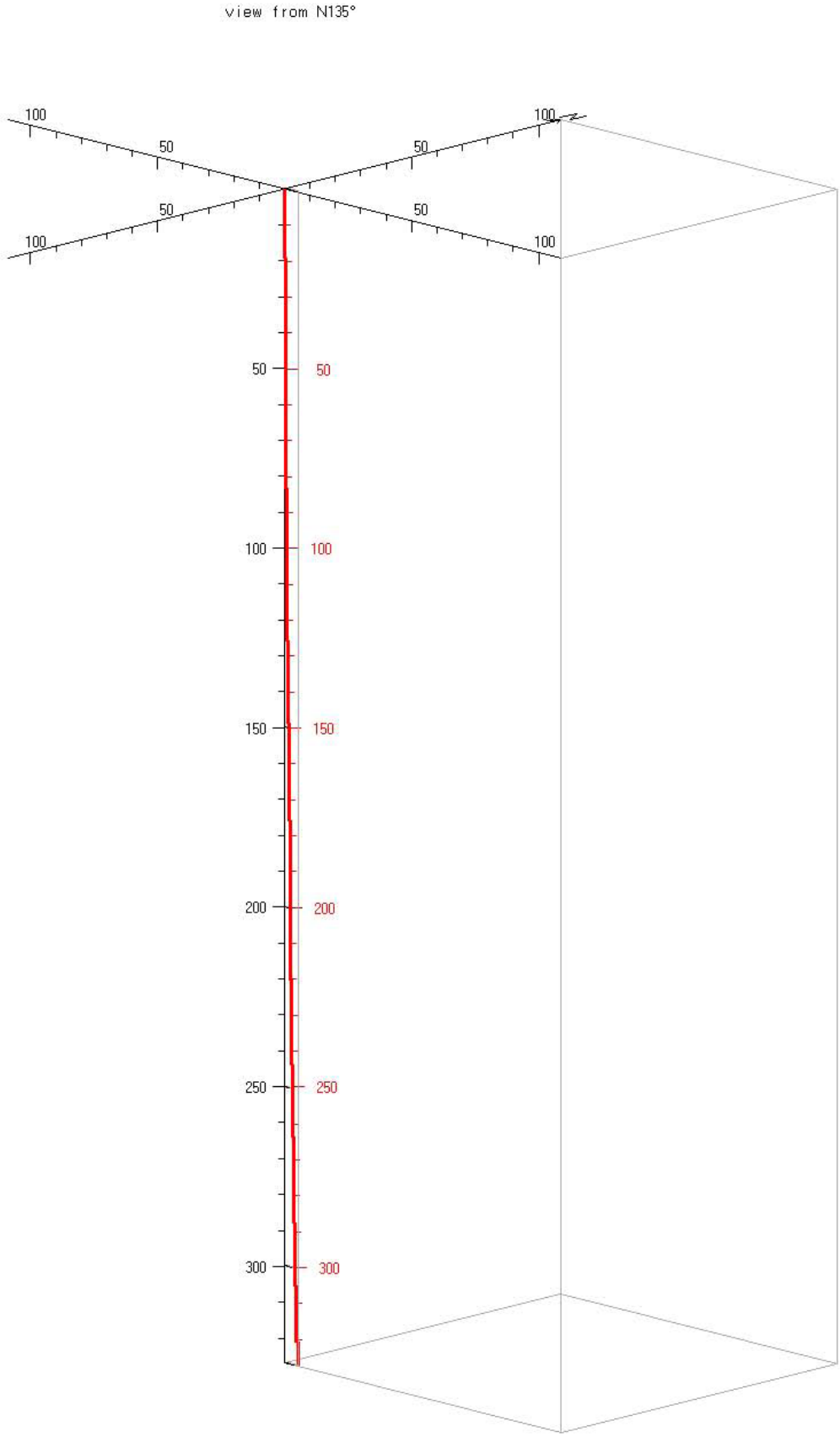

Figure 8. Boring B-1003, Deviation Projection (dimensions in meters)

Depth (ft)	V_s (ft/sec)	V_p (ft/sec)
75.5	2010	5570
77.1	2460	5220
78.7	2140	5760
80.4	2290	5970
82.0	2550	6430
83.7	3310	7960
85.3	2460	6960
86.9	1620	5860
88.6	1470	5570
90.2	1430	5660
91.9	1760	6080
93.5	2060	6310
95.1	1650	6080
96.8	1940	7260
98.4	2610	7110
100.1	2460	6960
101.7	1860	6430
103.4	1400	6080
105.0	1490	5570
106.6	2270	6680
108.3	2510	6430
109.9	2330	6890
111.6	2630	6750
113.2	2300	6820
114.8	2490	6750
116.5	2710	7260
118.1	2720	7190
119.8	2190	6680
121.4	2400	6890
123.0	2550	7510
124.7	2760	7590
126.3	2930	7590
128.0	2720	7510
129.6	2710	7110
131.2	2670	7110
132.9	2580	6890
134.5	2470	6820
136.2	2410	6890
137.8	2480	6960
139.4	2600	7040
141.1	2680	7040
142.7	2620	7190
144.4	2630	7110
146.0	2590	6890
147.6	2440	7040
149.3	2010	6550
150.9	1710	6190
152.6	1730	6080
154.2	1890	6370
155.8	2000	6250

Depth (ft)	V_s (ft/sec)	V_p (ft/sec)
157.5	1820	6020
160.8	2100	6250
164.0	2480	6310
167.3	2540	6430
170.6	1680	5810
173.9	1560	5710
177.2	1570	5910
180.5	1860	6190
183.7	1700	5910
187.0	1670	5860
190.3	1690	5860
193.6	1700	5910
196.9	1880	6190
200.1	1950	6430
203.4	2610	6820
206.7	2690	6890
210.0	2130	6080
213.3	2660	6080
216.5	2170	6750
219.8	2200	6490
223.1	2040	6490
226.4	2490	6680
229.7	2270	6490
232.9	2350	6550
236.2	2040	6490
239.5	2530	6890
242.8	2180	6080
246.1	1930	6080
249.3	1880	6190
252.6	1980	6020
255.9	2180	6680
259.2	2160	6490
262.5	2200	6190
265.8	1950	6020
269.0	1850	6080
272.3	1820	5970
275.6	1920	6130
278.9	1880	6130
282.2	1910	6370
285.4	2010	6130
288.7	2100	6750
292.0	2060	6490
295.3	2180	6550
298.6	2060	6370
301.8	2240	6680
305.1	2270	6430
308.4	2030	6130
311.7	2000	6080
315.0	1990	6130
318.2	2140	6370

Depth (ft)	V_s (ft/sec)	V_p (ft/sec)
321.5	1570	5910
324.8	1570	5860
328.1	1300	6310
331.4	1070	5970
334.7	1100	7040
337.9	1700	7190
341.2	2040	6620
344.5	1420	5970
347.8	1430	5660
351.1	1710	5860
354.3	2110	6680
357.6	2690	7260
360.9	2970	7040
364.2	2730	7040
367.5	1450	5970
370.7	1480	5860
374.0	1610	5970
377.3	1580	6080
380.6	1990	6430
383.9	1830	6680
387.1	2260	6620
390.4	2300	6430
393.7	2570	6550
397.0	2400	6890
400.3	1940	6250
403.5	2150	6370
406.8	1890	6190
410.1	2160	7040
413.4	2430	6190
416.7	2210	6680
420.0	2450	6960
423.2	2680	6750
426.5	2290	6190
429.8	1920	6310
433.1	2250	6550
436.4	1760	6820
439.6	2560	6750
442.9	1980	6250
446.2	2220	6370
449.5	2240	6310
452.8	2330	6310
456.0	2510	6430
459.3	2170	6750
462.6	2550	6020
465.9	2300	6960
469.2	2490	6890
472.4	2370	6490
475.7	2480	6890
479.0	2450	6550
482.3	2350	6620

Table 5. Boring B-1003, Suspension R1-R2 depths and P- and S_H-wave velocities

Depth (ft)	V_s (ft/sec)	V_p (ft/sec)
485.6	2650	6820
488.9	2330	6890
492.1	2620	6750
495.4	2490	6820
498.7	2740	6890
502.0	2600	6680
505.3	2480	6620
508.5	2610	7040
511.8	2620	6680
515.1	2530	6680
518.4	2480	6620
521.7	2460	6490
528.2	2740	6890
531.5	3610	8150
534.8	3070	7340
538.1	2620	6550
541.3	2630	6250
544.6	3050	6750
547.9	2730	6750
551.2	2870	6620
555.5	2880	6960
557.7	2580	6890
561.0	2820	6890
564.3	2750	6960
567.6	2660	6960
570.9	2910	7110
574.2	2880	6890
577.4	3110	7430
580.7	3200	7430
584.0	2720	6820
587.3	2740	6890
590.6	2780	7190
593.8	2840	7260
597.1	2930	7040
600.4	2820	6890
603.7	2800	7040
607.0	2770	7590
610.2	2770	7430
613.5	2780	6820
616.8	2780	7430
620.1	2940	6960
623.4	2930	7510
626.6	3280	7430
629.9	2690	7110
633.2	2580	6820
636.5	2690	6960
639.8	2770	7040
643.0	2460	6750
646.3	2640	7340
649.6	3080	7260

Depth (ft)	V_s (ft/sec)	V_p (ft/sec)
652.9	2490	8050
656.2	2930	6890
659.5	2660	6750
662.7	2640	7110
666.0	2620	6750
669.3	2730	6890
672.6	2960	7260
675.9	3010	7770
679.1	3180	7430
682.4	3260	7430
685.7	3090	6960
689.0	2910	6820
692.3	2750	6890
695.5	2760	7340
698.8	3000	6890
702.1	2860	6890
705.4	2800	6890
708.7	2750	7040
711.9	2920	6960
715.2	2770	6820
718.5	2970	7040
721.8	2710	6620
725.1	2820	7040
728.4	2810	7190
731.6	3180	7590
734.9	3330	7510
738.2	2840	7110
741.5	2890	7040
744.8	2760	7190
748.0	2760	7040
751.3	2730	7260
754.6	3240	8350
757.9	3550	7680
761.2	2820	7510
764.4	2870	7510
767.7	3000	7190
771.0	3200	7590
774.3	3080	7430
777.6	2870	7190
780.8	2970	7340
784.1	2930	6960
787.4	3050	7110
790.7	2930	7190
794.0	2970	7260
797.2	2810	7190
800.5	2840	7190
803.8	2740	6960
807.1	2810	6960
810.4	2680	6960
813.7	2690	7040

Depth (ft)	V_s (ft/sec)	V_p (ft/sec)
816.9	2830	7110
820.2	2890	7190
823.5	2870	7040
826.8	2870	7110
830.1	2980	7110
833.3	2890	6960
836.6	3070	7190
839.9	2780	7110
843.2	3050	7340
846.5	2920	7190
849.7	2970	7590
853.0	2880	7190
856.3	2970	7430
859.6	3140	7680
862.9	2840	7510
866.1	3540	8050
869.4	2860	7260
872.7	2680	7510
876.0	3080	7510
879.3	2840	7680
882.6	4130	8790
885.8	4670	9030
889.1	3500	7260
892.4	2570	7260
895.7	2810	8250
899.0	2510	7430
902.2	1880	6620
905.5	2040	6750
908.8	2340	7110
912.1	3140	7680
915.4	3080	7430
918.6	3260	7340
922.2	2710	7260
925.2	2600	7040
928.5	2620	6960
931.8	2460	6820
935.0	2480	6960
938.3	2770	7260
941.6	2910	7040
944.9	2860	7260
948.2	2800	7040
951.4	2420	6490
954.7	2620	7340
958.0	2980	7260
961.3	2930	7260
964.6	2550	6750
967.9	2170	6620
971.1	2670	7340
974.4	2910	7190
977.7	2490	7040

Table 5, continued. Boring B-1003, Suspension R1-R2 depths and P- and S_H-wave velocities

Depth (ft)	V_s (ft/sec)	V_p (ft/sec)
981.0	2570	7260
984.3	2410	7340
987.5	2780	7340
990.8	3120	7770
994.1	3230	7770
997.4	3230	7860
1000.7	3140	7960
1003.9	2960	7340
1007.2	2710	7190
1010.5	2280	6820
1013.8	2180	6750
1017.1	2300	6960
1020.3	2430	7110
1023.6	2400	6820
1026.9	2240	6750
1030.2	2160	6750
1033.5	2410	7110
1035.1	2460	7110
1036.8	2480	6890
1038.4	2590	6750
1040.0	2360	6680
1041.7	2330	7040
1043.3	2430	6890
1045.0	2230	6750
1046.6	2180	6890
1047.9	2530	7510
1049.9	3040	8680
1051.5	2710	7860
1053.2	2400	7340
1054.8	2640	7340
1056.4	3090	7300
1058.1	2940	8520
1059.7	2320	8400
1061.4	3210	7660
1063.0	3190	8070
1064.6	3200	8440
1066.3	3380	8440
1067.9	3850	9130
1069.6	3550	9080
1071.2	4470	9230
1072.8	3810	9600
1074.5	4580	9710
1076.1	3940	8750
1077.8	3950	9660
1079.4	4030	10070
1081.0	4300	9180
1082.7	4670	10850
1084.3	4610	10510
1086.0	4670	9490
1087.6	4830	10640

Depth (ft)	V_s (ft/sec)	V_p (ft/sec)
1089.2	4660	9330
1090.9	5550	10250
1092.5	5500	10850
1094.2	5520	11370
1095.8	5350	13370
1097.4	4900	8890
1099.1	5350	11520
1100.7	6220	13700
1102.4	5410	11770
1104.0	4860	10190
1105.6	4810	10510
1107.3	4560	10920
1108.9	4880	10250
1110.6	5100	10000
1112.2	4930	9180
1113.9	4950	10310
1115.5	5060	10920
1117.1	5410	10380
1118.8	6620	12950
1120.4	6490	10000
1122.1	5660	12290
1123.7	5010	11140
1125.3	5030	10380
1127.0	5990	9830
1128.6	6580	14160
1130.3	5910	12750
1131.9	6100	11930
1133.5	6310	14660
1135.2	5220	12560
1136.8	5060	11070
1138.5	4950	10510
1140.1	4740	9180
1141.7	4520	9550
1143.4	5060	9890
1145.0	4900	10510
1146.7	5940	12950
1148.3	5860	12660
1149.9	5300	11290
1151.6	4910	10380
1153.2	4580	11140
1154.9	4550	10850
1156.5	5260	9950
1158.1	4350	8150
1159.8	5500	10190
1161.4	6890	11680
1163.1	9030	15190
1164.7	7550	13050
1166.3	6960	11140
1168.0	8100	15050
1169.6	8000	10710

Depth (ft)	V_s (ft/sec)	V_p (ft/sec)
1171.3	6820	13050
1172.9	6220	10920
1174.5	6680	13050
1176.2	7150	13370
1177.8	7110	12850
1179.5	7110	12750
1181.1	5500	10850
1182.7	4880	10310
1184.4	5180	11070
1186.0	5590	11210
1187.7	5100	10380
1189.3	5120	10310
1190.9	5370	10710
1192.6	5620	11290
1194.2	5500	11290
1195.9	5200	10570
1197.5	5140	10710
1199.2	5990	11290
1200.8	6130	12200
1202.4	5330	10640
1204.1	5480	10510
1205.7	5370	10570
1207.4	5500	10920
1209.0	6130	11680
1210.6	6750	12110
1212.3	7230	12850
1213.9	7640	13160
1215.6	8150	14920
1217.2	7470	14530
1218.8	6550	11850
1220.5	6310	11770
1222.1	7230	13920
1223.8	7820	15330
1225.4	8570	12110
1227.0	8570	14920
1228.7	8050	13580
1230.3	7040	12950
1232.0	6370	12020
1233.6	5790	12560
1235.2	5810	11290
1236.9	6280	12380
1238.5	7300	14040
1240.2	7190	12850
1241.8	7470	12380
1243.4	6960	12560
1245.1	6520	12200
1246.7	6490	12110
1248.4	6680	13260
1250.0	6720	12200
1251.6	6330	12290

Table 5, continued. Boring B-1003, Suspension R1-R2 depths and P- and S_H-wave velocities

Depth (ft)	V_s (ft/sec)	V_p (ft/sec)
1253.3	6370	11370
1254.9	7070	11930
1256.6	7470	13810
1258.2	6960	12850
1259.8	7110	13580
1261.5	7510	12850
1263.1	8350	12560
1264.8	9350	18360
1266.4	7770	16220
1268.0	7150	13260
1269.7	6750	15330
1271.3	6490	14530
1273.0	7860	14790
1274.6	8150	13160
1276.3	7260	14660
1277.9	8300	14920
1279.5	6750	12850
1281.2	7470	13580
1282.8	7960	14660
1284.5	7770	13370
1286.1	8200	16070
1287.7	7590	12750
1289.4	8300	13810
1291.0	7230	13920
1292.7	6050	11600
1294.3	6490	11930
1295.9	7070	12290
1297.6	6960	12470
1299.2	7590	13700
1300.9	7190	14920
1302.5	7430	13810
1302.5	7510	14530
1304.1	8050	14530
1305.8	8350	16300
1307.4	7380	14660
1309.1	7190	18360
1310.7	7340	13160
1312.3	7380	16880
1314.0	7510	12660
1315.6	8250	13470
1317.3	7820	15760
1318.9	6430	12020
1320.5	6130	11850
1322.2	5990	12290
1323.8	5860	11520
1325.5	5970	11520
1327.1	6520	12380

Table 5, continued. Boring B-1003, Suspension R1-R2 depths and P- and S_H-wave velocities

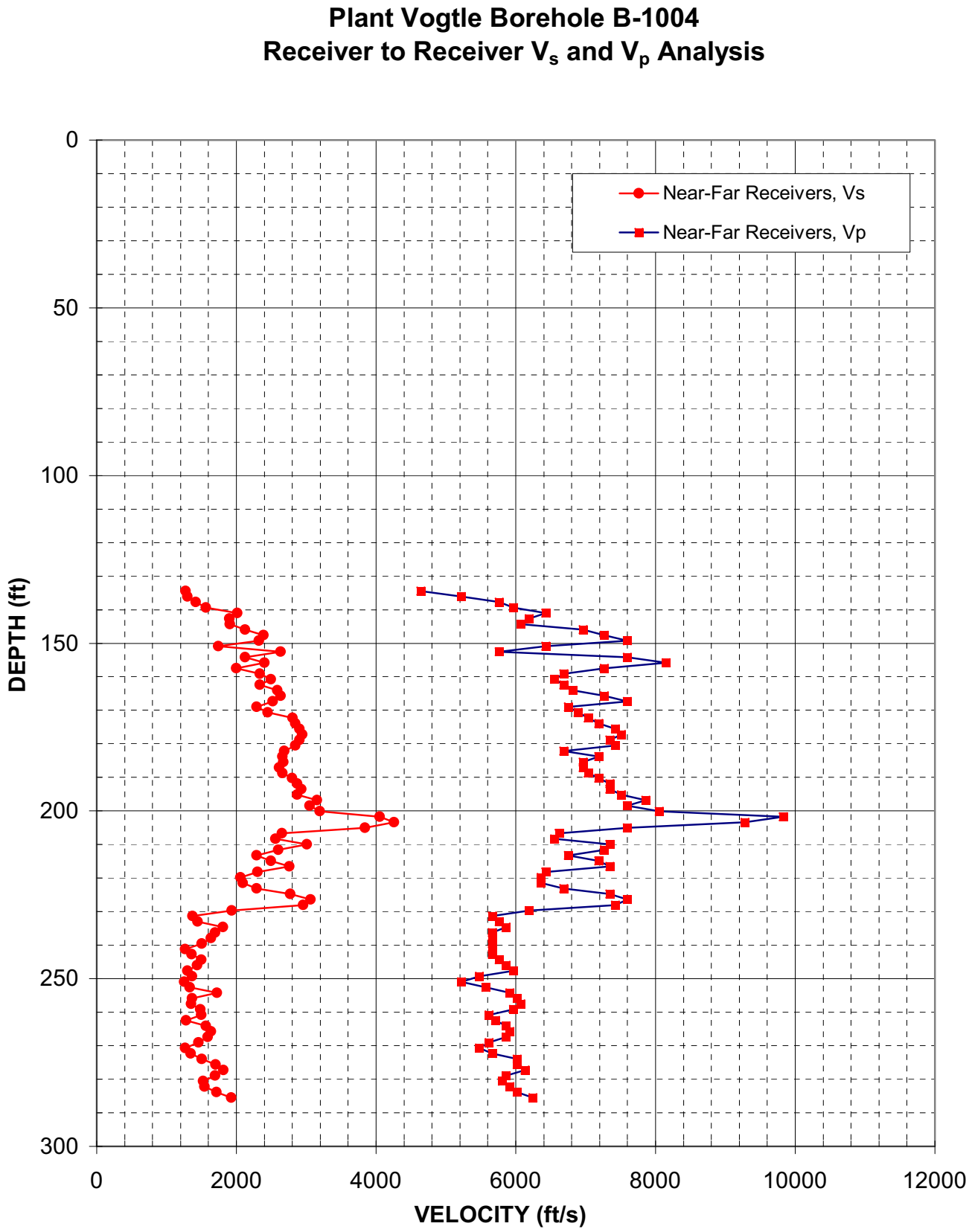

Figure 9. Boring B-1004, Suspension R1-R2 P- and S_H-wave velocities

Depth (ft)	V_s (ft/sec)	V_p (ft/sec)
134.5	1270	4640
136.2	1300	5220
137.8	1420	5760
139.4	1560	5970
141.1	2010	6430
142.7	1900	6190
144.4	1910	6080
146.0	2130	6960
147.6	2390	7260
149.3	2320	7590
150.9	1740	6430
152.6	2630	5760
154.2	2130	7590
155.8	2400	8150
157.5	2000	7260
159.1	2340	6680
160.8	2490	6550
162.4	2340	6680
164.0	2590	6820
165.7	2630	7260
167.3	2520	7590
169.0	2290	6750
170.6	2450	6890
172.2	2810	7040
173.9	2840	7190
175.5	2910	7430
177.2	2940	7510
178.8	2910	7340
180.5	2840	7430
182.1	2680	6680
183.7	2660	7190
185.4	2670	6960
187.0	2610	6960
188.7	2660	7040
190.3	2800	7190
191.9	2870	7340
193.6	2930	7340
195.2	2870	7510
196.9	3150	7860
198.5	3050	7590
200.1	3200	8050
201.8	4050	9830
203.4	4260	9280
205.1	3840	7590
206.7	2650	6620
208.3	2560	6550
210.0	3010	7340
211.6	2600	7260
213.3	2290	6750
214.9	2490	7190

Depth (ft)	V_s (ft/sec)	V_p (ft/sec)
216.5	2760	7340
218.2	2300	6430
219.8	2060	6370
221.5	2100	6370
223.1	2290	6680
224.7	2770	7340
226.4	3070	7590
228.0	2960	7430
229.7	1930	6190
231.3	1380	5660
232.9	1450	5760
234.6	1810	5860
236.2	1700	5660
237.9	1640	5660
239.5	1510	5660
241.1	1270	5660
242.8	1360	5660
244.4	1500	5760
246.1	1440	5860
247.7	1300	5970
249.3	1370	5480
251.0	1250	5220
252.6	1330	5570
254.3	1720	5910
255.9	1360	6020
257.6	1350	6080
259.2	1490	5970
260.8	1500	5620
262.5	1280	5710
264.1	1560	5860
265.8	1640	5910
267.4	1590	5860
269.0	1460	5620
270.7	1270	5480
272.3	1350	5660
274.0	1510	6020
275.6	1700	6020
277.2	1820	6130
278.9	1700	5860
280.5	1530	5810
282.2	1540	5910
283.8	1720	6020
285.4	1930	6250

Table 6. Boring B-1004 Suspension R1-R2 depths and P- and S_H-wave velocities

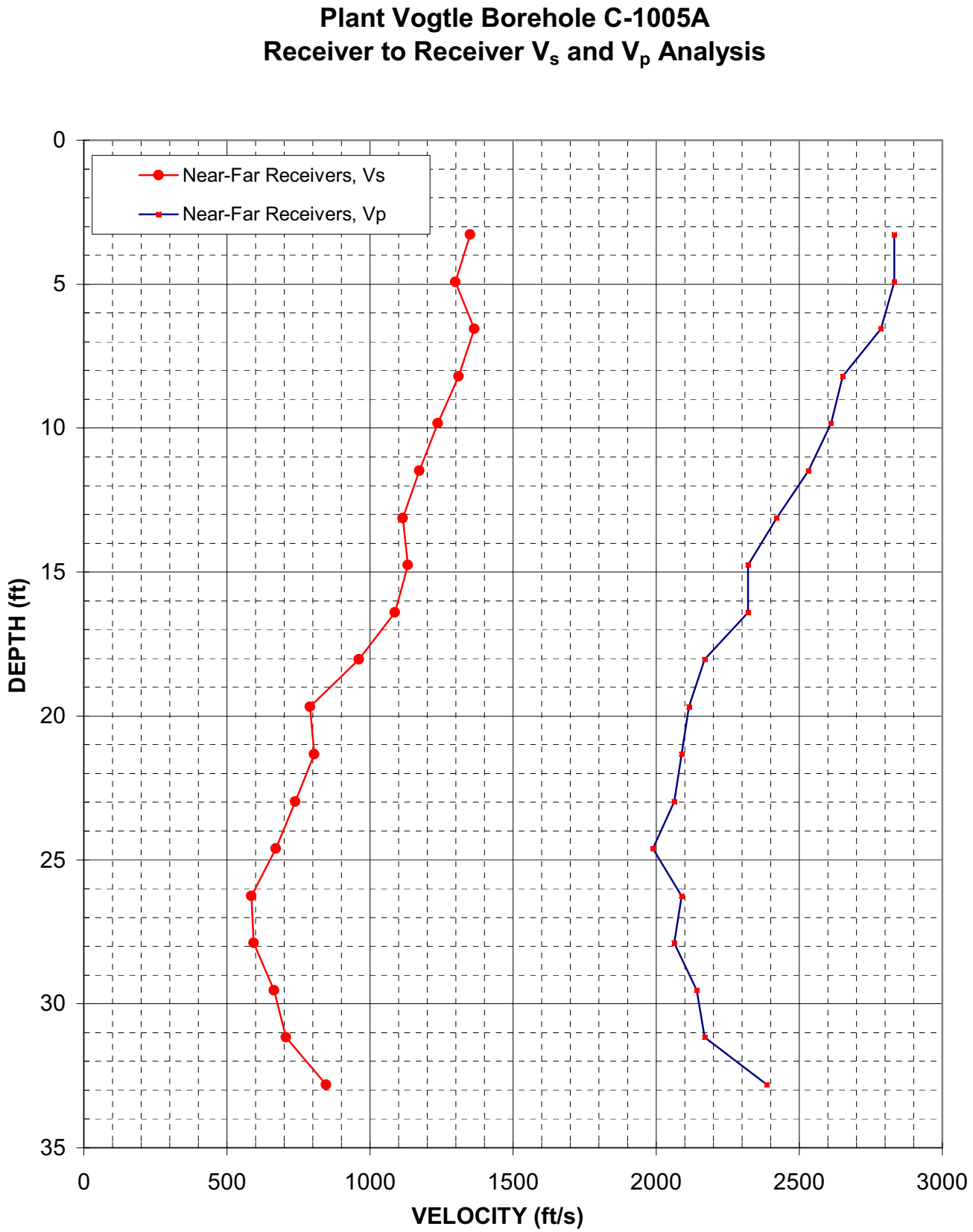

Figure 10. Boring C-1005A, Suspension R1-R2 P- and S_H-wave velocities

Depth (ft)	V_s (ft/sec)	V_p (ft/sec)
3.3	1350	2830
4.9	1300	2830
6.6	1360	2780
8.2	1310	2650
9.8	1240	2610
11.5	1170	2530
13.1	1110	2420
14.8	1130	2320
16.4	1090	2320
18.0	960	2170
19.7	790	2110
21.3	810	2090
23.0	740	2060
24.6	670	1990
26.3	590	2090
27.9	590	2060
29.5	670	2140
31.2	710	2170
32.8	850	2390

Table 7. Boring C-1005A, Suspension R1-R2 depths and P- and S_H-wave velocities